CO-PYROLYSIS OF MICROALGAE, SLUDGE AND LIGNOCELLULOSIC BIOMASS FOR AROMATIC HYDROCARBON PRODUCTION

By

SOURABH CHAKRABORTY

Bachelor of Technology in Biotechnology
West Bengal University of Technology
Kolkata, West Bengal
2013

Master of Technology in Biotechnology and Biochemical Engineering
Indian Institute of Technology – Kharagpur
Kharagpur, West Bengal
2015

Submitted to the Faculty of the
Graduate College of the
Oklahoma State University
in partial fulfillment of
the requirements for
the Degree of
DOCTOR OF PHILOSOPHY
December, 2019

CO-PYROLYSIS OF MICROALGAE, SLUDGE, AND LIGNOCELLULOSIC BIOMASS FOR AROMATIC HYDROCARBON PRODUCTION

Dissertation Approved:

Dr. Nurhan Turgut Dunford

Dissertation Adviser

Dr. Ajay Kumar

Dr. Robert Scott Frazier

Dr. Marimuthu Andiappan

ACKNOWLEDGEMENTS

Firstly, I am thankful to my adviser Dr. Nurhan Dunford for selecting me in carrying out this dissertation work and providing me with encouragement, support and guidance for the past three and a half years. Her passion and determination for resolving the problems from its root has always motivated me in carrying out my work and will continue doing so for my future goals. Additionally, I would like to thank my committee members Dr. Ajay Kumar, Dr. Robert Scott Frazier and Dr. Marimuthu Andiappan for their support and feedback. Their time and effort are deeply appreciated. Outside my committee, I am extremely gratified for the time contributed by Dr. Carla Goad in helping me with the experimental design and statistical analysis of my work. Furthermore, I would like to extend my gratitude to Dr. Sayeed Mohammad for his help with ASPEN PLUS simulation for my work.

Moreover, I strongly appreciate the help provided in my work especially at the time of need, by Wayne Kiner (the former manager of BAE (Biosystems and Agricultural Engineering) Laboratory), Joe Preston (the current manager of BAE Laboratory), and Jacob Nelson. By interacting with them, I've learned about the fine aspects of my work.

I also thank Dr. David Jacobs for help with GC – MS analysis of samples in the Chemistry department. Additionally, I am grateful to Larry Vaughn and his team at the Instrument workshop at the Physical Science building for their support on repairing and fixing furnace instrument parts during the furnace runs.

Finally, I am thankful to my parents and family for their support, faith, and belief in me throughout this journey.

Name: SOURABH CHAKRABORTY

Date of Degree: DECEMBER, 2019

Title of Study: CO-PYROLYSIS OF MICROALGAE, SLUDGE, AND LIGNOCELLULOSIC BIOMASS FOR AROMATIC HYDROCARBON PRODUCTION

Major Field: BIOSYSTEMS AND AGRICULTURAL ENGINEERING

Abstract:

Co-pyrolysis, where a mixture of two or more different biomasses are subjected to pyrolysis, has gained attention over the years. Many studies have revealed that it leads to bio-oil production with desirable properties like reduced moisture content and enhanced caloric value. In the present study, blends of cedar wood (CW), algal biomass (AB), and digested sludge (DS) were subjected to co-pyrolysis in presence and absence of the catalyst ZSM-5. Differential Scanning Calorimetry (DSC) analysis was carried out for 18 different combinations of these biomasses to assess the total activation energy (E_a), change in enthalpy (ΔH), and change in Gibb's free energy (ΔG) for these blends. The lowest value of E_a (87.28 kJ/mol) and ΔH (80.49 kJ/mol) were obtained for the 2:1 wt/wt catalyst to 1:1:1 wt/wt biomass blend of CW: AB: DS with ΔG value of 207.62 kJ/mol.

Statistical analysis of the DSC data resulted in significant response surface models (RSM) for Ea and ΔH, but could not model ΔG well. Additionally, it has demonstrated that the catalyst addition to blends reduced the energy requirement for pyrolysis. Therefore, based on the RSM models for E_a and ΔH, 2:1 wt/wt blend of ZSM–5 to biomass: 57.14 wt % DS, 4.29 wt % AB and 38.57 wt % CW was chosen as the optimum combination (OC). The 2:1 wt/wt ZSM–5: biomass blend containing equal weight fractions of three biomasses produced a bio-oil with the highest aromatic hydrocarbon yield of 89.38 wt %. The aromatic hydrocarbon content of 83.12 wt % was obtained in the bio-oil produced from pyrolysis of OC. Naphthalene, anthracene and their methyl derivatives were the main aromatic hydrocarbons in the bio-oil.

ASPEN PLUS simulation of the AB, DS and CW co-pyrolysis system confirmed the findings obtained with the DSC experiments indicating that co-pyrolysis can reduce energy requirement and allowed both mass and energy balance calculations for the process.

TABLE OF CONTENTS

Chapter Page

LIST OF TABLES

Table Page

LIST OF FIGURES

Figure Page

Figure Page

CHAPTER I

INTRODUCTION

1.1 PROBLEM STATEMENT

Solar radiation (from sun), wind, and biomass have been evaluated as energy sources for decades (Akella et al., 2009; Gutermuth, 1998; Painuly, 2001). Initially, oil from oilseed crops such as soybean, jatropha, rapeseed, and canola have been utilized for production of biodiesel (Chisti, 2008; Demirbas, 2007). However, biofuel production using these crops competes with the availability of agricultural land for food, fiber, and feed production. Thus, a potential alternative is utilization of microalgal biomass for biofuel production as most of the problems associated with crop production are either eliminated or reduced, i.e. faster growth, lower nutrient requirement and no need for agricultural land for algae growth (Anand et al., 2016). Lipids and carbohydrates from microalgae have been utilized for biodiesel and bioethanol production, respectively (Chisti, 2008; Harun et al., 2010; Markou et al., 2012). During the last decade, conversion of algal biomass to bio-oil via various thermochemical conversion techniques has been gaining attention (Lam & Lee, 2012).

Pyrolysis and hydrothermal liquefaction techniques are widely used for bio-oil production. From these methods, the bio-oil produced can be utilized as feedstock to produce fuels and valuable chemicals including levoglucosan (precursor for pharmaceuticals, surfactants, pesticides etc.) and formic acid (precursor for preservative, antibacterial agent) (Isahak et al., 2012; Lam & Lee, 2012; Mohan et al., 2006).

There is also interest in bio-oil production via pyrolysis of wood, and digested sludge (Fabbri & Torri, 2016; Fonts et al., 2012; Kim et al., 2011; Mohamed et al., 2016).

Eastern red cedar is considered an invasive plant in Oklahoma due to its adaptability to diverse conditions of soil, climate and topography leading to environmental problems such as degradation of grasslands, water absorption from soil, and displacement of native wildlife and plant species (Dunford et al., 2007; Ramachandriya et al., 2013). Thus, utilization of eastern red cedar in production of bio-oil could be beneficial in mitigation of some of the environmental problems.

Sewage sludge is another potential pyrolytic feedstock. Sludge generated during municipal waste treatment comprise of a heterogeneous mixture of organic and inorganic materials. The conventional disposal methods such as landfill, land disposal, and incineration have limitations mainly due to the presence of toxic heavy metals (Cr, Cu, Ni, Zn, Fe etc.) present in the sludge (Fonts et al., 2012). The release of these heavy metals may have a detrimental effect on the environment. As a remedy to this problem, pyrolysis of sludge is helpful as it produces an oil that emits less pollutants (various nitrates and sulfates) than the fuels produced from other biomass. For example, no toxic organic compounds like dioxins are formed during sludge pyrolysis. Anaerobically digested sludge is produced in high quantities at urban wastewater treatment plants. Hence, digested sludge is another suitable feedstock for biomass pyrolysis (Agrafioti et al., 2013; Kim & Parker, 2008).

1.2. OBJECTIVES

The main objective of this study is optimization of a pyrolysis oil production process which uses underutilized biomass resources available in Oklahoma. The goal is development of a process that converts biomass mixtures rather than a single type of biomass to bio-oil that can be further processed into biofuels and/or high value industrial chemicals. Our hypothesis is that utilization of more than one type of biomass in the process will improve the sustainability of long-term

feedstock supply and allow flexibility in the formulation of the chemical composition of the bio-oil produced during the process.

Three types of biomass will be examined in this study: cedar wood, digested sludge, and algal biomass.

The specific objectives of the study are;

1) Determine three-biomass blend compositions with favourable thermodynamic properties (low activation energy, enthalpy change, and high Gibb's Free energy change) for a co-pyrolysis process using Differential Scanning Calorimetry (DSC) technique.

2) Use the biomass blends selected in objective 1 for large scale pyrolysis and determine the chemical composition of the bio-oil produced.

3) Evaluate the co-pyrolysis process mass and energy balances using the RYield model in ASPEN PLUS simulation software.

.

CHAPTER II

LITERATURE REVIEW

The term "Pyrolysis" refers to thermal degradation of biomass at a high temperature (usually above 350 ^{o}C) in the absence of oxygen. Biomass degradation occurs in four stages. The first step involves evaporation of moisture and light volatile materials. Following this, degradation of proteins, carbohydrates, and lipids take place (Bordoloi et al., 2016).

Although, bio-oil is the main product of pyrolysis, bio-char and non-condensable gases including CO, CO_2, and CH_4 are also produced during this process (Marcilla et al., 2013). The yields of the pyrolysis products vary with process conditions. There are two types of pyrolysis: fast pyrolysis (high heating rate and short residence time) and slow pyrolysis (low heating rate and long residence time). Fast pyrolysis is known to produce a higher yield of bio-oil than slow pyrolysis (Mohan et al., 2006). Co-pyrolysis, which refers to the pyrolysis of feedstock comprising two or more biomass types, has gained importance with time (Chen et al., 2017a).

2.1 Pyrolysis of Pure Biomass

Biomass degradation is affected by temperature as stated below (Mehrabadi et al., 2017).

1) **Stage 1:** below 200 ^{o}C – Loss of water and volatiles from the biomass;
2) **Stage 2:** 200 to 500 ^{o}C – Decomposition of major organic materials like proteins, carbohydrates, and lipids from biomass and,

3) **Stage 3:** Above 500 ºC – Decomposition of residual carbonaceous material from the biomass leading to char formation.

For a given heating rate and residence time, the thermal degradation profile of various biomass cellular components is temperature dependent (Mehrabadi et al., 2017). Thus, yield and chemical composition of the bio-oil vary with the heating rate and the final temperature which determine the reaction kinetics during pyrolysis.

2.1.1 Biomass Degradation Kinetics

Important thermodynamic parameters such as Activation Energy (E_a), Pre-exponential or Frequency Factor (A), Change in Enthalpy (ΔH) and Change in Gibb's Free Energy (ΔG) can be determined by studying biomass pyrolysis kinetics. Estimation of pyrolysis kinetic parameters like E_a, A, ΔH, and ΔG helps us to understand the thermal characteristics of the biomass. It is known that pyrolysis is an important step in many other thermochemical conversion processes such as combustion and gasification. Hence, it is essential to understand the pyrolysis kinetics in order to evaluate the economic and technical feasibility, design, and scale up biomass conversion processes for applications such as producing gaseous and liquid fuels, and various chemical products at industrial scale.

Knowledge of E_a for biomass pyrolysis helps in understanding the energy requirement for biomass decomposition during the process. E_a represents an energy barrier that needs to be overcome before pyrolysis reaction starts. A low value of E_a is indicative of faster reaction rate during pyrolysis as the energy required for breakage of the chemical bonds between the atoms is low (Anca-Couce et al., 2014; Ounas et al., 2011; White et al., 2011; Xu & Chen, 2013; Zhou & Dunford, 2017).

The pre-exponential factor (A) conveys information about the reaction mechanism during biomass pyrolysis. A low A value ($<10^9$ s^{-1}) signifies pyrolysis reactions occurring at the biomass

surface. However, a higher value of A (> 10^9 s^{-1}) suggests that a chemical complex is formed before the final products are generated (Ahmad et al., 2017b; Turmanova et al., 2008).

The change in enthalpy (ΔH) for biomass pyrolysis represents the energy required for raising the temperature of the biomass from room temperature to the pyrolysis temperature and ultimately forming the activated complex from which the biomass pyrolysis products are generated. Thereby, enthalpy specifies the energy required for biomass degradation (Ahmad et al., 2017a; Daugaard & Brown, 2003).

The change in Gibb's Free Energy (ΔG) indicates the increase in total energy of the system (biomass), as it approaches to the temperature at which an activated complex is formed during pyrolysis. Thus, the energy that is available from the biomass upon pyrolysis can be determined. A high ΔG value indicates a spontaneous and efficient biomass pyrolysis (Ahmad et al., 2017b; Maia & de Morais, 2016; Xu & Chen, 2013).

The optimal operating conditions for biomass pyrolysis and suitability of biomass as a potential bioenergy feedstock can be evaluated based on the thermal properties and reaction kinetic parameters (Fernandez et al., 2016). Two mathematical approaches exist for obtaining information on the kinetics of biomass pyrolysis, especially E_a and frequency or pre-exponential factor A; (a) Model fitting (model-based), and (b) Model free (Iso-conversion) methods.

In the model-based method, a reaction order is assumed. Here, the reaction rate is directly related to the amount of unreacted substance raised to an exponent i.e. the reaction order:

$$\frac{d\alpha}{dT} = k(T)\,(1 - \alpha)^n = A\,exp^{\frac{-E_a}{RT}}\,(1 - \alpha)^n \qquad (1)$$

Where, α = mass fraction of the decomposed biomass,

T = Temperature,

k(T) = Reaction rate constant at temperature T,

1 – α = mass fraction of the residual biomass after decomposition,

n = order of the reaction,

A = frequency or pre-exponential factor

E_a = Activation energy

R = Universal gas constant

The data obtained from pyrolysis experiment is fitted into this model assuming a value of n. A major drawback of using this model is inaccurate estimation of E_a and A, based on incorrect reaction order and thus, improper reaction model chosen. This problem of model-based method can be overcome using an iso-conversion model. In the latter case, no assumption for n is necessary in estimation of E_a and A. Instead, different heating rates at a specific temperature (specific for a certain fraction conversion of biomass) is used for estimation of E_a and A based on the following formula:

$$\ln \frac{\beta}{T^2} = -\frac{E_a}{R}\left(\frac{1}{T}\right) - \ln \frac{AR}{E_a\, G(\alpha)} \qquad (2)$$

Where, β = the heating rate,

E_a = apparent activation energy,

T = Peak temperature,

A = Frequency or pre- exponential factor,

α = fraction of biomass conversion = $(W_o - W_t)/(W_o - W_\infty)$,

W_o = Initial weight of the biomass before the pyrolysis,

W_t = Weight of the biomass at any instance of time 't' during pyrolysis,

W_∞ = Final weight of the biomass after the pyrolysis is over,

$$G(\alpha) = \int_0^\alpha \frac{d\alpha}{f(\alpha)} \quad (3)$$

This technique for estimating E_a is referred to as KAS (Kissinger-Akahira-Sunose) which is a popular model free method used frequently. Here, from the slope of the plot of "ln (β/T^2)" vs "1/T", $-E_a/R$, is obtained, and then the activation energy, E_a, is calculated.

Floor Wynn Ozawa (FWO) is another iso-conversion method (White et al., 2011) for estimation of E_a. Here, E_a is calculated from the slope of the plot of "log β" vs "1/T".

$$\log\beta = \log\frac{A\,E_\alpha}{R\,G(\alpha)} - 2.315 - 0.4567\,\frac{E_a}{R}\left(\frac{1}{T}\right) \quad (4)$$

Other iso-conversion methods also exist for estimation of E_a besides KAS and FWO. For instance, Coats-Redfern method estimates E_a from the slope of the "ln[-ln(1 – α)/T^2]" vs "1/T" plot.

$$\ln\left[\frac{-\ln(1-\alpha)}{T^2}\right] = -\frac{E_a}{R}\left(\frac{1}{T}\right) - \ln\frac{A\,R}{\beta\,E_a} \quad (5)$$

E_a calculation using the Distributed Activation Energy Model (DAEM) assumes that a large number of independent reactions each having their own E_a proceed during biomass degradation. It is further assumed that A is same for all the reactions. So, E_a is represented by a continuous distribution function f(E_a) (White et al., 2011). Using the equations (4) and (5) the following relationships can be written.

$$\alpha(T) = \int_0^\infty \left\{1 - \exp\left[-\frac{A}{\beta}\int_0^T \exp\left(\frac{-E_a}{RT}\right)\,dT\right]\right\} F(E_a)\,dE_a \quad (6)$$

$$\frac{d\,\alpha(T)}{dT} = \int_0^{\infty} \frac{A}{\beta} \exp\left[-\frac{E_a}{RT} - \frac{A}{\beta}\int_0^{T} \exp\left(-\frac{E_a}{RT}\right) dT\right] F(E_a)\, dE_a \qquad (7)$$

A software like MATLAB can be used to solve equations (6) and (7) numerically (White et al., 2011).

The following relationship can be used for calculating pre-exponential factor A after calculating E_a (Ahmad et al., 2017b):

$$A = \frac{\beta\, E_a\, exp^{\frac{E_a}{RT}}}{R\, T^2} \qquad (8)$$

After calculating E_a and A, estimation of ΔG and ΔH is done using the following mathematical equation (Ahmad et al., 2017b):

$$\Delta H = E_a - RT \qquad (9)$$

$$\Delta G = E_a + \left(RT \ln \frac{K_B\, T}{hA}\right) \qquad (10)$$

A study on the pyrolysis kinetics and thermal characterization of *Nannochloropsis oculata* and *Tetraselmis* sp. (Ceylan & Kazan, 2015) used a Thermogravimetric Analysis (TGA) method involving three different heating rates of 5, 10, and 20 ^{o}C / min. The biomass conversion fractions were varied from 0.1 to 0.8 and the apparent E_a was calculated from the slope of the plot of "ln (a/T^2)" vs "1/T" ["T" = Pyrolysis temperature and "a" = heating rate for pyrolysis] plot for each biomass conversion fraction, which was found to be different for *Nannochloropsis oculata* and *Tetraselmis* sp. Since, the thermal decomposition of biomass during pyrolysis is comprised of multiple steps, a single reaction mechanism for the overall process was not valid for either strain (Ali et al., 2015; López-González et al., 2014). The average values of apparent E_a (KAS method) were calculated as 136.26 kJ/mol and 171.93 kJ/mol for *Nannochloropsis oculata* and *Tetraselmis* sp., respectively.

Besides TGA, Differential Scanning Calorimetry (DSC), another thermoanalytical technique, can also be utilized for estimation of E_a for endothermic processes like pyrolysis (Foltin et al., 2017). In this case, the change in heat flow per unit mass with time and temperature is measured with respect to an inert reference (usually empty crucible of the same material as that of the crucible with sample). Heat consumption of the sample during its thermal decomposition is monitored (Zhao et al., 2017b).

Pyrolysis kinetics of shale oil (100 to 900 ^oC) at eight different heating rates (2, 5, 10, 15, 20, 25, 40, and 50 ^oC/min) were evaluated using DSC, and E_a and A values, were estimated (Foltin et al., 2017). For each heating rate, the endothermic peak temperatures were obtained from the DSC thermograms and utilized to estimate E_a (268.5 kJ/mol) and A (7.9×10^{16} min^{-1}) values according to the FWO model. In another study (Kok & Gundogar, 2013), pyrolysis kinetics for four different crude oil samples were evaluated from room temperature to 600 ^oC at the heating rates of 5, 10, and 15 ^oC/min using a DSC method. The E_a values calculated using the FWO model were found to be different for each sample: Crude oil-1 – 104 kJ/mol, Crude oil-2 – 149 kJ/mol, Crude oil-3 – 91 kJ/mol, and Crude oil-4 – 108 kJ/mol. Here, the E_a value was highest for Crude oil-4 as compared to the remaining three. A probable reason for this was due to the highest content (4.58 wt %) of asphaltene (complex ring structure comprising of C, H, N, O, and S) in Crude oil-4. It is known that asphaltene decomposes thermally at 520 ^oC, thereby leading to higher energy requirement (Ciajolo & Barbella, 1984).

2.1.1.1 Algal Biomass Degradation Kinetics

A stepwise pyrolysis experiment via TGA was performed on a mixed consortium (*Coleastrum sp., Actinustrum sp., Diatom sp. and Mucidosphaerium pulchellum*) of microalgae biomass (cultivated in an open raceway pond in wastewater) for understanding the mechanism of weight loss at different temperatures (Mehrabadi et al., 2017). The sample was heated from room

temperature to 200 ^{o}C at a rate of 20 ^{o}C/min while argon gas was flowing at 75 mL min^{-1}, then, from 200 to 500 ^{o}C, at an interval of 100 ^{o}C, (with a holding time of 30 minutes at each step). It was found that weight loss (23 ± 2 % of the initial dry weight of the mixed algal consortium) was the highest between 200 and 300 ^{o}C. Beyond 300 ^{o}C, weight loss from the biomass declined. This happened because water from the biomass had evaporated below 200 ^{o}C. Furthermore, the mixed consortium algal biomass had a very high protein content (42 wt %). Therefore, at 300 ^{o}C, most of the proteins had decomposed, as the energy needed for its degradation was low. Consequently, the weight loss from the biomass was highest at 300 ^{o}C. Other organic materials like lipids and/or carbohydrates could have started to decompose above 300 ^{o}C till 500 ^{o}C, leading to complete biomass degradation (Agrawal & Chakraborty, 2013). Thus, bio-oil yield was highest at 400 – 500 ^{o}C (4.7 wt % of the initial biomass) as compared to that from 300 – 400 ^{o}C or below 300 ^{o}C (< 1.5 wt % of the initial biomass). Therefore, major decomposition of cellular organic materials started at 200 ^{o}C and continued until 500 ^{o}C. Hence, with increasing temperature, the bio-oil yield has also increased.

Qualitative GC-MS analysis of the liquid fraction showed that both the bio-oil and the aqueous phase of the liquid fraction contained nitrogenous and oxygenated compounds (Mehrabadi et al., 2017). The nitrogenous compounds comprised of pyrroles, indoles, and amides. These were probably formed due to Maillard reaction taking place between the proteins and carbohydrates present in the biomass (carbonyl groups of sugar molecules reacting with amino groups of protein). The oxygenated compounds are comprised of acids and alcohols formed due to decomposition of carbohydrates and lipids. The compounds in both fractions were identified in three classes based on their chemical structures: aromatics, hydrocarbons, and acids. Among these, aromatics and hydrocarbons dominated the bio-oil phase of the liquid fraction. As the pyrolysis temperature increased, the aromatic concentration in the bio-oil increased. So, pyrolysis at higher temperature has an advantage of producing aromatics which are industrially important

chemicals. Nevertheless, the amount of the hydrocarbons in the bio-oil gradually declined with increasing temperature. Presence of greater quantity of aromatic compounds in bio-oil relative to other compounds leads to its higher energy content (Campanella et al., 2012; Harman-Ware et al., 2013). For example, the energy content of an oil obtained from stepwise pyrolysis at 400-500 ^{o}C was 37 ± 0.8 kJ/g with an aromatic hydrocarbon content of 33.8 area %. This yield of aromatic hydrocarbon is relatively higher than the bio-oil obtained from pyrolysis at 300-400 ^{o}C (21 area %), which had a lower energy content of 35.3 ± 0.5 kJ/g (Mehrabadi et al., 2017). Additionally, higher content of carbon (73.9 ± 1.5 wt % of initial biomass) and hydrogen (9.5 ± 0.5 wt % of initial biomass), and lower content of oxygen (8.9 wt % of initial biomass) in the bio-oil obtained from the microalgal biomass could also have influenced the energy content (Miao et al., 2004). The energy content of the oil obtained from mixed culture microalgal biomass was relatively higher than the monoculture algae based bio-oil and comparable to that of fossil fuel (Babich et al., 2011; Du et al., 2011; Harman-Ware et al., 2013).

2.1.1.2 Lignocellulosic Biomass Degradation Kinetics

E_a, ΔH, and ΔG for pyrolysis of *Urochloa mutica* (para grass) were measured to assess its bioenergy potential (Ahmad et al., 2017a). TGA-DSC analyses were performed at three different heating rates (10, 30 and 50 ^{o}C. min^{-1}) starting from room temperature up to 1000 ^{o}C. E_a was calculated for different biomass conversion fractions (α) using the KAS method and the average E_a for pyrolysis was found to be 178.72 kJ/mol. The E_a for the para grass was lower than those for cellulose (191 kJ/mol), rice husk (229.1 kJ/mol), and elephant grass (218.2 kJ/mol). This suggests that para grass can be blended with other biomass having higher E_a values for co-firing and potentially lowering the energy barrier of the mixed feedstock to be used for pyrolysis (Braga et al., 2014; Sánchez-Jiménez et al., 2013). The average ΔH for para grass was 173.66 kJ/mol. This value is relatively lower than that of the perennial grass *Typha latifolia* (179.42 kJ/mol) (Ahmad et al., 2017b). In the same study (Ahmad et al., 2017a), it was also established that for each para

grass conversion fraction, the difference between the E_a and ΔH values were relatively small (~ 5 – 6 kJ/mol). This signifies that activated complex formation was favored at each stage of para grass pyrolysis. The average ΔG for para grass (170 kJ/mol) (Ahmad et al., 2017a), was higher than that of rice straw (164.59 kJ/mol), rice bran (167.17 kJ/mol), and red pepper waste (139.4 kJ/mol) (Maia & de Morais, 2016; Xu & Chen, 2013). This suggests that para grass biomass can be a potential bioenergy source for biofuel production.

The activation energy of eight different lignocellulosic biomass (corn stover, cotton stalk, wheat straw (obtained from a farm in Jiangxi province, China), palm oil husk, pine wood, red oak, sugarcane bagasse, and switchgrass obtained from a local farm in Amherst, Massachusetts, USA) were examined via TGA (biomass heated from room temperature to 800 ^{o}C in an inert atmosphere of helium at a flowrate of 100 mL min^{-1} and 5 ^{o}C min^{-1} heating rate) (Cai et al., 2013). The DAEM analysis was used to evaluate the TGA data. E_a for corn stover, cotton stalk, wheat straw, palm oil husk, pine wood, red oak, sugarcane bagasse, and switchgrass were established as 179.60 – 239.34, 178.19 – 239.46, 175.51 – 240.61, 169.71 – 236.11, 186.70 – 271.76, 183.11 – 242.15, 184.75 – 234.76, and 186.78 – 260.95 kJ/mol, respectively. The activation energy distribution was based on decomposition of three components: 1) hemicellulose, 2) cellulose, and 3) lignin. In the DAEM technique used, it was assumed that there was no interaction between the three components, so degradation of the three components occurred in a parallel and independent manner. The difference in E_a calculated for each of the three components in the biomass was the highest for lignin, 26.5 – 41.8 kJ/mol. From this, it was inferred that the thermal decomposition of lignin component of the lignocellulosic biomass occurs over a wide range of temperature (approximately 200 to 1000 ^{o}C) (Cho et al., 2012). So, higher lignin content for a lignocellulosic biomass could lead to higher energy requirements for its thermal decomposition (Li et al., 2014; Yang et al., 2017).

Among the various lignocellulosic biomass used for pyrolysis, eastern red cedar wood is one having limited report in the literature. Maximum bio-oil yield of 35.9 wt % was obtained from slow pyrolysis (heating rate of 6 ^{o}C/min and holding time of 30 min) of sapwood (SW) (soft outer part of the cedar wood tree that lies between heartwood and bark) at 450 ^{o}C (Yang et al., 2016). However, the highest yield of 34.3 wt % was achieved at 500 ^{o}C from slow pyrolysis of heartwood (HW) (dense inner part of the cedar wood tree). Acetic acid (at 450 ^{o}C, 18.18 % of the total Py-GC/MS peak area in SW and 11.25 % in HW; at 500 ^{o}C, 18.1 % in SW and 9.75% in HW) and furfural (at 450 ^{o}C, 22.69% in SW and 26.20% in HW; at 500 ^{o}C, 20.10% in SW and 21.80% in HW) were the major components in the bio-oil. The reason behind such high yield of acetic acid and furfural was due to thermal decomposition of hemicellulose components xylan, arabinan, galactan and mannan in both SW and HW. It is well established that hemicellulose has the least thermal stability as compared to cellulose and lignin (Mohan et al., 2006). Furfural and acetic acid are precursors for production of many chemical compounds (Isahak et al., 2012). Hence, pyrolysis oil from cedar wood can be used in the chemical industry. The bio-oil from fast pyrolysis (heating rate = 1000 ^{o}C/s and holding time = 20 s) of both HW and SW from cedar wood resulted in higher guaiacol content (at 450 ^{o}C, 38.06 % in SW and 34.73% in HW; at 500 ^{o}C, 35.91% in SW and 44.36% in HW) than other chemical components in the bio-oil. Additionally, the phenol content of bio-oil (obtained from depolymerization of lignin) was relatively higher at 500 ^{o}C (8.56 % from HW and 4.95 % from SW) than that at 450^{o}C (4.30 % from HW and 1.66 % from SW). Enhanced yield of guaiacols and phenol in bio-oil from fast pyrolysis (at 500 ^{o}C) of HW was due to the fact that lignin is thermally more stable than cellulose and hemicellulose, hence, higher energy is needed for the breakdown of lignin (Li et al., 2014; Mohan et al., 2006). Phenols are precursors for phenolic resins that are used in synthesis of wood adhesive, antiseptic, dyes, and pharmaceuticals. Bio-oil with a greater phenol content could be useful in wood industries where it could be an inexpensive feedstock (Effendi et al., 2008; Kim et al., 2010). This is because the common method of phenol production via partial oxidation of

benzene or cumene is expensive (Pilato, 2010). Also, bio-oil with higher concentration of guaiacol relative to other components can be a useful feedstock in pharmaceuticals owing to its antioxidant, anti – inflammatory and antibacterial activity (Scozzafava et al., 2015) and as a substrate for peroxidase assay in chemical industries (Mäkinen & Tenovuo, 1982).

The energy requirement for cedar wood pyrolysis has not been reported, hence, a study on the pyrolysis kinetics of cedar wood would fill the current knowledge gap.

Pyrolysis of *Chlorella vulgaris*, pine needle, peanut shell, and corncob (Yuan et al., 2015) was performed in a fixed bed reactor at temperatures from 300 to 900 ^{o}C at an interval of 100 ^{o}C. The highest bio-oil yields of 20.76, 17.75 and 32.69 wt % (% of initial biomass) from pine needle, peanut shell and *Chlorella vulgaris*, respectively, were obtained at 500 ^{o}C. The lowest bio-oil yield was from corncob (11.38 wt %) at 500 ^{o}C, which was similar to the yield at 400 ^{o}C (11.43 wt %). *Chlorella vulgaris* produced the highest bio-oil yield, probably due to lack of lignin in it. (Li et al., 2014; Yang et al., 2007). Lignin is difficult to pyrolyze leading to lower yield of bio-oil from lignocellulosic biomass. Aromatic hydrocarbon content in bio-oil from lignocellulosic biomass was higher than that from *Chlorella vulgaris*. This was due to thermal decomposition of lignin during pyrolysis contributing to aromatic hydrocarbons like benzene and their derivatives. Benzene and phenols found in bio-oil obtained from *Chlorella vulgaris* was due to the degradation of oxygen containing compounds like acids, aldehydes, and ketones (Li et al., 2014). E_a of the latter four biomass was examined via a TGA method by heating the biomass from room temperature to 800 ^{o}C at the heating rates of 5, 10, and 20 ^{o}C/min. The average E_a for *Chlorella vulgaris* biomass (FWO method: 220.79 kJ/mol; KAS Method: 211.09 kJ/mol) was found to be lower than that for the lignocellulosic biomass (FWO method: pine needle – 291.49 kJ/mol, peanut shell – 253.9 kJ/mol and corncob – 258.98 kJ/mol; KAS Method: pine needle – 281.50 kJ/mol, peanut shell – 244.29 kJ/mol and corncob – 249.25 kJ/mol). This can be due to the higher

volatile matter and less thermally resistant biomass components in *Chlorella vulgaris* as compared to those in lignocellulosic biomass (Li et al., 2014; Sanchez-Silva et al., 2012).

2.1.1.3 Sewage Sludge Degradation Kinetics

Pyrolysis kinetics of two types of sewage sludge-L (anaerobically digested) and F (treated with $Ca(OH)_2$ and $FeCl_3$) were examined using a TGA method by heating the sample from room temperature to 800 °C at a 10 °C/min rate (Folgueras et al., 2013). The estimation of E_a was done using equation 11 (the slope of the "ln (α/T) – ln f(α)" vs "1/T" plot:

$$\ln\left[\frac{\alpha}{T}\right] - \ln f(\alpha) = -\frac{E_a}{R}\left(\frac{1}{T}\right) + \ln\left(\frac{A}{\beta}\right) \qquad (11)$$

When L type sludge was heated from 180 to 390 °C and from 390 to 510 °C, E_a was found to be 49.4 kJ/mol and 197.7 kJ/mol, respectively. When F type sludge was heated from 200 to 385 °C and from 385 to 510 °C, E_a was 50 kJ/mol and 169.6 kJ/mol, respectively. So, the average E_a for each sludge was calculated as 123.55 (Type L) and 109.8 kJ/mol (Type F).

In another report (Gao et al., 2014) on the pyrolysis of dried sewage sludge (collected from a drying plant in Dalian, China) using a TGA method by heating the sample from 30 to 800 °C at 10 °C/min, E_a determined using the Coat-Redfern model was 82.28 kJ/mol for the temperature range of 186 – 296 °C and 48.34 kJ/mol for 296 – 518 °C. So, the average E_a was 65.31 kJ/mol. The values reported in the latter two studies are relatively lower than those obtained with microalgal and lignocellulosic biomass. The reason for that is that the biomass components in dried sewage sludge are thermally less resistant to degradation as compared to microalgae and other lignocellulosic biomasses, owing to lower content of cellulose and lack of lignin (Li et al., 2014; Sanchez-Silva et al., 2012). It is worth noting that digested sludge has high ash content with catalytic activity due to the presence of metals in the ash (Luo et al., 2004; Sharma et al., 2015; Xie et al., 2014).

In summary, energy barrier for pyrolysis of microalgae and sewage sludge is low owing to lack of lignin (Sanchez-Silva et al., 2012). Furthermore, aromatic hydrocarbon yield in bio-oil can be enhanced by co-pyrolyzing algal biomass and sewage sludge with lignocellulosic biomass like cedar wood (Eom et al., 2012; Li et al., 2014; Sanchez-Silva et al., 2012; Zabeti et al., 2012).

2.1.2 Catalytic Pyrolysis

The effect of catalysts on pyrolysis of pure biomass has been evaluated (Anand et al., 2016). Among various catalysts available, zeolites have gained prominence due to their dual, acid-base characteristics which are helpful in selective enhancement of desirable chemical compounds in the bio-oil obtained from pyrolysis, their lower cost than other catalysts, lower environmental problems and reusability. Zeolite refers to a crystalline complex molecule comprising of different ratios of the oxides of aluminum and silicon. Structurally, it contains tetrahedral form of AlO_4^{5-} and SiO_4^{4-}, bonded together by oxygen atoms in a 3D structure. Their general formula is $M_{x/n}[AlO_2)_x(SiO_2)_y].{}_zH_2O$, where, M represents the extra cation (usually from a metal) which is involved in balancing the anion in the 3D frame. Zeolites have a highly porous structure with well – defined micron-sized pores (0.4 to 1 nm) which make them excellent catalysts for loading exchangeable cations to their 3D structure and facilitating ion exchange between feedstock and the catalyst (Ennaert et al., 2016; Shahinuzzaman et al., 2017).

The effects of zeolite type, mass ratio of zeolite: algae, and temperature on catalytic fast pyrolysis of *Arthrospira platensis* were evaluated using the catalyst ZSM-5, Zeolite-β, and Zeolite-Y (Anand et al., 2016). It was found that the bio-oil composition, specifically the yield of aromatic hydrocarbons determined by Py-GC/MS was affected by the type of zeolite used. For example, at catalyst loading ratio of 10:1 (catalyst: biomass, wt/wt) and temperature of 600 ^oC, the yield of monoaromatics (29.56% of the Py-GC/MS peak area) was higher with ZSM-5 than that with Zeolite-β (24.66 %) and Zeolite-Y (21.47 %). Aromatic compounds are known to be useful

solvents for dissolution of grease or oil-based compounds. Additionally, they have potential applications in wood adhesives, bio-plastics, and fragrance production, and as octane enhancer (prevent pre-ignition knocking in engines) in transportation fuels (De Wild et al., 2009). Hence, ZSM-5 is a preferred catalyst for high aromatics production via pyrolysis (Anand et al., 2016; Rego & Roley, 1999).

Fast microwave-assisted catalytic pyrolysis of sewage sludge (mix of primary and secondary sludge from Metropolitan Wastewater Treatment Plant, Saint Paul, Minnesota) was examined at different temperatures: 450, 500, 550 and 600 ^{o}C, with HZSM-5 as the catalyst (catalyst: biomass (wt/wt) = 2:1) (Xie et al., 2014). As the temperature increased, the bio-oil yield increased to the highest value of 20.9 wt % at 550 ^{o}C due to the devolatilization of organic material in the sludge. At high temperatures, more energy is available for the dissociation of strong organic bonds leading to devolatilization (Encinar et al., 2000). Aromatic hydrocarbon content in the bio-oil increased from about 2 to 32 wt % with increasing temperature from 450 to 550 ^{o}C. This was due to Diels-Alder reaction mechanism occurring during pyrolysis by either addition of 1,3 – butadiene to ethylene, followed by removal of hydrogen atoms leading to aromatization or trimerization of alkenes into rings (Cunliffe & Williams, 1998; Fonts et al., 2009; Park et al., 2008; Richter & Howard, 2000).

Therefore, combining biomass with zeolites can be helpful in enhancement of aromatic hydrocarbons in the bio–oil obtained.

2.2 Co-pyrolysis

Co-pyrolysis refers to the mixture of two or more different types of biomass being subjected to pyrolysis. Co-pyrolysis may improve the quality of the pyrolysis oil, enhance oil yield, and reduce water content of the oil (Abnisa & Daud, 2014).

Co-pyrolysis of bamboo waste and *Nannochloropsis* sp., was examined at 600 ^{o}C at a pure argon gas flow rate of 200 mL min^{-1} (Chen et al., 2017a). Hemicellulose, cellulose and lignin contents in the bamboo waste were 18.8, 46.5 and 25.7 wt %, respectively. The latter components could not be detected in biomass of *Nannochloropsis* sp. Lipid, protein, and carbohydrate contents in algal biomass were 30, 40.8 and 19.2 wt %, respectively. The latter compounds were not detected in the bamboo waste. So, for a 1:1 (w/w) blend of bamboo waste and algal biomass, hemicellulose, cellulose, and lignin contents are expected to be lower i.e. 9.4, 23.25, and 12.85 wt %, respectively. Lower lignin content in feedstock to be used for pyrolysis is desirable (Brebu & Vasile, 2010; Yang et al., 2017). Moreover, algal biomass and bamboo waste had moisture contents of 4.01 and 6.22 wt %, respectively. Hence, for a 1:1 (w/w) blend, the moisture content of the mixture is expected to be lower, 5.12 wt %. The bio-oil yield from the microalgae: bamboo blend (1:3) was relatively higher (66 wt % of initial biomass) than that from bamboo waste (61 wt % of initial biomass) and *Nannochloropsis* sp. (60 wt % of initial biomass) alone. As the algal biomass weight ratio in the blend increased (2:1, 3:1 wt/wt), the bio-oil yield decreased from 65% to 60 wt %. However, the latter values were still greater than that from individual pyrolysis of *Nannochloropsis* sp. and bamboo waste. A probable reason for the latter result could be that co-pyrolysis inhibited secondary decomposition of the pyrolytic volatiles and thus, hampered generation of smaller molecular weight gas products. This helped in formation of larger molecules in char and bio-oil (Hua & Li, 2016). For the biomass mixtures, the long chain fatty acids (50 % in 1:1 microalgae-bamboo and 46 % in 3:1 microalgae-bamboo blend) and aliphatic contents (12% in 1:1 microalgae-bamboo and 13% in 3:1 microalgae-bamboo blend) were relatively higher than all the other compounds present in the bio-oil. Furthermore, the weight fraction of the long chain fatty acids was significantly greater in the bio-oil from the co-pyrolysis of the biomass blends having microalgae weight fraction up to 50 wt % than that obtained from pyrolysis of pure biomass of either *Nannochloropsis* sp or bamboo waste. This can be attributed

to the decomposition of lipids in the blend (Chen et al., 2017b). Bio-oil with a higher content of long-chain fatty acids can be used as a precursor for production of transportation fuels, as they can be transformed to hydrocarbons via a suitable catalyst (Zhang et al., 2016).

The highest bio-oil yield (about 58%) was obtained by mixing peanut shells and cassava starch at a weight ratio of 1:3 (Messina et al., 2015). Pure peanut shell and pure cassava starch produced lower bio-oil yields (about 54 % from pure cassava starch and 32 % from pure peanut shell) as compared to that from the 1:3 wt/wt blend of peanut shell: cassava starch. As the content of the peanut shell increased in the biomass mixture, the bio-oil yield decreased, i.e. for blends of peanut shells-cassava starch, the bio-oil yield decreased from 58% (1:3 of peanut shells-cassava starch) to approximately 50% (1:1 of peanut shells-cassava starch) and 45% (3:1 of peanut shells-cassava starch). These results can be explained with the higher lignin content in peanut shell which leads to lower bio-oil yield as it is thermally more resistant to decomposition as compared to starch. Additionally, increasing starch content in the feedstock could have reduced the thermal stability of cellulose during pyrolysis, as starch is thermally less stable than cellulose and lignin (Li et al., 2014; Wang et al., 2011).

DTG curves obtained from the TGA study of the mixtures (1:1 wt/wt) of cellulose and cassava starch, and lignin and cassava starch, indicated that the peak temperature for thermal degradation of the starch-cellulose and starch-lignin mix was lower than 350 ^{o}C and approximately 300 ^{o}C, respectively. When compared with the DTG curves for the pyrolysis of pure cellulose and lignin, the peak temperature for maximum decomposition was found to be approximately 350 ^{O}C and 370 ^{o}C, respectively. There was no peak at the pure cellulose degradation temperature in the DTG curve for the starch, hemicellulose, cellulose and lignin which can be explained by the reduced thermal stability of cellulose in the presence of starch. It is also possible that the thermal stability of lignin was decreased as well (Cornelissen et al., 2008; Lin et al., 2013; Wang et al., 2011).

Hence, chemical composition of the feedstock has a significant effect on its thermal degradation profile during pyrolysis.

Fast co-pyrolysis of a 50 wt % mixture of sewage sludge (anaerobically digested and thermally dried from an urban wastewater treatment plant in Barcelona, Spain) and pinewood sawdust was examined (Alvarez et al., 2015). The process was carried out in a conical spouted reactor at 500 ^{o}C. The highest bio-oil yield from the blend was 55%. When the experimental value of bio-oil yield was compared with the theoretical value, the experimental value was found to be lower, 12 wt %. This difference could be due to the ash content of the sewage sludge containing metal, which may have catalytic activity promoting secondary reactions like cracking and dehydration and thus, further degradation of the pyrolysis products, especially long chain cyclic and non-cyclic hydrocarbons (Eom et al., 2012; Stefanidis et al., 2011; Zabeti et al., 2012), increasing the gas yield and reducing the bio-oil yield.

Sawdust and sludge obtained from an urban wastewater treatment plant in Barcelona, Spain (anaerobically digested and thermally dried) were co-pyrolyzed using a TGA method by heating the sample from 30 ^{o}C to 900 ^{o}C, at a heating rate of 15 ^{o}C/min in an inert environment of nitrogen flowing at the rate of 100 mL min^{-1} (Alvarez et al., 2015). The DTG curve obtained from the TGA runs indicated that sawdust had decomposed mainly between 200 and 575 ^{o}C. There was a shoulder in the DTG curve between 300 and 375 ^{o}C which corresponded to hemicellulose degradation. The highest peak was attained at approximately 375 ^{o}C at which weight loss for sawdust was the highest owing to cellulose decomposition. Finally, a long tail was observed in the high temperature region after 375 ^{o}C, which was attributed to lignin decomposition in the sawdust (Amutio et al., 2011; Yang et al., 2007). On the DTG curve obtained during sewage sludge pyrolysis, there was a shoulder between 100 and 200 ^{o}C, corresponding to the release of moisture and light molecular weight volatile compounds. There were also peaks at 255 and 300 ^{o}C which corresponded to the degradation of lipid and carbohydrates, respectively. The shoulder

on the DTG curve between 360 and 525 ^{o}C corresponded to decomposition of proteins (Cao et al., 2013; Francioso et al., 2010). Sludge contained small amount of wastewater constituents like plant fragments containing lignin which was confirmed via FT-IR analysis of the sludge (Parnaudeau & Dignac, 2007). Hence, lignin decomposition may have occurred between 360 and 525^{o}C. First peak on the DTG curve for the blend was between 75 and 150 ^{o}C which corresponded to the loss of moisture and light volatile matter. There was a shoulder between 200 and 275 ^{o}C which was linked to degradation of lipids in the blend. Another shoulder between 300 and 370 ^{o}C corresponded to the degradation of hemicellulose and carbohydrates in the blend. The highest peak at 370 ^{o}C was due to the cellulose degradation in sawdust. The final shoulder in the temperature range of 375 and 450 ^{o}C corresponded to the combined degradation of proteins and lipids in the blend (Antal & Varhegyi, 1995; Branca et al., 2005; Yao et al., 2008). Thus, the weight loss pattern for the blend was different than that of the sludge and the sawdust alone. When experimental and theoretical DTG curves for the biomass blend were compared, a clear synergetic effect was found at low pyrolysis temperatures. The synergy was asserted by shifting of the shoulder related to lipid degradation in sewage sludge from 200 to 150 ^{o}C. The experimental and theoretical curves had similar decomposition patterns beyond 300 ^{o}C. Henceforth, no interaction between carbohydrates and protein constituents of the sludge and pinewood sawdust components were detected (Shuang-quan et al., 2009). Phenols (20.12 wt %) were the main class of organic compounds present in the oil obtained from the sawdust and sludge blend (Alvarez et al., 2015). Phenol content in the oil obtained from the blended biomass was between that of the bio-oil obtained from individual pyrolysis of sewage sludge (17.85 wt %) and sawdust (21.88 wt %). Phenols are produced during the depolymerization of lignin, formed along with alkyl phenols and benzenediols. The high ash content of the sludge had catalytic activity that favored the secondary dissociation of methoxyphenols yielding alkyl phenols and benzenediols (Alvarez et al., 2014; Demirbaş, 2000). Similar findings have been reported in other studies (Li et al., 2014) examining co-pyrolysis of rice straw and Shenfu bituminous coal. The

phenol content of the bio-oil from the blended biomass enhanced with increasing rice straw amount in the blend (Rice straw: Coal wt/wt ratio – 1:5-38.99 vol %, 2:5-43.45 vol % and 3:5-44 vol %). The phenol content of the bio-oil obtained from pure rice straw and coal were 18.11% and 33.77 vol %, respectively. Synergistic interaction between the biomass and coal components in the blend lower the vapor residence time (about 30 to 40 s) in the reactor reducing the time for secondary reactions and leading to increased gas production and enhanced decomposition of oxygen containing compounds in the bio-oil (Bridgwater et al., 1999).

Co-pyrolysis of *Isochrisis* sp. and sewage sludge (obtained from a wastewater treatment plant in Beijing, China, where it was treated by a traditional aeration process) (Wang et al., 2016) showed that as the weight fraction of the sewage sludge increased in the blend, aromatic hydrocarbon content in the bio-oil increased. The contents of aromatic hydrocarbon in the oil obtained from the blend weight ratios of 1:2, 1:1 and 2:1 were found to be 9.3, 9.5, and 12.9 wt %, respectively. The latter values were lower than the aromatic hydrocarbon yield from sewage sludge (28.1 wt %), but higher (only for the blend of 2:1 wt/wt) than the microalgae alone (10.9 wt %).

Co-pyrolysis of *Chlorella vulgaris* and coal (semi-anthracite provided by Huangpu power plant in Guangzhou, China) was studied by using a TGA method, where the sample was heated from room temperature to 900 ^{o}C at rates of 5, 10, 15, 20, and 25 ^{o}C/min in a nitrogen environment, at a flowrate of 400 mL min^{-1} (Chen et al., 2012). The average E_a (as per KAS method) for the microalgae and coal (MCR) blends of 3:7, 5:5, and 7:3 were found to be 416.01, 320.77, and 407.57 kJ/mol, respectively. E_a was the lowest (320.77 kJ/mol) for the 5:5 (wt/wt) microalgae-coal mixture as compared to that from *Chlorella vulgaris* alone (335.69 kJ/mol). This could be due to the synergistic effect of volatiles released from the microalgae reacting with the solid phase during thermal decomposition, thereby reducing the energy barrier for pyrolysis (Haykiri-Acma & Yaman, 2010; Lee et al., 2010). Average E_a increased as the microalgae ratio in the blend increased. This could be due to an inhibitive effect which can be explained via the

following mechanism: initially, algal biomass decomposition was faster than that of coal. The algal decomposition products deposited on the coal surface at a time when the coal molecules were about to undergo various polymerization and condensation reactions, blocking the pores on the coal surface which were involved in the removal of the volatile matters generated during pyrolysis. Thus, further thermal degradation of coal was hampered by the blocked pores increasing the energy barrier for pyrolysis (Effendi et al., 2008).

Co-pyrolysis of four lignocellulosic agricultural waste [Cotton Stalk (CS), Hazelnut Shell (HS), Sunflower Residue (SFR) and *Euphorbia rigida* (ER)] with two different plastic waste (Polyvinyl Chloride-PVC and Polyethylene Terephthalate-PET) was performed using a 1:1 (wt/wt) blend (Çepelioğullar & Pütün, 2013). The kinetic study for the co-pyrolysis was carried out using a TGA method which involved heating the samples from room temperature to 800 ^{o}C at a heating rate of 10 ^{o}C/min and a nitrogen flow rate of 100 mL min^{-1}. The weight loss occurred at a slow rate from room temperature to 120 ^{o}C. This was due to the loss of moisture from the biomass-PVC blend. Around 200 to 250 ^{o}C, the cellulose component of the biomass started degrading and there was simultaneous degradation of PVC polymeric structure in the mixture. Beyond this, significant peaks were obtained depending on the biomass used in the blend, i.e. for CS, at 284.1 ^{o}C, for HS at 283 ^{o}C, for SFR at 274.4 ^{o}C, and for ER at 274.3 ^{o}C. Following the latter peaks, there was a tailing region till about 400 ^{o}C on the weight loss curve. This was possibly due to lignin degradation in the blend as lignin has a broad degradation temperature range (200 to 800 ^{o}C) (Liu et al., 2008). Additionally, there was another peak in the temperature range of 400 to 450 ^{o}C, which could be due to the secondary degradation of the products released during the prior breakdown of lignin (Branca et al., 2005; Ma et al., 2002; Yao et al., 2008). For the biomass-PET blend, a similar trend was observed, except that cellulose degradation in the blend started between 200 and 350 ^{o}C. The highest peak corresponding to the maximum weight loss depended on the blend used as follows; for CS-PET at 427.4 ^{o}C, for HS-PET at 427.3 ^{o}C, for SFR-PET at 425.2

°C, and for ER-PET at 420.4 °C. The shift in decomposition temperature pattern happened due to the higher energy required for thermal degradation of the aromatic ring structure of the PET in the blend (Holland & Hay, 2002; Ma et al., 2002). This was confirmed by calculating the activation energy for co-pyrolysis of the biomass-PET blend. The range of activation energy varied depending on the blend used, CS-PET = 68.59 to 171.48 kJ/mol, HS-PET = 73.94 to 139.04 kJ/mol, SFR-PET = 66.63 to 261.32 kJ/mol, and ER-PET = 63.36 to 316.34 kJ/mol. The activation energy for biomass-PVC blend was lower than those for biomass-PET blends, CS-PVC = 51.08-190.13 kJ/mol, HS-PVC = 45.06- 135.99 kJ/mol, SFR-PVC = 45.88- 197.72 kJ/mol, and ER-PVC = 42.1- 228.6 kJ/mol. E_a for the plastic waste (for PVC, 108.12 to 246.78 kJ/mol; for PET, 172.6 – 347.4 kJ/mol) were higher than that of the lignocellulosic biomass (CS, 38.9 to 79.48 kJ/mol; HS, 38.53 to 82.45 kJ/mol; SFR, 30.64 to 74.2 kJ/mol and ER, 36.13 to 88.87 kJ/mol). The structural difference between biomass and complex polymeric structure of the plastics (especially aromatic backbone of PET) lead to variations in pyrolysis reactivity at various temperatures (Holland & Hay, 2002). During PVC pyrolysis, the HCl in the PVC structure is volatilized in the temperature range of 285 to 520 °C. Beyond 340 °C, the PVC waste undergoes further decomposition to form low chain linear or cyclic hydrocarbons (C1 to C7 compounds) (Ma et al., 2002). In the case of PET waste, owing to the aromatic ring structure, the thermal degradation starts at a higher temperature (above 360 °C). Degradation of PET waste comprises of two processes: intramolecular rearrangement between the dimers (terephthalic acid and ethylene glycol) of PET and β – C – H hydrogen transfer from the terephtahlic acid unit of one dimer to the ethylene glycol of the other dimer. PET loses more of its aliphatic components than aromatic components during the thermal degradation (Girija et al., 2005; Holland & Hay, 2002). It is worth noting that for a given biomass-plastic blend, the activation energy was relatively higher for ER-plastic blend as compared to other biomass (CS, HS, ER and SFR) in the blend. This could possibly be due to the higher lignin content in ER (37.92 wt % dry basis) as compared

to other biomass (CS: 22.16 wt % dry basis, HS: 23.46 wt % dry basis and SFR: 20.94 wt % dry basis), thereby leading to a greater energy barrier for thermal degradation.

2.3 Co-Pyrolysis vs Pure Biomass Pyrolysis

The main advantage of co-pyrolysis is that it allows the formulation of a desirable feedstock chemical composition, i.e. moisture, hemicellulose, cellulose and lignin contents (Abnisa & Daud, 2014). Co-pyrolysis may lead to synergistic interactions among biomass components, resulting in higher bio-oil yield and desirable chemical composition (Chen et al., 2017a; Li et al., 2014; Messina et al., 2015). The activation energy of a feedstock to be used for pyrolysis can be adjusted using biomass blends as desired (Chen et al., 2012).

However, if the biomass blend is not formulated correctly, blending could have inhibitive effects leading to reduction in the bio-oil yield and undesirable chemical composition (Wang et al., 2016), and higher activation energy as compared to that from its pure biomass components (Çepelioğullar & Pütün, 2013; Chen et al., 2012). Hence, it is imperative that various biomass blends are carefully evaluated to optimize a pyrolysis process that will produce final products with high yield and desirable quality.

2.4 Response Surface Methodology (RSM)

Response Surface Methodology (RSM) refers to an assemblage of statistical and mathematical techniques for development and optimization of products and processes (Danmaliki et al., 2017). It is very useful when the output of a production process is affected by multiple factors. Additionally, RSM helps in understanding the factors that are significant in the process. The purpose of using the RSM technique is reduction in the number of experimental runs while maximizing the output from the generated data (Bezerra et al., 2008).

In a report (Sarkar & Chowdhury, 2016), RSM has been used for optimization of paper waste (PW) and mustard press cake (MPC) co-pyrolysis in a semi-batch reactor. The process duration was 1 h, and the PW to MPC weight ratio varied from 2.33:1 to 9:1 and the temperature range from 400 to 900 ^{o}C were examined. Based on the results obtained from 17 experiments selected using the Design Expert software (Statistical Software), two process parameters, weight ratio and temperature, were optimized via RSM. The following quadratic response surface model was attained for the maximum yield of bio-oil:

$$Bio - oil\ Yield\ (wt\ \%) = 1.57 * A^2 - 10.21\ B^2 + 0.65 * A - 3.03 * B - 0.97 * A * B + 44.33$$

Where; A = weight ratio of PW-MPC and B = Pyrolysis temperature (K). The R^2 for this model was 0.8233. To ensure the fitness of the model, ANOVA (Analysis of Variance) was performed on the model and the following terms were found to be significant at p = 0.05 level; linear term for B (– 3.03 * B) and Quadratic term for B (– 10.21 * B^2). Therefore, from the ANOVA analysis of the model, it can be inferred that temperature has a significant effect on the bio-oil yield. From this model, maximum bio-oil yield of 46.95 wt % was attained at 874.75 K (601.75 ^{o}C) and PW: MPC weight ratio of 9:1. Individual pyrolysis of PW and MPC resulted in the highest bio-oil yield of 48 wt % at 600 ^{o}C for PW and 46 wt % at 700 ^{o}C for MPC.

2.5 ASPEN PLUS simulation

Validation of the experimental pyrolysis data is of utmost importance due to the complex nature of the feedstock chemical and physical properties and the reactions taking place during the process. Simulation of the pyrolysis process is necessary for the process design and scale-up (Zhai et al., 2016). ASPEN PLUS software is commonly used for process modelling and simulation. The unit operations within the process are represented by operation blocks in the software. For instance, the RYIELD block is best suited for modelling the pyrolysis reactor and

the SEP block is well known to model separation of the gas released into condensable bio-oil and non-condensable gases (Ward et al., 2014). To run the ASPEN simulation the following input data are needed; chemical composition of the biomass described by the proximate, ultimate and sulfur analyses, feed flow rate, temperature, and pressure of the operation.

ASPEN PLUS has been used for modelling pyrolysis of rice straw at different temperature (350 to 600 ^{o}C) and validation of the quantitative yield of various products (bio-oil, bio-char and gases) (Xianjun et al., 2015). In the simulation, because of its complex physical and chemical structure rice straw was defined as a nonconventional feed, rather than a conventional type which refers to a pure compound. So, MIXCINC was used as the stream structure in the simulation for specifying the nonconventional feed as no particle size distribution data was available. The pyrolysis process was expressed so that the biomass passes through a SEP block where biomass is fractionated in to its components: cellulose, hemicellulose, lignin, extractables and ash. Then, these components pass through the RYIELD block for the reactor where pyrolysis takes place yielding final products. The enthalpy and density of these components were calculated using the HCOALGEN enthalpy and DCOALIGT density models embedded in the software, respectively. In order to have the enthalpy modelled via HCOALGEN, proximate, ultimate and sulphur analysis of biomass are required (Darmawan et al., 2017). The program utilizes a number of different correlations for enthalpy estimation. For instance, the Boie, Kirov, and heat of combustion based correlations are used to estimate the heat of combustion, heat capacity and heat of formation, respectively, based on the input biomass elemental composition (Hoffmann et al., 2013). Ultimate and sulphur analyses of the biomass are required for density estimation via DCOALIGT (Asif et al., 2015). The following process conditions were used in the rice straw simulation: Environment temperature = 20 ^{o}C, reactor operating pressure = 0.1 MPa, reactor temperature = 350 to 600 ^{o}C and biomass flow rate = 1000 kg/h. The thermodynamic method used in the simulation was RKS-BM (Withag et al., 2012) and the following assumptions were

made: uniform temperature distribution for particles, no effect of biomass particle size, chemical equilibrium for reaction inside the pyrolysis reactor, same pressure throughout the reactor and ash component of biomass is inert throughout the process. The enthalpy and density of rice straw biomass was found to be -1.51 x 10^9 kcal/hr and 1546.098 kg/m^3 respectively. The simulation demonstrated that increasing temperature resulted in a gradual decrease in the yield of bio-char and bio-oil while the yield of non-condensable gases increased. The latter findings were in agreement with the experimental results.

Co-pyrolysis of coal (Yilan Subbituminous) and corncob in a fluidized bed reactor at 600 ^oC was examined (Atsonios et al., 2017). Through the ASPEN PLUS simulation, co-pyrolysis process mass and energy analyses were performed and the effect of different coal blending ratios (wt % of coal in the blend = 0, 20, 40, 60, 80 and 100) on the process performance was evaluated. RYIELD model was used for the reactor analysis. The product yields used in this simulation study were based on experimental data obtained with coal-corncob co-pyrolysis from another study (Wang et al., 2014b). The results indicated that the weight fraction of coal in the blend had a beneficial effect by producing bio-oil with high hydrocarbon content. For example, when the coal weight ratio in the blend was 20 wt %, the yield of hydrocarbons was the highest (17.9 wt %). Increasing coal fraction in the blend resulted in a reduction of hydrocarbon content in the bio-oil. This was because of the higher coal amount in the mixture reducing the volatile content in the blend. Hence, formation of organic compounds like hydrocarbons and alcohols was not favored. From this simulation, it was clear that blending had a beneficial effect on the pyrolysis products and there is an optimum blend composition that favors hydrocarbon production.

Hence, ASPEN PLUS simulation for co-pyrolysis of microalgae, cedar wood and digested sludge for maximum production of aromatic hydrocarbons does have its significance.

CHAPTER III

MATERIALS AND METHODS

3.1 MATERIALS

3.1.1 BIOMASS

3.1.1.1 Microalgae: A mixed consortium of the following 15 strains of microalgae purchased from the Culture Collection of Algae at University of Texas (UTEX), Austin, are used in this work:

- *Navicula sp.* SP 11,
- *Tetraselmis striata* SP 22,
- *Aphanothece sp.* SP 25,
- *Geitlerinema amphibium* SP 27,
- *Geitlerinema carotinosum* SP 28,
- *Komvophoron sp.* SP 33,
- *Phormidium keutzingianum* SP 38,
- *Pseudanabena sp.* SP 46,
- *Pseudanabena sp.* SP 47,
- *Pseudanabena sp.* SP 48,
- *Dunaliella sp.* SP19,
- *Dunaliella sp.* SP 20,

- *Aphanocapsa sp.* SP 23,
- *Tychonema bornetii* SP 50 and
- *Picochlorum oklahomensis.*

The strains were maintained in regular medium and cultivated in animal wastewater (autoclaved prior to inoculation). They were grown in 2 L (working volume = 1.4 L), 5 L (working volume = 3.5 L), and 10 L (working volume = 7 L) glass bioreactors inside a wooden chamber of dimensions: 9 m x 9 m x 18 m. There were 12 white fluorescent bulbs (Osram Sylvania Inc., Wilmington, MA; 60 W; 800 lumens; Color Rendering Index ≥ 80; Color temperature = 2427 ^{o}C) which were attached to the ceiling of the growth chamber as light source. The average light intensity of these bulbs were calculated to be 96 µmol m^{-2} s^{-1} at four different locations on the bioreactor surface with the help of a quantum meter (model QMSW–SS, Apogee Instruments, Inc., Logan, Utah). The gas provided for growth was air supplemented with 2 % (v/v) CO_2 (Industry Grade, Stillwater Steel Supply, Stillwater, Oklahoma, USA) and bubbled through each reactor at the flow rate of 20 mL min^{-1} maintained with the help of flowmeters (Cole – Parmer, Vernon Hills, Illinois, USA). The cultures were inoculated at the inoculation rate of 7 % v/v. After the culture in each reactor reached stationary phase, the microalgal biomass was harvested by centrifugation, dried, pulverized using a mortar and pestle, and then ground using a coffee grinder (Mr. Coffee W183ME, Boca Raton, Florida, USA) before use.

3.1.1.2 Cedar wood: The sample was a mixture of the heartwood and sapwood parts of eastern red cedar trees harvested in Oklahoma. The cedar wood samples were ground using a Perten grinder (Model No: 3600, Huddinge, Sweden), followed by hammer mill (Fitz Mill DAS06, Elmhurst, Illinois, USA) and finally a coffee grinder (Mr. Coffee W183ME, Boca Raton, Florida, USA).

3.1.1.3 Digested Sludge: The sample was collected from Stillwater, OK, wastewater treatment plant, dried, and pulverized using a mortar and pestle. Finally, it was further ground using a coffee grinder (Mr. Coffee W183ME, Boca Raton, Florida, USA) before use.

3.1.2 Catalyst: Zeolite ZSM–5 (Si/Al = 38) was purchased from ACS Material (Pasadena, California, USA).

3.2 METHODS

3.2.1 Elemental Analyses of Biomass

3.2.1.1 Proximate Analysis

The ash (A), moisture (M) and volatile matter (VM) contents (wt %) of the biomass samples were analyzed according to the AOAC 1995 (Intl, 1995), ASTM E-871 (E871-72, 1998) and ASTM E-872 (E872-82, 2013) methods, respectively. The fixed carbon content (FC) of the biomass was determined based on the weight difference (Speight et al., 2015) as:

$$FC\ (wt\ \%) = 100 - (A + M + VM) \qquad (12)$$

All the tests were performed in duplicates.

3.2.1.2 Ultimate Analyses

The elemental composition (C, H, N, S, and O) of the three biomasses were analyzed using an elemental analyzer (model 2400 Series 2, PerkinElmer, Inc.) at the department of Biological and Agricultural Engineering, Kansas State University. Here, the tests were performed in duplicates (Zhou & Dunford, 2017). In summary, about 3 mg of each biomass was finely ground and then pressed into a pellet in a tin capsule. Then, the biomass pellets were treated in the combustion chamber where the temperature was set at 975 ^{o}C. Gases generated during combustion were separated in a quartz column containing copper wires and detected with the help of a

thermoconductometer detector. The helium, oxygen and nitrogen gas pressures were set at 20, 18 and 60 psi, respectively.

3.2.1.3 Sulphur Analysis

The sulphate content of biomass was determined using a Spectro Arcos ICP – OES (Inductively Coupled Plasma – Optic Emission Spectroscopy) analyzer (Miller et al., 2013). In summary, about 100 mg of dry sample was placed in an extraction vessel and 25 mL of 2 % acetic acid was added. Then, the vessel was placed in a reciprocating mechanical shaker for about 30 minutes. Finally, the extract was filtered and the filtrate was analyzed using the ICP – OES. All tests were performed in duplicates. The pyritic and organic sulphur contents (wt %) were calculated on the assumption that the remaining forms of sulphur in the biomass, (Total sulphur from elemental analyses – Sulphate), comprised of pyritic and organic sulphur based on the ash content (wt %) as follows:

$$Pyritic\ Sulphur = \ Ash\ content * Residual\ sulphur \quad (13)$$

$$Organic\ Sulphur = (100 - Ash\ Content) * Residual\ sulphur \quad (14)$$

3.2.2 Lipid Content Analysis

3.2.2.1 Lignocellulosic Biomass

Lipid content in cedar wood was determined using a Soxtec apparatus (Foss, ST 243, Hilleroed, Denmark). In summary, about 1 g of sample was dried in an oven (Barnstead International, F6020 C, Dubuque, Iowa, USA) at 110 ^{o}C for 1 hour. Then, it was placed in a thimble, where it was mixed with at least two scoops of celite powder. Pre-weighed aluminum cups containing 40 ml of hexane were used for extracting lipids from biomass. The samples were treated with hexane for 20 minutes, followed by rinsing for 40 minutes and hexane stream containing extracted lipids was collected. The residual sample in the thimble was subjected to a second set of extraction in order

to extract remaining lipids. The difference in original weight of the aluminum cup after lipid extraction and solvent removal denoted the lipid content of the biomass sample. All the tests were performed in duplicates.

3.2.2.2 Algae and Sludge Biomass

Lipid content of dry algal and sludge biomass were determined as follows (Lee et al., 1998):

(i) About 200 mg of dry biomass was suspended in 25 mL of phosphate buffer (pH = 7.4) and transferred into a bead beater (Model HBB908, Hamilton Beach, Richmond, VA) that was filled about halfway covering the rotor blade with 1mm beads.

(ii) The biomass suspended in phosphate buffer was treated in the bead beater for 1 min.

(iii) The slurry obtained from step (ii) was transferred into a separatory funnel and about 30 mL of 2:1 (v/v) chloroform-methanol mixture was added. Then, the mixture was allowed to rest for 30 minutes after shaking the funnel vigorously.

(iv) The bottom layer containing the organic phase was collected in a beaker.

(v) Step (iii) was repeated again using 30 mL of 2:1 (v/v) chloroform-methanol mixture. A third extraction was carried out using 20 mL of solvent. Each time, the bottom layer was collected in the same beaker used in step (iv).

(vi) The organic phase was vacuum filtered through a Whatman filter paper (Filter No 4, GE Healthcare, Pittsburgh, PA) using a ceramic funnel to remove remaining biomass. Then, the filter paper was washed with chloroform in the funnel to remove the residual extract on the filter.

(vii) The filtered organic phase was transferred into a separatory funnel, where it washed with 20 mL of a 5 % (w/v) NaCl solution.

(viii) The washed organic phase was collected in a pre-weighed beaker and placed in a RapidVap (LABCONCO Corporation, Kansas City, KS) to evaporate the solvent under vacuum at 40 ^{o}C for 5 hours until a constant weight was reached. The lipid content was determined by weight difference; weight of the beaker with dry extract – weight of the empty beaker.

All tests were performed in duplicates.

3.2.3 Particle size analysis

The analysis of the cedar wood biomass particle size was carried out according to the AACC 66 - 20 method (AACCI, 1999). In summary, about 50 g of biomass sample was subjected to shaking in a ro-tap sieve shaker (W.S. Tyler, RX – 29, Mentor, OH) for 5 minutes. The shaker was equipped with the following sieves having sieve numbers of 20, 45, 60, 100, 140, 200 and Pan which collected particles in the size range of 850 and higher, 355 to 850, 250 to 355, 150 to 250, 106 to 150, 75 to 106, and below 75 µm, respectively. These sieves were pre – weighed before the run. After the completion of the run, each sieves were weighed and the weight difference before and after sieving denoted the weight fraction of the particles in each size range. This procedure was performed in duplicate.

3.2.4 Differential Scanning Calorimetry (DSC) Analysis

A DSC 823e from Mettler Toledo (Columbus, OH, USA) was used for the analysis. Initially, the instrument was calibrated using indium and zinc within their module specifications (Indium: onset temperature – 156.6 ± 0.3 ^{o}C; heat flow – 28.45 ± 0.6 J/g; Zinc: onset temperature – 419.6 ± 0.7 ^{o}C; heat flow – 107.5 ± 3.2 J/g). Once successfully calibrated, 7 mg of biomass sample was placed in an aluminium crucible (100 µl) with a lid. The sample was heated from 25 to 500 ^{o}C, at three different heating rates (10, 15 and 20 ^{o}C/min) to estimate the thermodynamic parameters (E_a

– Activation energy; A – Pre-exponential factor; ΔH – Change in enthalpy, and ΔG – Change in Gibb's Free Energy). There were 18 different biomass combinations (Table 1).

This experimental design is a mixture experiment with a process variable (Pradhan et al., 2017). The effect of proportion of each biomass component in the blend of three biomasses (AB, CW and DS; each at four levels – 0, 33.33, 66.67 and 100 wt %) and the catalyst effect (catalyst to biomass ratio; tested at two levels: 0 (off) and 2 (on)) is checked on the estimated parameters (E_a, A, ΔH, and ΔG). Based on the constraint that the weight fractions of AB, CW and DS sum to 100 and two levels of catalyst effect, there are twenty total combinations possible (Goos et al., 2020). This would lead to 60 number of experimental runs. Here, the constraint for experimental runs was the control of three pure biomasses at the two catalyst levels. Additionally, for error estimation in ANOVA test for the RSM model obtained, the central point (Combination 13 and 14) was replicated twice. So, to get a second degree RSM model (Equation 15) for the parameters from the design (Pradhan et al., 2017) with minimal experimental runs (60), two combinations for the biomass mixtures had to be removed.

$$Y_i = \beta_0 + \sum_{i=1}^{3} \beta_i x_i + \sum_{i=1}^{3} \beta_{ii} {x_i}^2 + \sum_{i=1}^{3} \sum_{i<j}^{2} \beta_{ij} x_i x_j + \delta_0 z + \sum_{i=1}^{3} \delta_i x_i z + \varepsilon \qquad (15)$$

Here, i = 1, 2 and 3; $Y_1 = E_a$, $Y_2 = \Delta H$ and $Y_3 = \Delta G$; β_0 = constant; δ_0 = coefficient of effect due to catalyst; β_i = regression coefficients; δ_i = interaction between catalyst and biomass component i; and x_i is the i^{th} biomass component.

With the aim of selecting one or more combinations with desirable thermodynamic properties among the three biomasses (as seen in literature survey), DS is known to have low energy barrier owing to its high ash content and CW being a lignocellulosic biomass, can be expected to have relatively higher value for the same (Li et al., 2014). Based on this, it was decided to keep all the biomass combinations of DS and to exclude two combinations containing CW at a higher weight fraction. Hence, combination of 33.33 wt % AB and 66.67 wt % CW (with and without ZSM–5)

were excluded as, the energy barrier for pyrolysis can be expected to be relatively higher as compared to other biomass mixtures (with and without catalyst), owing to greater lignin content in the blend. Thus, there were 18 combinations that were studied for the three biomasses involving catalyst use.

STAR e software (Mettler Toledo, Version 9.01) was used to identify the endothermic peak temperatures at each heating rate. A plot of "log of heating rate" vs "reciprocal of temperature" was generated according to the FWO model (Foltin et al., 2017). E_a was determined from the slope of the plot. The remaining parameters i.e. A, ΔH, and ΔG were determined as per equations (8) through (10) shown earlier in the literature survey section. The temperature, T, used in the calculations corresponds to the peak temperature closest to the average of the peak temperatures obtained from each of the three heating rates used for calculation of E_a (Foltin et al., 2017). This value of T was also used in calculation of the remaining three thermodynamic parameters. For any combination, the final values of E_a, A, ΔG, and ΔH were determined as summation of the values for all the peaks that appeared in the thermograms. The bio-char yield (wt %) was also recorded after each DSC run as the weight difference of the empty crucible and weight of the crucible with residual solid.

For pure biomass or biomass mixture ('X' mg) used in the DSC runs, the bio-char yield was calculated as:

$$Bio - char\ yield, C\ (wt\ \%) = \left(\frac{S}{X}\right) * 100 \qquad (16)$$

Where, S = Mass of residual solid left in the crucible (mg),

In case of catalytic blends (2:1 wt/wt ZSM–5: Biomass blend) of pure biomass or biomass mixture ('D' mg of combined blend), it was assumed that the bio-char came only from biomass or

biomass mixture and two-third of the blend comprised of catalyst only. Based on this, the bio-char yield (C_{cb}) was calculated as:

$$Bio - char\ yield, C_{cb}\ (wt\ \%) = \left(\frac{3S-2D}{D}\right) * 100 \quad (17)$$

3.2.5 Pyrolysis Tests

A muffle furnace (Barnstead International, F6020 C, Dubuque, Iowa, USA) was used to pyrolyze 20 g of pure biomass or biomass blend with or without catalyst. The biomass was weighed and placed in a quartz crucible inside a closed quartz reactor. The reactor was connected to a condenser system (Figure 1) through quartz and steel tubing which was heated (Temperature set = 125 ^{o}C) with a heating tape (Omega Engineering Inc., Stamford, Connecticut, USA) and insulated by wrapping the tubing with insulation material, to minimize heat loss and condensation before the gas phase reached to the condenser unit. Industrial grade nitrogen (Airgas, Stillwater, Oklahoma, USA) was used to purge inside the system for at least 30 minutes at a flow rate of 100 mL min^{-1}, before the experiment began and was continued for at least 10 minutes after the experiment was over. The non-condensable gases were expelled in the fume hood. The biomass was heated from room temperature to 500 ^{o}C in the following four segments controlled via a PID controller:

(i) Heating from room temperature to 100 ^{o}C.

(ii) Isothermal treatment at 100 ^{o}C for 1 minute.

(iii) Increase in temperature from 100 to 500 ^{o}C and

(iv) Isothermal treatment at 500 ^{o}C for 60 minutes.

For each heating segment, a holdback value of 5 ^{o}C was used in the PID controller to ensure that the final temperature did not deviate beyond 5 ^{o}C from the set point temperature for that segment.

During the temperature ramp segments (i) and (iii), the average heating rate was approximately 14 ^{o}C/min, which was within the heating rate range used for the DSC experiments.

For 'X' g of pure biomass or blend used, the yield of bio-char was calculated from equation 16, while the other products were calculated as:

$$Pyrolysis\ Liquid\ Yield, P\ (wt\ \%) = \left(\frac{L}{X}\right) \quad (18)$$

$$Loss\ and\ Gas\ Yield, G\ (wt\ \%) = 100 - C - P \quad (19)$$

Here, L = Combined weight of the condensed liquid in three flasks of the condenser system.

For calculation of loss and gas yield from equation 19, the following mass balance was assumed:

$$Total\ weight\ of\ biomass\ used\ in\ pyrolysis = (Weight\ of\ bio - char) + (Weight\ of\ pyrolysis\ liquid) + (Weight\ of\ gasses\ and\ losses) \quad (20)$$

In case of catalytic pyrolysis runs, 'B' g of catalyst and 'X' g of either pure biomass or biomass mixture were used. Two assumptions were made for product yield calculation; a) the bio-char was generated from biomass only. So, the amount of catalyst was deducted from the weight of solid residue after run. B) the moisture present in the catalyst contributed to the aqueous phase part of pyrolysis liquid obtained. Based on this, the yield of bio-char and pyrolysis liquid were calculated as:

$$Bio - char\ yield, C_c\ (wt\ \%) = \left(\frac{S-B}{X}\right) * 100 \quad (21)$$

$$Pyrolysis\ Liquid, P_c\ (wt\ \%) = \left(\frac{L}{B}\right) * 100 \quad (22)$$

The yield of gas and losses were calculated from equation 19.

After an experimental run, all the system components were disconnected, and the quartz tubing connections were heated to 850 ^{o}C for 2.5 hours to clean up the residue prior to the next run. The larger system components like the steel tubing, condenser columns and connecting glasswares were cleaned using methanol.

3.2.6 GC-MS Analysis of Bio-oil

The collected bio-oil was analyzed using a GC-MS (QP2010S, Shimadzu USA Manufacturing inc., Columbia, MD, USA). The samples were diluted 40 times using dichloromethane (HPLC grade, Sigma Aldrich, St Louis, MO, USA) prior to injecting 1 µL of sample to a GC-MS equipped with DB5-MS capillary column (Part Number: 122 – 5532, 30 m length, 0.25 mm inner diameter and 0.25 µm film thickness, Agilent, Santa Clara, CA, USA) using an autosampler (AOC – 20i model, Shimadzu Corporation, Kyoto, Japan). The following oven method was used for the separation; i) hold at 40 ^{o}C for 4 minutes, ii) increase the temperature to 280^{o}C at a rate of 5 ^{o}C/min, iii) hold at this temperature for 20 minutes. The injector temperature was set at 250 ^{o}C in splitless mode. The carrier gas was helium at a flow rate of 1 mL min^{-1}. The NIST mass spectral data library (2002, Baltimore, MD, USA) was used for the identification of the peaks on the chromatograms. The area percentage of the total ion chromatogram was used for determining the bio-oil composition using GC-MS solution (v 2.4, Shimadzu USA Manufacturing Inc, Columbia, MD, USA). The analysis of each bio-oil sample was performed in duplicate.

3.2.7 Statistical Analysis

Microsoft Excel 2013 was used for linear regression for the estimation of E_a, which was subsequently used for determination of A, ΔH, and ΔG. Response surface modelling for the relevant parameters and ANOVA analysis for the corresponding model was done using SAS (v 9.4, SAS Institute Inc., Cary, NC, USA). The ANOVA tests were performed at $\alpha = 0.15$ and the mean comparisons were done at $\alpha = 0.05$ level.

3.2.8 Process Modelling

The flow of energy and mass across various streams in the pyrolysis process starting from the biomass to the end products, were evaluated using the ASPEN PLUS software (V 10, Bedford, MA).

CHAPTER IV

RESULTS AND DISCUSSION

4.1 Chemical Composition of Biomass

The ultimate, proximate, sulphur, and lipid compositions of the biomass samples examined in this study are shown in Table 2-a, b, c and d. Algal biomass (AB) had relatively higher contents of C (43.66%), H (7.30%), and lower content of O (41%) as compared to those for the cedar wood (CW) and digested sludge (DS) samples. The elemental composition of AB determined in this study is comparable to the data reported in literature for other microalgae strains: *Pseudanabena* sp. SP 46 (Zhou & Dunford, 2017), *Nannochloropsis gaditana* (Sanchez-Silva et al., 2013), *Nannochloropsis oculata* and *Tetraselmis* sp. (Ceylan & Kazan, 2015). Relatively higher content of N in AB and DS (Table 2-a) is due to the higher protein content in these samples than that in the CW. Lower S and N content in the feedstock to be used for biofuel production is desirable, since higher content of these compounds increases harmful sulphur and nitric oxide emissions during fuel combustion. Although CW had significantly lower N content than that of AB and DS, sulphur contents of all three biomass examined in this study were similar.

The carbon content of the biomass is directly proportional to the heating value of the biofuel, while the oxygen content inversely affects the heating value.

Presence of oxygen containing compounds such as lignin, cellulose, and hemicellulose in CW is the reason for its high O content, Table 2-a, (Praveen et al., 2016). The high fixed carbon content in CW (Table 2-b) could potentially be due to its high content of lignin which is composed of a very complex cross-linked network of aromatic compounds with very high thermal stability (Quan et al., 2016; Zhao et al., 2017a).

The DS had extremely high ash content reducing its volatile matter and fixed carbon content (Table 2-b). This is due to the fact that DS tends to accumulate more heavy metals than the anaerobic waste (Agrafioti et al., 2013; Alvarez et al., 2002). Hence, the AB used in this study appears to be a better candidate for biofuel production than CW and DS. This conclusion is further supported by the finding that AB also has higher volatile matter and lower ash content than those of DS and CW (Table 2-b). High volatile matter and fixed carbon contents are desirable features for feedstock to be used for thermochemical production of biofuel.

The speciation of sulfur in the biomass is very important for understanding chemical composition of the gas, liquid and solid phases formed during the pyrolysis process. The biomass samples examined in this study has similar total S content, Table 2-a. Although there were slight differences in the sulphur species (Table, 2-c) present in AB, CW and DS, the differences were not significant for practical purposes.

Among the three biomass samples examined in this study, AB had the highest oil content (Table 2-d). This result was expected considering that algae strains used for this study are salt water species which tend to accumulate lipids. The Lipids in DS is most probably due to the oil and fat present in foods and feces carried with municipal wastewater. The presence of lipid in biomass increases its energy content and significantly affect pyrolysis kinetics and the products formed during the process.

The chemical composition of the biomass selected for this study, AB, CW and DS, are very diverse. Hence, co-pyrolysis of these feedstock would allow greater flexibility in process optimization and final product properties.

4.2 Particle size analysis

Particle size distribution of the AB and DS could not be determined due to the very limited amount of biomass available for this study. A small fraction of the CW particles obtained after grinding was larger than 850 mm (4.31 wt %) and between 75 to 150 µm (12.62 wt %) (Table 3). Majority of the CW particles (40.07 wt %) had a particle size between 355 to 850 µm. The fraction of the particles between 150 and 355 was also significant (33.38 wt %). The remaining weight fraction of the CW biomass had particles size smaller than 75 µm.

It is known that smaller particle size for pyrolysis feedstock decreases the path length for pore diffusion during pyrolysis. This, in turn minimizes the secondary interaction of volatiles, thereby increasing the rate of devolatilization of biomass (Tian et al., 2016). Therefore, enhanced intraparticle heat and mass transfer lead to an increase in the yield of bio-oil (Kan et al., 2016).

4.3 Differential Scanning Calorimetry Analysis

4.3.1 Pyrolysis Kinetics

Pyrolysis kinetics of AB, CW, DS and their mixtures were examined with and without catalyst. The experimental design consisted of 18 combinations of biomass which were determined via statistical mixture experimental design, Table 1. Typical DSC thermograms for pure and mixed biomass at 3 different heating rates are shown in Figures 2-4. The peak temperatures obtained from the thermograms and used for the calculations are listed in Table 4. The data clearly indicate that peak temperatures vary significantly with biomass type and the heating rate, consequently affecting the calculated kinetic parameters.

Among the 3 biomass samples examined in this study, pure AB had the lowest E_a and ΔH (Table 5). The latter results were due to the lack of lignin content in AB as compared to the other types of biomass (Maddi et al., 2011). Pure DS had higher E_a and ΔH than those of AB, probably due to the presence of fibrous waste carried in the municipal wastewater (Ahmad & Eskicioglu, 2019). Additionally, DS might have higher amount of O containing hydrocarbons than AB (Table 2-a). Since the energy needed to break C – O bonds is high (about 400 kJ/mol) (Politzer & Ranganathan, 1986), the energy requirement for DS degradation is expected to be higher than AB.

It is well established that thermal behavior of a biomass during pyrolysis is correlated with its chemical composition (Shuping et al., 2010). The pyrolysis of pure CW with no catalyst had the highest energy requirement. This is due to its high lignin content which is thermally more stable than the other biomass components such as proteins and carbohydrates (Li et al., 2014; Mohan et al., 2006). The DSC thermograms for CW (Figure 2-4) displayed a peak in the temperature range of 120 to 160 ^{o}C, which was not present in the thermograms for AB and DS. This temperature range has been attributed to the degradation of light volatiles and simple sugar molecules like glucose, galactose and fructose in the biomass (Ahmad et al., 2017b). The occurrence of this reaction at such an early stage of pyrolysis could have possibly led to a high value of ΔG, 489.77 kJ/mol, for CW (Table 4).

The values of E_a, ΔH and ΔG for biomass mixtures varied from 192.39 to 398.55 kJ/mol, 179.96 to 382.61 kJ/mol and 329.99 to 494.75 kJ/mol, respectively, depending on the composition of the biomass blend (Table 5). It appears that addition of DS into the CW (combinations 7 and 9) significantly reduced the energy requirement for the pyrolysis process (Table 5). A possible reason for this trend could be that high ash content in DS produced catalytic activity reducing the energy barrier for CW degradation (Eom et al., 2012; Sanchez-Silva et al., 2012), and indicating synergistic interactions of biomass blends. A comparison of the degradation behaviours of AB

and DS mixtures (Combinations 11 and 15) indicates that higher AB fraction in the mixture significantly increases E_a due to the higher amount of lipids present in AB (Bui et al., 2016).

One of the objectives of this study was to determine the biomass mixture combinations that resulted in low E_a and ΔH in an effort to minimize the energy requirement for the process. The biomass mixture with 66.6% AB, 33.3% CW and no DS with catalyst (combination 16) gave the lowest E_a, 57.03 kJ/mol, and ΔH, 50.14 kJ/mol (Table 5).

The ΔG of the CW (66.67 %) and DS (33.33 %) with no AB, combination 9, (329.99 kJ/mol) was lower than those for all three pure biomass. The DSC thermograms for the latter combination displayed an additional fourth peak between 339 and 384 ^oC at the heating rate of 10 ^oC/min. However, this peak was not present at the heating rates of 15 and 20 ^oC/min. Since this combination contained higher CW fraction than the other mixtures, it could be possible that there was not enough time for degradation of all the lignin and cellulose present in the blend at high heating rates. So, the ΔG calculated for the combination 9 might be a slight underestimation of the true value.

The highest ΔG value among the mixtures was obtained for the combination 15, 66.6% AB, 33.3% CW and no DS, 494.75 kJ/mol. The DSC thermograms for this blend showed an additional peak in the temperature range of 155 to 171 ^oC which was not present in the thermogram for pure CW and AB (Figure 2-4) indicating the synergistic interaction of blend components and enhancement of the spontaneity of biomass degradation.

For all biomass combinations, addition of catalyst in the combination reduced pyrolysis energy requirement (Table 5). A possible explanation for the latter results is that O containing functional groups on organic molecules present in the biomass like – OH, – C = O, and – C – O – C – formed acidic sites on the inner surface of Si – Al framework of ZSM-5. These sites are capable of easily interacting with complex molecules like polyaromatic rings and fatty acids and reducing

the energy needed for the reactions like decarbonylation, decarboxylation, cyclization, and deoxygenation that occur during biomass degradation (Wang et al., 2014a). The lowest energy barrier was obtained for the combination 16, 2:1 AB: CW mixture. The catalyst addition drastically lowered the pyrolysis energy barrier (E_a = 57.03 kJ/mol and ΔH = 50.14 kJ/mol) for this combination as compared to the blend without the catalyst, due to the catalytic activity (Li et al., 2014; Sanchez-Silva et al., 2012). Although there was an endothermic peak at 341.80 ^oC in the thermogram obtained at 20 ^oC/min corresponding to lignin and cellulose degradation, it tailed off at the heating rates of 10 and 15 ^oC/min (Figure 5 (a), (b) and (c)). This could have possibly happened because lignin and cellulose degraded around this temperature at high heating rates but lower heating rates did not provide sufficient energy for this reaction to complete.

Other kinetic parameter studied was pre-exponential factor, A (Table 4) which helps to explain mechanism of the reactions occurring at different temperatures represented by endothermic peaks.

For all the combinations, in the temperature range of 75 to 110 ^oC, the value of A (min^{-1}) was below $6x10^{10}$, corresponding to removal of moisture from the biomass surface. (Ahmad et al., 2017b; Turmanova et al., 2008). For non-catalytic blends 1, 3, 5, 7, and 17 the value of A was higher than $6x10^{10}$ at temperatures from 140 to 260 ^oC, which was probably due to the initiation of the degradation of complex macromolecules like cellulose, hemicellulose, lipids and/or lignin in the blend. For the remaining combinations, A values were around 6 $x10^{10}$. The latter results indicate lower energy requirement for the catalytic pyrolysis. The thermal degradation of the biomass components was probably initiated at a lower temperature in the presence of a catalyst.

Above results further support the previous findings that catalyst addition reduced energy requirement for biomass degradation possibly by initiating degradation of complex macromolecules on the catalyst surface (Ahmad et al., 2017b) as revealed by the lower A values obtained for the catalytic pyrolysis than those obtained without catalyst.

4.3.2 Bio-char Yield

Table 6 summarizes the bio-char yields from the DSC experiments. For pure AB and DS, the yield of bio-char was similar at heating rates of 10 and 15 ^{o}C/min. However, at the higher heating rate of 20 ^{o}C/min, bio-char production reduced from 34.29 to 31.43 and 54.28 to 48.27 wt % for AB and DS, respectively. The latter results can be explained by the improved heat and mass transfer at higher heating rates (Kan et al., 2016). The bio-char yield from CW decreased from 40 to 37.14 wt % as the heating rate was increased from 10 to 15 ^{o}C/min. However, there was no significant change in the bio-char yield at the heating rate of 20 ^{o}C/min. This could have been due to the fact that the mass and heat transfer limitation in CW biomass was already overcome at 15 ^{o}C/min, thereby not affecting the bio-char yield with increasing heating rate to 20 ^{o}C/min (Kan et al., 2016).

The variations in the bio-char production with the change in the heating rate were more complex for the biomass blends. Presence or absence of the catalyst further complicated the bio-char production kinetics due to the very complex interactions and reactions occurring during the pyrolysis process. Very small biomass amount used in the DSC experiments is expected to introduce a large error in the bio-char measurements. Hence, no apparent trend could be established for bio-char production from the data collected from the pyrolysis of biomass blends with and without catalyst.

4.4 Process Evaluation Using Surface Response Methodology

Response surface modelling (RSM) was performed for E_a, ΔH, and ΔG using the RSREG procedure in SAS 9.4. The model comprised of the weight of two biomass components in the blend and the presence or absence of the catalyst. For pyrolysis of a complicated system comprising of a mixture of at least two different biomasses (especially combined with catalyst), statistical analysis at the commonly used $\alpha = 0.05$ level, can lead to exclusion of essential

variables (especially the interaction between the biomass components) from the ANOVA test for the RSM model of both E_a and ΔH (Bursac et al., 2008). So, hypothesis testing for ANOVA tests at $\alpha = 0.05$ level is not convenient. Furthermore, the total degree of freedom in the RSM models for both E_a and ΔH are 19 (Table 1; Total number of combinations = 20, including replication for combinations 13 and 14). When total degree of freedom for a response surface model is within 20, testing at a higher significance level of 0.15 ($\alpha = 0.15$) can be possibly considered as the best option (Bendel & Afifi., 1977). Hence, the ANOVA test was performed at $\alpha = 0.15$ level.

The models (equations 23 – 28) were found to be statistically significant ($p < 0.0001$) for both E_a and ΔH, for any of the three pairs of biomass components chosen, AB - CW, AB - DS and CW-DS and there was no significant lack of fit ($p > 0.38$) (Table 7 - 8). The models based on parameter estimates (Table 9 – 14) are listed below.

(a) RSM model for biomass pair AB and CW:

$$E_a = 13.43 * CW^2 - 71.93 * CW - 8.95 * AB + 11.73 * CW * AB - 113.89 * Catratio + 367.38 \quad (23)$$

$$\Delta H = 12.86 * CW^2 - 68.2 * CW - 8.21 * AB + 11.15 * CW * AB - 112.1 * Catratio + 350.72 \quad (24)$$

Where, CW = Weight of cedar wood in the blend (mg), CW

AB = Weight of microalgae mixed culture in the blend (mg), AB

CW * AB = Interaction between CW and AB in the blend,

Catratio = Catalyst to biomass weight ratio (wt/wt), Catratio = 0 or 2.

(b) RSM model for biomass pair DS and CW:

$$E_a = 4.49 * DS^2 - 20.82 * DS + 28.03 * CW - 9.59 * DS * CW - 113.89 * Catratio + 319.92 \quad (25)$$

$$\Delta H = 4.53 * DS^2 - 21.84 * DS + 26.99 * CW - 8.98 * DS * CW - 112.1 * Catratio + 308.63 \quad (26)$$

Where, DS = Weight of digested sludge in the blend (mg), DS

DS * AB = Interaction between the DS and AB in the blend,

(c) RSM model for biomass pair AB and DS:

$$E_a = 14.08 * DS^2 - 115.98 * DS - 28.03 * AB + 9.59 * DS * AB - 113.89 * Catratio + 516.141 \quad (27)$$

$$\Delta H = 13.51 * DS^2 - 111.7 * DS - 26.99 * AB + 8.98 * DS * AB - 112.1 * Catratio + 497.56 \quad (28)$$

The ANOVA analysis showed that the value of R^2 for E_a was higher, 0.8428 for DS - CW, and AB - DS than that of CW - AB (R^2 = 0.8298). The R^2 value of 0.8428 signifies that 84.28 % of the variation in response could be significantly explained by the model (DS - CW and AB - DS). The models also confirm that effect of catalyst on E_a and ΔH are significant ($p < 0.0001$).

A significant quadratic effect ($p < 0.005$) for DS was found in the model based on AB - DS blends (Tables 13 and 14). A statistically significant interaction exists between the DS and AB for both E_a ($p = 0.0939$) and ΔH ($p = 0.1085$). Hence, the final RSM model chosen was based on the AB – DS.

From the known value of DS and AB, CW can be calculated as:

$$CW = 7 - DS - AB \quad (29)$$

The statistical analysis of ΔG (Table 15) indicate a significant lack of fit ($p < 0.0001$) for the model attained. Hence, the given experimental design does not model ΔG well. Among the thermodynamic triplets, E_a, and ΔH are more important than ΔG, as they confer to energy barrier for pyrolysis (Ahmad et al., 2017 b; Xu & Chen, 2013; Zhou & Dunford, 2017). ΔG gives us the measure of the spontaneity for the pyrolysis process (Ahmad et al., 2017a; Xu & Chen, 2013). This measure of spontaneity for pyrolysis can also be inferred from the relative difference between E_a and ΔH (Vlaev et al., 2007). For all the 18 combinations, this difference (for each peak in the DSC thermograms used for calculating E_a and ΔH) was found to be approximately 5 kJ/mol, which indicates a low energy barrier for pyrolysis favoring formation of an activated complex prior to final product formation (Ahmad et al., 2017a; Sánchez-Jiménez et al., 2013). Thus, the likelihood of all the possible reactions (decarbonylation, decarboxylation, cyclization, and deoxygenation) occurring during pyrolysis is high for all 18 combinations (Ahmad et al., 2017b).

The 3-D and contour plots for both E_a and ΔH (Figure 6-29) indicate that catalytic pyrolysis reduces energy requirement for the process. The plots also show that when the weight fraction of DS and AB was in the range of 42.86 - 57.14% and 0 - 14.29%, respectively, the energy requirement was minimized ($\leq$ 75 kJ/mol for E_a and $\leq$ 50 kJ/mol for ΔH). Based on the RSM model from equation 27 and 28, and the blend fraction region identified earlier, the following blend (with ZSM-5: Biomass blend = 2:1) with E_a and ΔH values of 52.75 and 45.37 kJ/mol, respectively, was chosen for further investigation: 57.14% DS - 4.29% AB - 38.57% CW. This combination with ZSM–5 is referred to as the “optimum combination” (OC) and the biomass mixture without ZSM–5 is designated as “optimum mixture” (OM) in the text from this point forward.

4.5 Bio-oil Yield

Due to the limitations of the pyrolysis system available to this study, it was not possible to collect and quantify bio-oil produced during the pyrolysis experiments accurately (Table 16). The lines between the reactor outlet and the condenser system was long causing bio-oil condensation before the gas stream reached the condenser. Insulation and even the heating of the lines did not eliminate large bio-oil loss in the system. However, bio-char yield produced during the pyrolysis runs could be measured accurately. The measurements for the pyrolysis liquid including bio-oil collected in the condenser could be measured with less accuracy due to the losses in the system as described earlier (Table 16). Hence, the amount for gases and losses reported in Figure 30 was calculated from the material balance. It appears that the relative amount of bio-oil recovered from pure AB without catalyst (14.8%) was higher than those for the CW (3.37%) and DS (5.32%). This result is expected due to the significantly higher volatile content of AB than CW and DS (Table 2-b). The high content of lignin in CW led to lower bio-oil yield as compared to the other two biomass (Maddi et al., 2011; Yang et al., 2007). Catalyst addition (Catalyst: biomass ratio = 2:1 wt/wt) to OM seems to lower the bio-oil yield, Figure 30. This can be attributed to the fact that catalyst addition at such a high amount leads to secondary degradation of large molecular weight volatiles, especially at a low heating rate used in this study, which enhances the gas yield, thereby reducing the bio-oil yield (Gao et al., 2017; Zhang et al., 2018a). Additionally, the volatile content of the OM is low owing to the high weight fraction of DS and low AB (Table 2-b). This could also have been another possible cause for low recovery of bio-oil from the blend of OC (Zhao et al., 2017a).

Pure DS resulted in the highest bio-char yield, 50%, followed by AB, 30.5%, and CW, 23%. The high ash content of DS, 32.97%, Table 2-b, led to highest yield of bio-char (Figure 30) (Agrafioti et al., 2013). Finally, the bio-oil recovery from OC, 1.04 %, was lower than that of combination 14 (2.73 wt %, ZSM-5: biomass blend = 2:1 wt/wt, where the blend has all the three biomass

components in equal weight fraction). This could be due to the fact that the volatile matter was relatively higher in the latter combination (Zhao et al., 2017a).

As the catalyst added to OM at increasing amounts, the bio-oil yield decreased significantly from 3.18% to 0.89%, 0.91% and 1% at 0.5, 1 and 2 catalysts : biomass ratio, respectively (Figure 30). The latter results also supported by the findings that as the catalyst to biomass ratio in the blend increased from 0.5 to 2, the yield of bio-char drastically decreased from 42.5 to 23.5%, while the yield of gases significantly enhanced from 35.11 to 55.18%. This could have happened, because increase in weight of catalyst added to the OM, led to further degradation of large molecules which promoted gas formation, thereby reducing the yield of bio-char and bio-oil recovery (Aho et al., 2008; Zhang et al., 2018a). Increased gas production with increasing catalyst amount can be attributed various reactions like dehydrogenation, cracking, and cyclization or aromatization that lead to hydrocarbon conversion from biomass at the acid sites of ZSM-5 (Iliopoulou et al., 2012).

4.6 Chemical Composition of Bio-oil

Chemical composition of bio-oil obtained from 11 different combinations (Table 17) was analyzed to assess the effects of biomass composition and catalyst amount in the mixture on aromatic hydrocarbon production. The experimental design used in this study was developed to minimize the process energy requirement, not the effect of presence or absence of a catalyst in the mixture on aromatic hydrocarbon production. To further evaluate the process variables for aromatic hydrocarbon production, the OC (OM with catalyst, ZSM–5: Biomass blend = 2:1) determined using the original experimental design in the previous section of this dissertation, OC, 57.14% DS - 4.29% AB - 38.57% CW, was pyrolyzed in a larger system to obtain sufficient bio-oil for chemical testing. The effect of the amount of catalyst in the mixture on chemical composition of the bio-oil produced was examined at 3 different catalyst: biomass ratio, 0.5, 1 and 2 using OM (Table 17).

Combination 14, 33.33% DS - 33.33% AB - 33.33% CW with ZSM-5: Biomass blend = 2:1 was also included in the large scale experiments to collect sufficient bio-oil for chemical testing for comparison purposes.

Major chemical groups identified in the bio-oil were aromatic hydrocarbons (AH), other aromatic compounds (OA) (all aromatic groups except hydrocarbons), acids, alcohols, aldehydes, ketones, amine, amides, esters, nitriles, paraffins, olefins, alkynes, furans and cholesterol-derived compounds.

A very low amount of AH, 1.27%, was found in the bio-oil obtained from CW while AB and DS did not produce detectable amount of AH when pure biomass samples were pyrolyzed without catalyst (Table 17). The highest OA yield was obtained with CW, 71.71%, and in decreasing amounts in bio-oils from DS, 12.98%, and AB, 2.46%. OA mainly comprised of different methoxy derivatives of phenol and trimethoxy benzene. The probable reason behind such a high yield of these aromatic compounds is thermal degradation of lignin in CW at 500 ^{o}C (Mullen & Boateng, 2010). Aromatic compounds are desirable for various chemical industries especially as solvent. Hence, the bio-oil from CW could be useful for various chemical industries. Furans were also present in the bio-oil from CW. These findings are in agreement with an earlier report on CW pyrolysis (Yang et al., 2016).

The main class of chemical compounds in bio-oil from AB was acids, n-hexadecanoic acid being the major one, 52.47%. This could have been due to incomplete thermal degradation of the long chain fatty acids such as n-hexadecanoic acid, under the pyrolysis conditions used in this study (Zhang et al., 2016). n-Hexadecanoic acid is known to have antimicrobial activities (Agatonovic-Kustrin et al., 2016; Tang et al., 2017). Hence, such a bio-oil rich in latter fatty acid could be useful in pharmaceutical industries.

The bio-oil from pure DS produced the highest amount, 53.97%, of cholesterol-derived compounds like cholestene, cholestane, and cholestanol acetate. This is due to the presence of cholesterol coming from food waste and human feces carried with municipal wastewater. The catalytic activity in DS which is due to its high ash content was helpful in converting some of the cholesterol molecules to OA during pyrolysis. This is evident from the yield of OA from DS, 12.98% that is relatively higher than that produced by AB, 2.46%. It is well established that bio-oil composition is dependent on pyrolysis temperature (Chen et al., 2016; Onay, 2007). The pyrolysis temperature used in this study, 500 ^{o}C, did not provide enough energy for complete degradation of cholesterol to aromatic compounds (including hydrocarbons) and other molecules (Hietala & Savage, 2015).

When OM was subjected to pyrolysis, no AH was found in the bio-oil (Table 17). However, the yield of OA was higher, 44.32%, than that from AB and DS alone. Also, bio-oil from OM contained cholesterol-derived molecules (cholestene and cholestane-diol) at a lower yield, 20.18% than that from DS alone. A prominent reason behind this could be that the catalytic activity in the blend due to its high content of DS and its high ash content, which aided in conversion of cholesterol and other molecules like olefins and acids to these aromatic compounds. Hence, this bio-oil can be used as a feedstock for various chemical industries requiring aromatic compounds.

Therefore, co-pyrolyzing AB, DS, and CW in the weight fractions as in OM improves the chemical composition of the bio-oil by increasing its aromatic content. But, it does not necessarily lead to formation of AH in high concentrations. This could be due to the fact that the hydrogen content of the blend was low as compared to other elements (C, O, N and S) (Table 2-a), which inherently was a barrier for AH formation (Zhang et al., 2018b). Additionally, the pyrolysis temperature, 500 ^{o}C, was insufficient for AH formation as higher energy is needed for AH formation than other compounds (Du et al., 2013).

When either pure biomass or biomass mixtures were combined with zeolite ZSM–5 at catalyst: biomass ratio of 2:1, AH were found in the bio-oil obtained. For instance, AH content of the bio-oil from DS was found to be 72.30% when catalytic pyrolysis was carried out. Additionally, the weight fraction of cholesterol derived compounds, alcohols, and OA had drastically decreased from 53.97 to 22.13%, 6.19 to 4.09%, and 12.98 to 4.09%, respectively. From this, it can be inferred that catalytic pyrolysis of DS facilitated the conversion of OA, alcohols, and cholesterol to AH. The possible reason behind it could be that catalyst facilitated disruption of the C – O bonds and aided with the dehydration, decarbonylation, decarboxylation, cyclization, alkylation, and aromatization reactions (Karnjanakom et al., 2016). As a result, oxygen from the biomass was removed as H_2O, CO_2, and CO, and subsequently carbon and hydrogen was converted to AH (Zhang et al., 2017). Similar findings were observed for the catalytic pyrolysis of CW and AB producing AH content of 84.90 and 57.76% in the bio-oils, respectively. CW being a lignocellulosic biomass with high lignin content and further deoxygenation of oxygen containing molecules could have led to such an enhanced yield of AH in the bio-oil (Zhang et al., 2018b). However, when the bio-oil from catalytic CW pyrolysis was diluted with HPLC grade dichloromethane, some precipitate formed which was removed prior to GC – MS analysis. So, the estimated value for AH content in the bio-oil could be a slight overestimation of the true value as some other compounds were removed from the bio-oil sample analyzed.

Catalytic pyrolysis of OC produced 83.12% AH in the bio-oil. It is worth noting the absence of OA and acids in the bio-oil for this catalytic blend. So, it was possible that these compounds were completely converted to AH in the presence of the catalyst (Karnjanakom et al., 2016; Zhang et al., 2017). The latter hypothesis is also supported by the drastic reduction of alcohols and cholesterol derived compounds from 9.21 to 0.69% and 20.18 to 10.94%, respectively, in the bio-oil with catalyst addition. GC – MS analyses indicate that AH are comprised of naphthalene and its methyl derivatives (79.29%), along with small amount of anthracene and its methyl derivatives

(2.91%). Naphthalene and anthracene are known to be useful as industrial solvents and precursors for different chemical industries (Erarpat et al., 2017; Hossain et al., 2016). Moreover, in the past few years, they have been recognized as promising candidates for highly conductive single molecular wires, where the Π electron on the benzene ring can directly couple to a metal electrode via metal - Π coupling (Liu et al., 2015). Hence, such a bio-oil could have potential application for conductive wire manufacturing industries in addition to various chemical industries.

Finally, when the bio-oil composition obtained from catalytic pyrolysis of OC (Table 17) and the biomass blend with equal weight proportions of AB, CW and DS (Table 17, combination 14) were compared, it was observed that AH content was slightly higher (89.38%) in combination 14 than that in OC (83.12%). Moreover, it is worth noting that the fraction of cholesterol derived compounds in the bio-oil from combination14 was lower (4.42%) than that in OC (10.94%). The lower weight fraction of DS in combination 14 (33.33%) as compared to that in OC (57.14%) could have led to such lower yield of cholesterol derived compounds in the bio-oil, since the cholesterol content of the combination 14 was lower than that for OC due to the higher cholesterol content in DS. The other compounds detected in these bio-oils were OA (2.40%), aldehydes (0.70%), alcohols (1.08%) and olefins (2.02%). The AH were comprised of naphthalene and its methyl derivatives (85.29%) with a small fraction of anthracene and its methyl derivatives (4.09%). The latter results clearly demonstrate that the yield and presence of various chemical compounds in the bio-oil from catalytic co-pyrolysis of the three biomasses are affected by their weight proportion in the mixture.

The effect of catalyst loading on AH production was examined by pyrolyzing OC at 3 catalyst loading levels, catalyst : biomass ratio of 0.5, 1 and 2. The combination with the lowest catalyst loading, combination OM – 0.5 (Table 17) produced 22.88% AH, 37.51% OA, 9.23% acids, 1.57% alcohols, 10.61% olefins, and 18.20% cholesterol derived compounds. The latter

compounds are produced in lower amounts with the exception of olefins when OC was pyrolyzed without a catalyst (combination OM, Table 17). The yield of olefins (α-cedrene) in the bio-oil from combination OM – 0.5 (10.62%) was relatively higher than that from combination OM (4.15%). The possible reason behind it could be that α-cedrene which is a major compound in CW essential oil was converted to different AH (naphthalene and its methyl derivative) in the presence of catalyst (Marcilla et al., 2008; Zhang et al., 2015). However, the amount of catalyst added was not sufficient to completely convert the polycyclic olefin to AH. From this it could be inferred that the addition of ZSM-5 to OM at 50 wt % of the biomass blend boosted the conversion of acids, alcohols, OA and cholesterol to AH and olefins.

As the catalyst loading with OM is increased (combination OM – 1.0, Table 17), AH content of the bio-oil increased significantly from 22.88 to 62.89% (Table 17). Yields of acids (3.55%), OA (10.78%), olefins (7.42%), and cholesterol derived compounds (12.01%) decreased with increasing catalyst amount in the blend. However, concentration of alcohols increased from 1.56% to 3.36% with increasing catalyst: biomass ratio from 0.5 to 1, but, a further increase in catalyst: biomass ratio to 2 resulted in a lower alcohol concentration in the bio-oil, 0.69%. The highest alcohol concentration was obtained with OM, 9.21%. The possible reason behind this was that catalytic pyrolysis facilitated further conversion of acids, alcohol, OA, cholesterol, and α-cedrene to AH. Additionally, it was possible that the acid (n-hexadecanoic acid) in the biomass blend was deoxygenated to form alcohol (1-dodecanol, 3,7,11-trimethyl) as an intermediate that got converted to AH (naphthalene and its methyl derivative) (Zhang et al., 2015). Increased catalyst loading with biomass provide more catalytic sites for pyrolysis reactions aiding further deoxygenation and cracking of different chemical compounds present in the bio-oil (Zhang et al., 2018b). Depending on the catalyst loading to the system, the amount of catalyst might not be enough for complete deoxygenation of the alcohol and subsequent formation of AH.

From these findings, it is clear that increased catalyst loading with the biomass blend enhances the yield of AH in the bio-oil. This finding is consistent with other reports in literature (Anand et al., 2016; Wang & Brown, 2013; Zhang et al., 2018b).

4.7 ASPEN PLUS Simulation

Information on the ASPEN PLUS simulation for modelling co-pyrolysis process optimization, and mass and energy balance evaluation is limited in the literature. Furthermore, an extensive literature review did not reveal any study on ASPEN PLUS simulation for co-pyrolysis using AB, DS and CW. Hence, this study is the first attempt for simulating co-pyrolysis of AB, DS and CW. The simulation comprised of 3 blocks and 6 streams (Figure 31).

The following streams were defined: "BLEND" – comprises either pure biomass or biomass mixtures; "PRODUCT" – decomposed products generated from pyrolysis of pure biomass or mixture; "SOLID" – bio-char generated from co-pyrolysis of BLEND; "PRODGAS" – gas generated from co-pyrolysis of BLEND; "LIQUID" – liquid stream comprising of both aqueous phase and bio-oil generated from condensation of the gas released from co-pyrolysis; and "GAS" – non-condensable gases released form the condenser unit of the co-pyrolysis system. The latter stream also accounts for the losses involved in the mass yield calculation of the three product streams.

Following blocks were used to generate and process the streams defined earlier:

- ✓ PYROLYSI – RYield reactor stream used for modelling the co-pyrolysis of "BLEND" stream at 500 ^{o}C. The stream "PRODUCT" is released from this block.
- ✓ SOLIDSEP – SSplit separator is used for separating the gas stream generated during pyrolysis of the "BLEND" from the solid formed. This block is used as RYield block which functions only as a reactor, does not model product separation. So, "PRODUCT" stream

formed from RYield block needs to be separated before further analysis can be performed on the solid, liquid and gas streams.

- ✓ CONDENSE – A flash separator that functions as a condenser for separating the liquid stream from the non-condensable gases formed.

The following assumptions were made for the simulation:

- ✓ The process is at steady state.
- ✓ The pressure inside the pyrolysis reactor and condenser unit is 1 atm.
- ✓ The stream BLEND was specified at 25 ^{o}C and 1 atm pressure.
- ✓ Ultimate, proximate and sulphur compositions of the biomass blends were calculated from the weight fraction of each biomass component in the blend. For example, the ash content of AB and DS was 11.5 and 32.97 wt % respectively. So, for combination 17 (AB: DS = 2:1 wt/wt), the ash content was calculated as 18.66 wt % [(11.5 x 0.6667) + (32.97 x 0.3333)].
- ✓ In ultimate analysis, the Cl content was assumed to be zero.
- ✓ Ultimate composition (C, H, N, Cl, S and O) of BLEND is the same in the PRODUCT (including both the solid and pyrolysis vapor products before their respective streams get separated via SEPSOLID block) stream coming out from the RYIELD reactor.

The physical property thermodynamic model used in this simulation was “PENG-ROB (Peng Robinson)”. MIXNC was used as the stream structure for defining the non-conventional input of “BLEND” stream. The density and enthalpy of these two streams were modelled using “DCOALIGT” and “HCOALGEN” models respectively. For this, proximate, ultimate and sulphur analysis of the blend had to be specified. The temperature for the blocks “PYROLYSI”, “SOLIDSEP” and “CONDENSE” were specified as 500 ^{o}C for the first two and 5 ^{o}C for the latter, respectively. For mass balance across the RYield reactor, several FORTRAN statements were written in the calculator block for the same.

The simulation was performed on 9 combinations (the pure biomass of AB, CW and DS, and their various non-catalytic mixture) selected from the experimental design used for the DSC runs (Table 1). For mass and energy balance, the system boundary for the whole pyrolysis unit comprised of the input stream of "BLEND" and the outlet streams of "SOLID", "GAS", and "LIQUID". Furthermore, each of the three blocks from the flowsheet represented a sub–boundary, where the mass and energy balance was performed for the input and output streams at that specific block. For instance, PYROLYSI block represented a sub-boundary for the input stream of BLEND and the output stream of PRODUCT from the block. In the same way, SOLIDSEP represented the sub-boundary for balancing mass and energy for the inlet stream of PRODUCT and outlet stream of PRODGAS and SOLID. Finally, CONDENSE was the sub-boundary for the inlet stream of PRODGAS and outlet of GAS and LIQUID stream.

Based on these defined unit boundaries, the stated assumptions and input (mass flow rate of BLEND = 20 g/day), mass balance was performed (Figure 32) for the 9 combinations. For the three pure biomasses, it was found that mass flow (g/day) was the highest (6.59) for SOLID stream for DS, while it was lowest (2.3) for AB. The latter results are due to the high ash content of DS and volatile content of AB. When considering the mass flow of GAS, it was highest for CW (10.23) and lowest (8.98) for DS. In case of LIQUID stream, the value obtained was maximum (7.73) for AB and was minimum for DS (4.43).

When considering the mass balance of the various mixtures of the three biomasses, mass flow rate of SOLID stream was the highest (5.47) for combination 7 [CW: DS = 1:2 wt/wt]. Consequently for the same combination the mass flow was lowest for LIQUID (5.14) stream. But, for combination 15 [AB: CW = 2:1 wt/wt], the mass flow rate of SOLID (2.6) was the lowest, while it was highest for the LIQUID (7.34) stream. A possible explanation for this trend, as seen from the mass flow balance for SOLID stream was that the higher content of heavy metals (along with low volatile matter) present in the DS component of combination 7, in

addition to the lignin from the CW component promoted secondary interaction of the volatiles released during co-pyrolysis of the blend. This enhanced the yield of bio-char i.e. SOLID and led to the higher mass flow of it as compared to that of LIQUID and GAS. As DS was replaced with AB in combination 7, in the same weight fraction (combination 15), the volatile matter content of the biomass mix was enhanced, which minimized these secondary interaction of the volatiles released during co-pyrolysis. This, possibly boosted the yield of bio-oil from combination 15, thereby, enhancing the mass flow for LIQUID stream. Comparing the LIQUID mass flow of combination 15 with that of the three pure biomasses, it was found to be higher than that of CW (6.56) and DS (4.43), but slightly lower than AB (7.73). From this, it can be inferred that there was possible synergistic interaction between the biomass components AB and CW in combination 15 as far as enhancement of the mass flow of LIQUID stream (and thereby yield of pyrolysis liquid product) was concerned.

While considering the enthalpy flow of the 6 streams for the three pure biomasses (Figure 33), it was found that the highest enthalpy flow for PRODUCT (4.07) and PRODGAS (4.11) was obtained for AB, while the same was lowest for DS [PRODUCT (2.36) and PRODGAS (2.46)]. As a result, the same trend was observed for LIQUID stream for a given biomass combination. So, for AB the enthalpy flow for LIQUID (1.95) was relatively higher than that of DS (1.12). In case of biomass mixtures, same trend like that of mass flow was observed in case of combination 7 and 15. Therefore, combination 7 had lowest enthalpy flow in the streams PRODUCT (2.71), PRODGAS (2.79) and LIQUID (1.30) as compared to that of combination 15 [PRODUCT (3.85), PRODGAS (3.89) and LIQUID (1.85)]. When the enthalpy flow for LIQUID stream for combination 7 was compared with that of the three pure biomasses, it was realized to be lower than that of AB (1.95) and CW (1.65), but slightly higher than that of DS (1.12).

It is known that biomass is a poor conductor of heat. So, blending CW with DS, at twice the amount of CW used, can potentially help improve the heat conduction through the biomass owing

to its high ash content. Thus, the energy consumption for production of pyrolysis liquid got reduced. This suggests possible synergistic interaction between CW and DS components of combination 7.

The enthalpy flow from SOLID stream was negative implying energy release due to char formation which is an exothermic reaction. This finding is consistent with that of reports in literature (Mok & Antal, 1983; Oyedun et al., 2013; Rath et al., 2003). As expected, high mass flow rate of liquid is associated with high enthalpy flow or energy consumption.

Another essential information gathered from enthalpy flow of the ASPEN PLUS simulation was heat duty (kJ/hr) for the PYROLYSI and CONDENSE block for the 9 combinations (Table 18). In case of PYROLYSI block functioning as pyrolysis reactor, heat duty gives an idea of the heat absorbed in the pyrolysis reactor during the pyrolysis of BLEND to give PRODUCT. This heat includes sensible heat, latent heat for vaporization as pyrolysis vapors get generated, and heat of different reactions (decarboxylation, decarbonylation, dehydration etc.) that occur during pyrolysis (Nwaoha et al., 2017). For CONDENSE block, heat duty is the amount of heat released from the cooling of the pyrolysis vapors.

For the three pure biomasses of AB, CW and DS, for PYROLYSI block heat duty (kJ/hr) was highest for CW (8.8) and lowest for DS (6.93). When considering the same for CONDENSE block, the heat duty was highest for AB (-2.05), but lowest for DS (-1.23). In case of biomass mixtures, heat duty for PYROLYSI block was found to be highest for combination 15 (8.72), but lowest for combination 11 [AB: DS = 1:2 wt/wt] (7.51). For CONDENSE block, it was highest for combination 15 (-1.93) but lowest for combination 7 (-1.39) [for combination 11, it was low (-1.50), but slightly higher than combination 7].

The catalytic activity of ash in DS is capable of reducing heat consumption in the pyrolysis reactor (PYROLYSI) during pyrolysis. As a result of this, the heat duty was lowest for

combination 11, as compared to other biomass mixture combinations. Therefore, co-pyrolysis using DS leads to decreased energy consumption in the pyrolysis reactor. Furthermore, heat released in the condenser unit (CONDENSE) of the pyrolysis system was correlated with the amount of heat consumed in the pyrolysis reactor. So, as more heat is absorbed by the reactor, more heat will be released in the condenser system. This study demonstrated that mass and heat balances of a co-pyrolysis process can be successfully analyzed via ASPEN PLUS simulation. Furthermore, the simulation results are in consistent with the findings of the DSC study.

CHAPTER V

CONCLUSIONS

This is the first study reporting investigation of co-pyrolysis of the biomass from AB, CW and DS with and without a catalyst (ZSM–5). The selected biomass samples had very diverse chemical composition indicating their suitability for optimizing a biomass blend for a given application.

A RSM design comprising 18 biomass mixtures with and without a catalyst was developed to model E_a, ΔH and ΔG for the process. The experimental data was collected via a DSC method at the heating rates of 10, 15 and 20 ^oC/min and biomass degradation kinetic parameter, E_a, ΔH, ΔG and pre-exponential factor A were calculated according to the Floor Wynn Ozawa (FWO) method. The models developed for E_a and ΔH were statistically significant and did not have lack of fit. However, ANOVA analysis indicated that RSM was not suitable for modeling ΔG using the experimental design developed for this study. The RSM model developed for AB and DS blends were used to determine the optimum biomass mixture (OM) for low pyrolysis energy requirement. The following blend composition was identified as the OM with catalyst, ZSM-5, at a catalyst: biomass weight ratio of 2:1 (OC) using the 3D contour plots and the RSM model developed: 57.14 wt % DS; 4.29 wt % AB and 38.57 wt % CW. OC had low E_a, 52.75 kJ/mol and ΔH, 45.37 kJ/mol. The experimental results clearly demonstrated that co-pyrolysis of AB, DS and CW at optimum weight fractions is capable of lowering system energy requirements for

pyrolysis i.e. E_a and ΔH. The results obtained from the DSC experiments also indicated that catalytic pyrolysis further reduced the energy required for the pyrolysis reactions.

Large scale pyrolysis tests carried out in a furnace were slow pyrolysis owing to the restriction on the average heating rate (14 ^{o}C/min). The results of the latter experiments demonstrated that biomass composition had a significant effect on the bio-oil, bio-char and gas yields and composition. The mass balance calculations based on the recovered bio-char and bio-oil amounts indicate that AB produced the highest amount of bio-oil, 14.8 wt %. The calculated bio-oil yields in the presence of the catalyst was even lower than those without a catalyst. However, it is important to note that absolute values of the calculated yields are underestimation of the actual liquid stream yields due to the large losses in the system especially with condensation of bio – oil in the steel tubing that connects the furnace outlet with the condenser unit.

Pyrolysis of pure AB, DS, CW and their mixtures without catalyst did not produce significant amount of AH. Catalytic pyrolysis significantly increased AH production. The highest AH was produced using OC and a catalytic blend (catalyst: biomass = 2:1 wt/wt) of biomass mixture containing equal amount of AB, DS and CW, 83.12 and 89.38 wt %, respectively. The experimental result obtained with OM at different catalyst loading ratio confirmed that higher catalyst loading enhances AH content of the bio-oil produced. For example, AH in the bio-oil increased from 22.88 to 83.12 wt % when catalyst: OM ratio increased from 0.5 to 2. AH in the bio-oil consisted of polyromantic hydrocarbons of naphthalene, anthracene and their methyl derivatives.

Finally, the mass and energy transfer across the various streams of the pyrolysis system were evaluated via ASPEN PLUS simulation. Since, the simulation software is developed for non-catalytic pyrolysis, only biomass mixtures without catalyst were examined. Heat duty for both the pyrolysis reactor and the condenser unit of the pyrolysis system were also determined.

The highest amount of PROGAS (LIQUID + GAS) was produced by pure AB. This is due to the higher volatile content of AB. The highest SOLID (bio-char) amount was produced from DS due to its very high ash content. Biomass blend with high DS amount also produced higher amount of SOLID. From these results it can be concluded that the mass balance simulation describes the system well and in agreement with the results obtained from DSC experiments.

Heat duty for the pure DS and the biomass blends with high DS amount, 66.67%, were lower due to their high ash and lower organic matter content to be decomposed in the blend. Heat released from the condenser was highest for the pure AB and the biomass mix with highest AB fraction, 66.67%, due to the high amount of PRODGAS processed in the CONDENSE block.

In conclusion, this study supports our hypothesis that co-pyrolysis of AB, DS and CW lowers the process energy requirement and catalytic co-pyrolysis allows customization of the final product, specifically bio-oil composition for desired applications.

CHAPTER VI

FUTURE WORK

1) Due to the limitations of the DSC instrument available for this study, the temperature range for the experiments was selected as 25 – 500^{o}C. Further research is needed to examine the bio-oil yield and composition from AB, DS and CW mixtures at higher temperatures.
2) The biomass blend optimization study examined the effect of catalyst at only one loading ratio, catalyst: biomass ratio of 2. Considering that high catalyst amount in the system reduces feedstock loading and increases operational cost, more research is needed to determine the optimal catalyst loading for desirable bio-oil yield and composition.
3) A better pyrolysis system design, i.e. shorter reactor and condenser system connections and better insulation, could have improved the product recovery and the results of mass balance calculations.
4) The experimental design used for the DSC experiments did not lead to a significant ΔG model. Hence, the RSM models can be further improved by including more biomass combinations into the experimental design.
5) A pyrolysis system with an online analysis system that will allow the evaluation of PRODGAS chemical composition would be helpful to better describe the chemical reactions as affected by the changes in feedstock composition.
6) Dilution of the bio-oil obtained from the catalytic pyrolysis of CW with HPLC grade dichloromethane caused precipitation of some of the bio-oil components. Further analytical

testing of the bio-oil and the precipitate could be helpful to better understand the bio-oil characteristics.

7) Utilization of the residual bio-char obtained from the co-pyrolysis tests with and without ZSM-5 as a catalyst should be explored to enhance the process economics.
8) This study only examined ZSM-5 for catalytic co-pyrolysis of AB, DS and CW. The effect of other catalysts on product yield and compositions could advance our understanding of the AB, DS and CW mixture behavior during pyrolysis.

REFERENCES

AACC Approved Methods of Analysis, 11th Ed. Method 66-20.01. Determination of Granularity of Semolina and Farina: Sieving Method (1999). Cereals & Grains Association, St. Paul, MN, U.S.A.

Abnisa, F., & Daud, W. M. A. W. (2014). A review on co-pyrolysis of biomass: an optional technique to obtain a high-grade pyrolysis oil. *Energy Conversion and Management, 87*, 71-85.

Agatonovic-Kustrin, S., Morton, D. W., & Ristivojević, P. (2016). Assessment of antioxidant activity in Victorian marine algal extracts using high performance thin-layer chromatography and multivariate analysis. *Journal of Chromatography A, 1468*, 228-235.

Agrafioti, E., Bouras, G., Kalderis, D., & Diamadopoulos, E. (2013). Biochar production by sewage sludge pyrolysis. *Journal of Analytical and Applied Pyrolysis, 101*, 72-78.

Agrawal, A., & Chakraborty, S. (2013). A kinetic study of pyrolysis and combustion of microalgae Chlorella vulgaris using thermo-gravimetric analysis. *Bioresource technology, 128*, 72-80.

Ahmad, M., & Eskicioglu, C. (2019). Fate of sterols, polycyclic aromatic hydrocarbons, pharmaceuticals, ammonia and solids in single-stage anaerobic and sequential anaerobic/aerobic/anoxic sludge digestion. *Waste Management, 93*, 72-82.

Ahmad, M.S., Mehmood, M. A., Al Ayed, O. S., Ye, G., Luo, H., Ibrahim, M., . . . Qadir, G. (2017a). Kinetic analyses and pyrolytic behavior of Para grass (Urochloa mutica) for its bioenergy potential. *Bioresource technology, 224*, 708-713.

Ahmad, M.S., Mehmood, M. A., Taqvi, S. T. H., Elkamel, A., Liu, C.-G., Xu, J., . . . Gull, M. (2017b). Pyrolysis, kinetics analysis, thermodynamics parameters and reaction mechanism of Typha latifolia to evaluate its bioenergy potential. *Bioresource technology, 245*, 491-501.

Aho, A., Kumar, N., Eränen, K., Salmi, T., Hupa, M., & Murzin, D. Y. (2008). Catalytic pyrolysis of woody biomass in a fluidized bed reactor: Influence of the zeolite structure. *Fuel, 87*(12), 2493-2501.

Akella, A., Saini, R., & Sharma, M. P. (2009). Social, economical and environmental impacts of renewable energy systems. *Renewable energy*, *34*(2), 390-396.

Ali, S. A. M., Razzak, S. A., & Hossain, M. M. (2015). Apparent kinetics of high temperature oxidative decomposition of microalgal biomass. *Bioresource technology*, *175*, 569-577.

Alvarez, E.A., Mochon, M. C., Sánchez, J. J., & Rodríguez, M. T. (2002). Heavy metal extractable forms in sludge from wastewater treatment plants. *Chemosphere*, *47*(7), 765-775.

Alvarez, J., Amutio, M., Lopez, G., Bilbao, J., & Olazar, M. (2015). Fast co-pyrolysis of sewage sludge and lignocellulosic biomass in a conical spouted bed reactor. *Fuel*, *159*, 810-818.

Alvarez, J., Lopez, G., Amutio, M., Bilbao, J., & Olazar, M. (2014). Bio-oil production from rice husk fast pyrolysis in a conical spouted bed reactor. *Fuel*, *128*, 162-169.

Amutio, M., Lopez, G., Aguado, R., Artetxe, M., Bilbao, J., & Olazar, M. (2011). Effect of vacuum on lignocellulosic biomass flash pyrolysis in a conical spouted bed reactor. *Energy & Fuels*, *25*(9), 3950-3960.

Anand, V., Sunjeev, V., & Vinu, R. (2016). Catalytic fast pyrolysis of Arthrospira platensis (spirulina) algae using zeolites. *Journal of Analytical and Applied Pyrolysis*, *118*, 298-307.

Anca-Couce, A., Berger, A., & Zobel, N. (2014). How to determine consistent biomass pyrolysis kinetics in a parallel reaction scheme. *Fuel*, *123*, 230-240.

Antal, M. J. J., & Varhegyi, G. (1995). Cellulose pyrolysis kinetics: the current state of knowledge. *Industrial & Engineering Chemistry Research*, *34*(3), 703-717.

Asif, M., Bak, C.-u., Saleem, M. W., & Kim, W.-S. (2015). Performance evaluation of integrated gasification combined cycle (IGCC) utilizing a blended solution of ammonia and 2-amino-2-methyl-1-propanol (AMP) for CO2 capture. *Fuel*, *160*, 513-524.

Atsonios, K., Kougioumtzis, M. A., Grammelis, P., & Kakaras, E. (2017). Process integration of a polygeneration plant with biomass/coal co-pyrolysis. *Energy & Fuels*, *31*(12), 14408-14422.

Babich, I., Van der Hulst, M., Lefferts, L., Moulijn, J., O'Connor, P., & Seshan, K. (2011). Catalytic pyrolysis of microalgae to high-quality liquid bio-fuels. *Biomass and Bioenergy*, *35*(7), 3199-3207.

Bendel, R. B., & Afifi, A. A. (1977). Comparison of stopping rules in forward "stepwise" regression. *Journal of the American Statistical association, 72*(357), 46-53.

Bezerra, M. A., Santelli, R. E., Oliveira, E. P., Villar, L. S., & Escaleira, L. A. (2008). Response surface methodology (RSM) as a tool for optimization in analytical chemistry. *Talanta, 76*(5), 965-977.

Bordoloi, N., Narzari, R., Sut, D., Saikia, R., Chutia, R. S., & Kataki, R. (2016). Characterization of bio-oil and its sub-fractions from pyrolysis of Scenedesmus dimorphus. *Renewable energy, 98*, 245-253.

Braga, R. M., Melo, D. M., Aquino, F. M., Freitas, J. C., Melo, M. A., Barros, J. M., & Fontes, M. S. (2014). Characterization and comparative study of pyrolysis kinetics of the rice husk and the elephant grass. *Journal of Thermal Analysis and Calorimetry, 115*(2), 1915-1920.

Branca, C., Albano, A., & Di Blasi, C. (2005). Critical evaluation of global mechanisms of wood devolatilization. *Thermochimica acta, 429*(2), 133-141.

Brebu, M., & Vasile, C. (2010). Thermal degradation of lignin—a review. *Cellulose Chemistry & Technology, 44*(9), 353.

Bridgwater, A., Meier, D., & Radlein, D. (1999). An overview of fast pyrolysis of biomass. *Organic geochemistry, 30*(12), 1479-1493.

Bui, H.-H., Tran, K.-Q., & Chen, W.-H. (2016). Pyrolysis of microalgae residues–a kinetic study. *Bioresource technology, 199*, 362-366.

Bursac, Z., Gauss, C. H., Williams, D. K., & Hosmer, D. W. (2008). Purposeful selection of variables in logistic regression. *Source code for biology and medicine, 3*(1), 17.

Cai, J., Wu, W., Liu, R., & Huber, G. W. (2013). A distributed activation energy model for the pyrolysis of lignocellulosic biomass. *Green Chemistry, 15*(5), 1331-1340.

Campanella, A., Muncrief, R., Harold, M. P., Griffith, D. C., Whitton, N. M., & Weber, R. S. (2012). Thermolysis of microalgae and duckweed in a CO2-swept fixed-bed reactor: bio-oil yield and compositional effects. *Bioresource technology, 109*, 154-162.

Cao, J.-P., Li, L.-Y., Morishita, K., Xiao, X.-B., Zhao, X.-Y., Wei, X.-Y., & Takarada, T. (2013). Nitrogen transformations during fast pyrolysis of sewage sludge. *Fuel, 104*, 1-6.

Çepelioğullar, Ö., & Pütün, A. E. (2013). Thermal and kinetic behaviors of biomass and plastic wastes in co-pyrolysis. *Energy Conversion and Management, 75*, 263-270.

Ceylan, S., & Kazan, D. (2015). Pyrolysis kinetics and thermal characteristics of microalgae Nannochloropsis oculata and Tetraselmis sp. *Bioresource technology, 187*, 1-5.

Chen, W., Chen, Y., Yang, H., Xia, M., Li, K., Chen, X., & Chen, H. (2017). Co-pyrolysis of lignocellulosic biomass and microalgae: Products characteristics and interaction effect. *Bioresource technology, 245*, 860-868.

Chen, D., Li, Y., Cen, K., Luo, M., Li, H., & Lu, B. (2016). Pyrolysis polygeneration of poplar wood: Effect of heating rate and pyrolysis temperature. *Bioresource technology, 218*, 780-788.

Chen, C., Ma, X., & He, Y. (2012). Co-pyrolysis characteristics of microalgae Chlorella vulgaris and coal through TGA. *Bioresource technology, 117*, 264-273.

Chen, W., Yang, H., Chen, Y., Xia, M., Yang, Wang, X., & Chen, H. (2017). Algae pyrolytic poly-generation: Influence of component difference and temperature on products characteristics. *Energy, 131*, 1-12.

Chisti, Y. (2008). Biodiesel from microalgae beats bioethanol. *Trends in biotechnology, 26*(3), 126-131.

Cho, J., Chu, S., Dauenhauer, P. J., & Huber, G. W. (2012). Kinetics and reaction chemistry for slow pyrolysis of enzymatic hydrolysis lignin and organosolv extracted lignin derived from maplewood. *Green Chemistry, 14*(2), 428-439.

Ciajolo, A., & Barbella, R. (1984). Pyrolysis and oxidation of heavy fuel oils and their fractions in a thermogravimetric apparatus. *Fuel, 63*(5), 657-661.

Cornelissen, T., Yperman, J., Reggers, G., Schreurs, S., & Carleer, R. (2008). Flash co-pyrolysis of biomass with polylactic acid. Part 1: Influence on bio-oil yield and heating value. *Fuel, 87*(7), 1031-1041.

Cunliffe, A. M., & Williams, P. T. (1998). Composition of oils derived from the batch pyrolysis of tyres. *Journal of Analytical and Applied Pyrolysis, 44*(2), 131-152.

Danmaliki, G. I., Saleh, T. A., & Shamsuddeen, A. A. (2017). Response surface methodology optimization of adsorptive desulfurization on nickel/activated carbon. *Chemical Engineering Journal, 313*, 993-1003.

Darmawan, A., Hardi, F., Yoshikawa, K., Aziz, M., & Tokimatsu, K. (2017). Enhanced process Integration of entrained flow gasification and combined cycle: modeling and simulation using Aspen Plus. *Energy Procedia, 105*, 303-308.

Daugaard, D. E., & Brown, R. C. (2003). Enthalpy for pyrolysis for several types of biomass. *Energy & Fuels*, *17*(4), 934-939.

De Wild, P., Van der Laan, R., Kloekhorst, A., & Heeres, E. (2009). Lignin valorisation for chemicals and (transportation) fuels via (catalytic) pyrolysis and hydrodeoxygenation. *Environmental Progress & Sustainable Energy: An Official Publication of the American Institute of Chemical Engineers, 28*(3), 461-469.

Demirbas, A. (2007). Importance of biodiesel as transportation fuel. *Energy policy, 35*(9), 4661-4670.

Demirbaş, A. (2000). Mechanisms of liquefaction and pyrolysis reactions of biomass. *Energy Conversion and Management, 41*(6), 633-646.

Du, Z., Hu, B., Ma, X., Cheng, Y., Liu, Y., Lin, X., . . . Ruan, R. (2013). Catalytic pyrolysis of microalgae and their three major components: carbohydrates, proteins, and lipids. *Bioresource technology, 130*, 777-782.

Du, Z., Li, Y., Wang, X., Wan, Y., Chen, Q., Wang, C., . . . Ruan, R. (2011). Microwave-assisted pyrolysis of microalgae for biofuel production. *Bioresource technology, 102*(7), 4890-4896.

Dunford, N., Hiziroglu, S., & Holcomb, R. (2007). Effect of age on the distribution of oil in Eastern redcedar tree segments. *Bioresource technology, 98*(14), 2636-2640.

E871-72, A. (1998). 871-82, 1998. *Standard test method for volatile matter in the analysis of particulate wood fuels*.

E872-82, A. A. (2013). Standard test method for volatile matter in the analysis of particulate wood fuels. In: ASTM International West Conshohocken, PA.

Effendi, A., Gerhauser, H., & Bridgwater, A. (2008). Production of renewable phenolic resins by thermochemical conversion of biomass: a review. *Renewable and Sustainable Energy Reviews, 12*(8), 2092-2116.

Encinar, J., Gonzalez, J., & Gonzalez, J. (2000). Fixed-bed pyrolysis of Cynara cardunculus L. Product yields and compositions. *Fuel Processing Technology, 68*(3), 209-222.

Ennaert, T., Van Aelst, J., Dijkmans, J., De Clercq, R., Schutyser, W., Dusselier, M., . . . Sels, B. F. (2016). Potential and challenges of zeolite chemistry in the catalytic conversion of biomass. *Chemical Society Reviews, 45*(3), 584-611.

Eom, I.-Y., Kim, J.-Y., Kim, T.-S., Lee, S.-M., Choi, D., Choi, I.-G., & Choi, J.-W. (2012). Effect of essential inorganic metals on primary thermal degradation of lignocellulosic biomass. *Bioresource technology, 104*, 687-694.

Erarpat, S., Özzeybek, G., Chormey, D. S., Erulaş, F., Turak, F., & Bakırdere, S. (2017). A novel liquid-liquid extraction for the determination of naphthalene by GC-MS with deuterated anthracene as internal standard. *Environmental monitoring and assessment, 189*(10), 528.

Fabbri, D., & Torri, C. (2016). Linking pyrolysis and anaerobic digestion (Py-AD) for the conversion of lignocellulosic biomass. *Current opinion in biotechnology, 38*, 167-173.

Fernandez, A., Saffe, A., Pereyra, R., Mazza, G., & Rodriguez, R. (2016). Kinetic study of regional agro-industrial wastes pyrolysis using non-isothermal TGA analysis. *Applied Thermal Engineering, 106*, 1157-1164.

Folgueras, M., Alonso, M., & Díaz, R. (2013). Influence of sewage sludge treatment on pyrolysis and combustion of dry sludge. *Energy, 55*, 426-435.

Foltin, J. P., Prado, G. N., & Lisbôa, A. C. (2017). Kinetic Analysis of the Oil Shale Pyrolysis using Thermogravimetry and Differential Scanning Calorimetry. *Chemical Engineering Transactions, 61*, 559-564.

Fonts, I., Azuara, M., Lázaro, L., Gea, G., & Murillo, M. (2009). Gas chromatography study of sewage sludge pyrolysis liquids obtained at different operational conditions in a fluidized bed. *Industrial & Engineering Chemistry Research, 48*(12), 5907-5915.

Fonts, I., Gea, G., Azuara, M., Ábrego, J., & Arauzo, J. (2012). Sewage sludge pyrolysis for liquid production: a review. *Renewable and Sustainable Energy Reviews, 16*(5), 2781-2805.

Francioso, O., Rodriguez-Estrada, M. T., Montecchio, D., Salomoni, C., Caputo, A., & Palenzona, D. (2010). Chemical characterization of municipal wastewater sludges produced by two-phase anaerobic digestion for biogas production. *Journal of hazardous materials, 175*(1-3), 740-746.

Gao, N., Li, J., Qi, B., Li, A., Duan, Y., & Wang, Z. (2014). Thermal analysis and products distribution of dried sewage sludge pyrolysis. *Journal of Analytical and Applied Pyrolysis, 105*, 43-48.

Gao, L., Sun, J., Xu, W., & Xiao, G. (2017). Catalytic pyrolysis of natural algae over Mg-Al layered double oxides/ZSM-5 (MgAl-LDO/ZSM-5) for producing bio-oil with low nitrogen content. *Bioresource technology, 225*, 293-298.

Girija, B., Sailaja, R., & Madras, G. (2005). Thermal degradation and mechanical properties of PET blends. *Polymer degradation and stability*, *90*(1), 147-153.

Goos, P., Syafitri, U., Sartono, B., & Vazquez, A. (2020). A nonlinear multidimensional knapsack problem in the optimal design of mixture experiments. *European Journal of Operational Research*, *281*(1), 201-221.

Gutermuth, P.-G. (1998). Financial measures by the state for the enhanced deployment of renewable energies. *Solar Energy, 64*(1-3), 67-78.

Harman-Ware, A. E., Morgan, T., Wilson, M., Crocker, M., Zhang, J., Liu, K., . . . Debolt, S. (2013). Microalgae as a renewable fuel source: fast pyrolysis of Scenedesmus sp. *Renewable energy, 60*, 625-632.

Harun, R., Danquah, M. K., & Forde, G. M. (2010). Microalgal biomass as a fermentation feedstock for bioethanol production. *Journal of Chemical Technology & Biotechnology*, *85*(2), 199-203.

Haykiri-Acma, H., & Yaman, S. (2010). Interaction between biomass and different rank coals during co-pyrolysis. *Renewable energy, 35*(1), 288-292.

Hietala, D. C., & Savage, P. E. (2015). Reaction pathways and kinetics of cholesterol in high-temperature water. *Chemical Engineering Journal, 265*, 129-137.

Hoffmann, J., Rudra, S., Toor, S. S., Holm-Nielsen, J. B., & Rosendahl, L. A. (2013). Conceptual design of an integrated hydrothermal liquefaction and biogas plant for sustainable bioenergy production. *Bioresource technology*, *129*, 402-410.

Holland, B., & Hay, J. (2002). The thermal degradation of PET and analogous polyesters measured by thermal analysis–Fourier transform infrared spectroscopy. *Polymer, 43*(6), 1835-1847.

Hossain, M. A., Yeasmin, F., Rahman, S. M., & Rana, M. (2016). Gas chromatograph–mass spectrometry determination of carcinogenic naphthalene, anthracene, phenanthrene and fluorene in the Bangsai river water of Bangladesh. *Arabian Journal of Chemistry, 9*, S109-S113.

Hua, M.-Y., & Li, B.-X. (2016). Co-pyrolysis characteristics of the sugarcane bagasse and Enteromorpha prolifera. *Energy Conversion and Management, 120*, 238-246.

Iliopoulou, E. F., Stefanidis, S., Kalogiannis, K., Delimitis, A., Lappas, A., & Triantafyllidis, K. (2012). Catalytic upgrading of biomass pyrolysis vapors using transition metal-modified ZSM-5 zeolite. *Applied Catalysis B: Environmental*, *127*, 281-290.

Intl, A. (1995). Official methods of analysis of AOAC International. *Arlington, Va.: AOAC Intl. pv (loose-leaf)*.

Isahak, W. N. R. W., Hisham, M. W., Yarmo, M. A., & Hin, T.-y. Y. (2012). A review on bio-oil production from biomass by using pyrolysis method. *Renewable and Sustainable Energy Reviews, 16*(8), 5910-5923.

Kan, T., Strezov, V., & Evans, T. J. (2016). Lignocellulosic biomass pyrolysis: A review of product properties and effects of pyrolysis parameters. *Renewable and Sustainable Energy Reviews, 57*, 1126-1140.

Karnjanakom, S., Bayu, A., Hao, X., Kongparakul, S., Samart, C., Abudula, A., & Guan, G. (2016). Selectively catalytic upgrading of bio-oil to aromatic hydrocarbons over Zn, Ce or Ni-doped mesoporous rod-like alumina catalysts. *Journal of Molecular Catalysis A: Chemical, 421*, 235-244.

Kim, S.J., Jung, S.-H., & Kim, J.-S. (2010). Fast pyrolysis of palm kernel shells: influence of operation parameters on the bio-oil yield and the yield of phenol and phenolic compounds. *Bioresource technology, 101*(23), 9294-9300.

Kim, P., Johnson, A., Edmunds, C. W., Radosevich, M., Vogt, F., Rials, T. G., & Labbé, N. (2011). Surface functionality and carbon structures in lignocellulosic-derived biochars produced by fast pyrolysis. *Energy & Fuels, 25*(10), 4693-4703.

Kim, Y., & Parker, W. (2008). A technical and economic evaluation of the pyrolysis of sewage sludge for the production of bio-oil. *Bioresource technology, 99*(5), 1409-1416.

Kok, M. V., & Gundogar, A. S. (2013). DSC study on combustion and pyrolysis behaviors of Turkish crude oils. *Fuel Processing Technology, 116*, 110-115.

Lam, M. K., & Lee, K. T. (2012). Microalgae biofuels: a critical review of issues, problems and the way forward. *Biotechnology advances, 30*(3), 673-690.

Lee, S., Kim, S.-B., Kim, J.-E., Kwon, G.-S., Yoon, B.-D., & Oh, H.-M. (1998). Effects of harvesting method and growth stage on the flocculation of the green alga Botryococcus braunii. *Letters in applied microbiology, 27*(1), 14-18.

Lee, J.Y., Yoo, C., Jun, S.-Y., Ahn, C.-Y., & Oh, H.-M. (2010). Comparison of several methods for effective lipid extraction from microalgae. *Bioresource technology, 101*(1), S75-S77.

Li, S., Chen, X., Liu, A., Wang, L., & Yu, G. (2014). Study on co-pyrolysis characteristics of rice straw and Shenfu bituminous coal blends in a fixed bed reactor. *Bioresource technology, 155*, 252-257.

Lin, T., Goos, E., & Riedel, U. (2013). A sectional approach for biomass: Modelling the pyrolysis of cellulose. *Fuel Processing Technology*, *115*, 246-253.

Liu, C., Kaneko, S., Komoto, Y., Fujii, S., & Kiguchi, M. (2015). Highly conductive single naphthalene and anthracene molecular junction with well-defined conductance. *Applied Physics Letters*, *106*(10), 103103.

Liu, Q., Wang, Zheng, Y., Luo, Z., & Cen, K. (2008). Mechanism study of wood lignin pyrolysis by using TG–FTIR analysis. *Journal of Analytical and Applied Pyrolysis*, *82*(1), 170-177.

López-González, D., Fernandez-Lopez, M., Valverde, J., & Sanchez-Silva, L. (2014). Kinetic analysis and thermal characterization of the microalgae combustion process by thermal analysis coupled to mass spectrometry. *Applied Energy*, *114*, 227-237.

Luo, Z., Wang, Liao, Y., Zhou, J., Gu, Y., & Cen, K. (2004). Research on biomass fast pyrolysis for liquid fuel. *Biomass and Bioenergy*, *26*(5), 455-462.

Ma, S., Lu, J., & Gao, J. (2002). Study of the low temperature pyrolysis of PVC. *Energy & Fuels*, *16*(2), 338-342.

Maddi, B., Viamajala, S., & Varanasi, S. (2011). Comparative study of pyrolysis of algal biomass from natural lake blooms with lignocellulosic biomass. *Bioresource technology*, *102*(23), 11018-11026.

Maia, A. A. D., & de Morais, L. C. (2016). Kinetic parameters of red pepper waste as biomass to solid biofuel. *Bioresource technology*, *204*, 157-163.

Mäkinen, K. K., & Tenovuo, J. (1982). Observations on the use of guaiacol and 2, 2′-azino-di (3-ethylbenzthiazoline-6-sulfonic acid) as peroxidase substrates. *Analytical biochemistry*, *126*(1), 100-108.

Marcilla, A., Beltrán, M., & Navarro, R. (2008). Evolution of products generated during the dynamic pyrolysis of LDPE and HDPE over HZSM5. *Energy & Fuels*, *22*(5), 2917-2924.

Marcilla, A., Catalá, L., García-Quesada, J. C., Valdés, F., & Hernández, M. (2013). A review of thermochemical conversion of microalgae. *Renewable and Sustainable Energy Reviews*, *27*, 11-19.

Markou, G., Angelidaki, I., & Georgakakis, D. (2012). Microalgal carbohydrates: an overview of the factors influencing carbohydrates production, and of main bioconversion technologies for production of biofuels. *Applied microbiology and biotechnology*, *96*(3), 631-645.

Mehrabadi, A., Craggs, R., & Farid, M. M. (2017). Pyrolysis of wastewater treatment high rate algal pond (WWT HRAP) biomass. *Algal Research, 24*, 509-519.

Messina, L. G., Bonelli, P., & Cukierman, A. (2015). Copyrolysis of peanut shells and cassava starch mixtures: Effect of the components proportion. *Journal of Analytical and Applied Pyrolysis, 113*, 508-517.

Miao, X., Wu, Q., & Yang, C. (2004). Fast pyrolysis of microalgae to produce renewable fuels. *Journal of Analytical and Applied Pyrolysis, 71*(2), 855-863.

Miller, R. O., Gavlak, R., & Horneck, D. (2013). Soil, plant, and water reference methods for the western region. *Western Regional Extension Publication (WREP), 125*.

Mohamed, B. A., Kim, C. S., Ellis, N., & Bi, X. (2016). Microwave-assisted catalytic pyrolysis of switchgrass for improving bio-oil and biochar properties. *Bioresource technology, 201*, 121-132.

Mohan, D., Pittman, C. U., & Steele, P. H. (2006). Pyrolysis of wood/biomass for bio-oil: a critical review. *Energy & Fuels, 20*(3), 848-889.

Mok, W. S.-L., & Antal Jr, M. J. (1983). Effects of pressure on biomass pyrolysis. II. Heats of reaction of cellulose pyrolysis. *Thermochimica acta, 68*(2-3), 165-186.

Mullen, C. A., & Boateng, A. A. (2010). Catalytic pyrolysis-GC/MS of lignin from several sources. *Fuel Processing Technology, 91*(11), 1446-1458.

Nwaoha, C., Idem, R., Supap, T., Saiwan, C., Tontiwachwuthikul, P., Rongwong, W., . . . Benamor, A. (2017). Heat duty, heat of absorption, sensible heat and heat of vaporization of 2–Amino–2–Methyl–1–Propanol (AMP), Piperazine (PZ) and Monoethanolamine (MEA) tri–solvent blend for carbon dioxide (CO2) capture. *Chemical Engineering Science, 170*, 26-35.

Onay, O. (2007). Influence of pyrolysis temperature and heating rate on the production of bio-oil and char from safflower seed by pyrolysis, using a well-swept fixed-bed reactor. *Fuel Processing Technology, 88*(5), 523-531.

Ounas, A., Aboulkas, A., Bacaoui, A., & Yaacoubi, A. (2011). Pyrolysis of olive residue and sugar cane bagasse: non-isothermal thermogravimetric kinetic analysis. *Bioresource technology, 102*(24), 11234-11238.

Oyedun, A. O., Gebreegziabher, T., & Hui, C. W. (2013). Mechanism and modelling of bamboo pyrolysis. *Fuel Processing Technology, 106*, 595-604.

Painuly, J. P. (2001). Barriers to renewable energy penetration; a framework for analysis. *Renewable energy, 24*(1), 73-89.

Park, E.-S., Kang, B.-S., & Kim, J.-S. (2008). Recovery of oils with high caloric value and low contaminant content by pyrolysis of digested and dried sewage sludge containing polymer flocculants. *Energy & Fuels, 22*(2), 1335-1340.

Parnaudeau, V., & Dignac, M.-F. (2007). The organic matter composition of various wastewater sludges and their neutral detergent fractions as revealed by pyrolysis-GC/MS. *Journal of Analytical and Applied Pyrolysis, 78*(1), 140-152.

Pilato, L. (2010). *Phenolic resins: a century of progress*: Springer.

Politzer, P., & Ranganathan, S. (1986). Bond-order-bond-energy correlations. *Chemical physics letters, 124*(6), 527-530.

Pradhan, U. K., Lal, K., Dash, S., & Singh, K. (2017). Design and analysis of mixture experiments with process variable. *Communications in Statistics-Theory and Methods, 46*(1), 259-270.

Praveen, K., Thomas, S., Grohens, Y., Mozetič, M., Junkar, I., Primc, G., & Gorjanc, M. (2016). Investigations of plasma induced effects on the surface properties of lignocellulosic natural coir fibres. *Applied surface science, 368*, 146-156.

Quan, C., Gao, & Song, Q. (2016). Pyrolysis of biomass components in a TGA and a fixed-bed reactor: Thermochemical behaviors, kinetics, and product characterization. *Journal of Analytical and Applied Pyrolysis, 121*, 84-92.

Ramachandriya, K. D., Wilkins, M. R., Hiziroglu, S., Dunford, N. T., & Atiyeh, H. K. (2013). Development of an efficient pretreatment process for enzymatic saccharification of Eastern redcedar. *Bioresource technology, 136*, 131-139.

Rath, J., Wolfinger, M., Steiner, G., Krammer, G., Barontini, F., & Cozzani, V. (2003). Heat of wood pyrolysis. *Fuel, 82*(1), 81-91.

Rego, A., & Roley, L. (1999). In-use barrier integrity of gloves: latex and nitrile superior to vinyl. *American Journal of Infection Control, 27*(5), 405-410.

Richter, H., & Howard, J. B. (2000). Formation of polycyclic aromatic hydrocarbons and their growth to soot—a review of chemical reaction pathways. *Progress in Energy and Combustion science, 26*(4-6), 565-608.

Sánchez-Jiménez, P. E., Pérez-Maqueda, L. A., Perejón, A., & Criado, J. M. (2013). Generalized master plots as a straightforward approach for determining the kinetic model: the case of cellulose pyrolysis. *Thermochimica acta, 552*, 54-59.

Sanchez-Silva, L., López-González, D., Garcia-Minguillan, A., & Valverde, J. (2013). Pyrolysis, combustion and gasification characteristics of Nannochloropsis gaditana microalgae. *Bioresource technology, 130,* 321-331.

Sanchez-Silva, L., López-González, D., Villaseñor, J., Sánchez, P., & Valverde, J. (2012). Thermogravimetric–mass spectrometric analysis of lignocellulosic and marine biomass pyrolysis. *Bioresource technology, 109,* 163-172.

Sarkar, A., & Chowdhury, R. (2016). Co-pyrolysis of paper waste and mustard press cake in a semi-batch pyrolyzer—optimization and bio-oil characterization. *International Journal of Green Energy, 13*(4), 373-382.

Scozzafava, A., Passaponti, M., Supuran, C. T., & Gülçin, İ. (2015). Carbonic anhydrase inhibitors: guaiacol and catechol derivatives effectively inhibit certain human carbonic anhydrase isoenzymes (hCA I, II, IX and XII). *Journal of enzyme inhibition and medicinal chemistry, 30*(4), 586-591.

Shahinuzzaman, M., Yaakob, Z., & Ahmed, Y. (2017). Non-sulphide zeolite catalyst for bio-jet-fuel conversion. *Renewable and Sustainable Energy Reviews*.

Sharma, A., Pareek, V., & Zhang, D. (2015). Biomass pyrolysis—A review of modelling, process parameters and catalytic studies. *Renewable and Sustainable Energy Reviews, 50,* 1081-1096.

Shuang-quan, Z., Xiao-ming, Y., Zhi-yuan, Y., Ting-ting, P., Ming-jian, D., & Tian-yu, S. (2009). Study of the co-pyrolysis behavior of sewage-sludge/rice-straw and the kinetics. *Procedia Earth and Planetary Science, 1*(1), 661-666.

Shuping, Z., Yulong, W., Mingde, Y., Chun, L., & Junmao, T. (2010). Pyrolysis characteristics and kinetics of the marine microalgae Dunaliella tertiolecta using thermogravimetric analyzer. *Bioresource technology, 101*(1), 359-365.

Speight, J., Luque, R., & Speight. (2015). Gasification for synthetic fuel production. *Synthetic liquid fuel production from gasification*, 147-174.

Stefanidis, S., Kalogiannis, K., Iliopoulou, E., Lappas, A., & Pilavachi, P. (2011). In-situ upgrading of biomass pyrolysis vapors: catalyst screening on a fixed bed reactor. *Bioresource technology, 102*(17), 8261-8267.

Tang, L., Chen, Y.-C., Jiang, Z.-B., Zhong, S.-P., Chen, W.-Z., Chen, W.-D., . . . Shi, G.-G. (2017). Phytochemical Investigation of the Marine Alga Grateloupia livida. *Chemistry of Natural Compounds, 53*(4), 770-774.

Tian, B., Qiao, Y. y., Tian, Y. y., & Liu, Q. (2016). Investigation on the effect of particle size and heating rate on pyrolysis characteristics of a bituminous coal by TG–FTIR. *Journal of Analytical and Applied Pyrolysis, 121*, 376-386.

Turmanova, S. C., Genieva, S., Dimitrova, A., & Vlaev, L. (2008). Non-isothermal degradation kinetics of filled with rise husk ash polypropene composites. *Express Polymer Letters, 2*(2), 133-146.

Vlaev, L., Georgieva, V., & Genieva, S. (2007). Products and kinetics of non-isothermal decomposition of vanadium (IV) oxide compounds. *Journal of Thermal Analysis and Calorimetry, 88*(3), 805-812.

Wang, F.J., Zhang, S., Chen, Z.-D., Liu, C., & Wang, Y.-G. (2014a). Tar reforming using char as catalyst during pyrolysis and gasification of Shengli brown coal. *Journal of Analytical and Applied Pyrolysis, 105*, 269-275.

Wang, J., Yan, Q., Zhao, J., Wang, Z., Huang, J., Gao, S., . . . Fang, Y. (2014b). Fast co-pyrolysis of coal and biomass in a fluidized-bed reactor. *Journal of Thermal Analysis and Calorimetry, 118*(3), 1663-1673.

Wang, K., & Brown, R. C. (2013). Catalytic pyrolysis of microalgae for production of aromatics and ammonia. *Green Chemistry, 15*(3), 675-681.

Wang, S., Guo, X., Wang, & Luo, Z. (2011). Influence of the interaction of components on the pyrolysis behavior of biomass. *Journal of Analytical and Applied Pyrolysis, 91*(1), 183-189.

Wang, X., Zhao, B., & Yang, X. (2016). Co-pyrolysis of microalgae and sewage sludge: Biocrude assessment and char yield prediction. *Energy Conversion and Management, 117*, 326-334.

Ward, J., Rasul, M., & Bhuiya, M. (2014). Energy recovery from biomass by fast pyrolysis. *Procedia Engineering, 90*, 669-674.

White, J. E., Catallo, W. J., & Legendre, B. L. (2011). Biomass pyrolysis kinetics: a comparative critical review with relevant agricultural residue case studies. *Journal of Analytical and Applied Pyrolysis, 91*(1), 1-33.

Withag, J. A., Smeets, J. R., Bramer, E. A., & Brem, G. (2012). System model for gasification of biomass model compounds in supercritical water–a thermodynamic analysis. *The Journal of Supercritical Fluids, 61*, 157-166.

Xianjun, X., Zongkang, S., & Peiyong, M. (2015). Establishment of three components of biomass pyrolysis yield model. *Energy Procedia, 66*, 293-296.

Xie, Q., Peng, P., Liu, S., Min, M., Cheng, Y., Wan, Y., . . . Chen, P. (2014). Fast microwave-assisted catalytic pyrolysis of sewage sludge for bio-oil production. *Bioresource technology, 172*, 162-168.

Xu, Y., & Chen, B. (2013). Investigation of thermodynamic parameters in the pyrolysis conversion of biomass and manure to biochars using thermogravimetric analysis. *Bioresource technology, 146*, 485-493.

Yang, Z., Kumar, A., Apblett, A. W., & Moneeb, A. M. (2017). Co-Pyrolysis of torrefied biomass and methane over molybdenum modified bimetallic HZSM-5 catalyst for hydrocarbons production. *Green Chemistry, 19*(3), 757-768.

Yang, Z., Kumar, A., Huhnke, R. L., Buser, M., & Capareda, S. (2016). Pyrolysis of eastern redcedar: Distribution and characteristics of fast and slow pyrolysis products. *Fuel, 166*, 157-165.

Yang, H., Yan, R., Chen, H., Lee, D. H., & Zheng, C. (2007). Characteristics of hemicellulose, cellulose and lignin pyrolysis. *Fuel, 86*(12-13), 1781-1788.

Yao, F., Wu, Q., Lei, Y., Guo, W., & Xu, Y. (2008). Thermal decomposition kinetics of natural fibers: activation energy with dynamic thermogravimetric analysis. *Polymer degradation and stability, 93*(1), 90-98.

Yuan, T., Tahmasebi, A., & Yu, J. (2015). Comparative study on pyrolysis of lignocellulosic and algal biomass using a thermogravimetric and a fixed-bed reactor. *Bioresource technology, 175*, 333-341.

Zabeti, M., Nguyen, T., Lefferts, L., Heeres, H., & Seshan, K. (2012). In situ catalytic pyrolysis of lignocellulose using alkali-modified amorphous silica alumina. *Bioresource technology, 118*, 374-381.

Zhai, M., Guo, L., Wang, Y., Zhang, Y., Dong, P., & Jin, H. (2016). Process simulation of staging pyrolysis and steam gasification for pine sawdust. *International Journal of Hydrogen Energy, 41*(47), 21926-21935.

Zhang, X., Lei, H., Yadavalli, G., Zhu, L., Wei, Y., & Liu, Y. (2015). Gasoline-range hydrocarbons produced from microwave-induced pyrolysis of low-density polyethylene over ZSM-5. *Fuel, 144*, 33-42.

Zhang, R., Li, L., Tong, D., & Hu, C. (2016). Microwave-enhanced pyrolysis of natural algae from water blooms. *Bioresource technology, 212*, 311-317.

Zhang, B., Tan, G., Zhong, Z., & Ruan, R. (2017). Microwave-assisted catalytic fast pyrolysis of spent edible mushroom substrate for bio-oil production using surface modified zeolite catalyst. *Journal of Analytical and Applied Pyrolysis, 123*, 92-98.

Zhang, S., Yang, M., Shao, J., Yang, Zeng, K., Chen, Y., . . . Chen, H. (2018a). The conversion of biomass to light olefins on Fe-modified ZSM-5 catalyst: Effect of pyrolysis parameters. *Science of the Total Environment, 628*, 350-357.

Zhang, B., Zhong, Z., Zhang, J., & Ruan, R. (2018b). Catalytic fast co-pyrolysis of biomass and fusel alcohol to enhance aromatic hydrocarbon production over ZSM-5 catalyst in a fluidized bed reactor. *Journal of Analytical and Applied Pyrolysis, 133*, 147-153.

Zhang, B., Zhong, Z., Ding, K., & Song, Z. (2015). Production of aromatic hydrocarbons from catalytic co-pyrolysis of biomass and high density polyethylene: analytical Py–GC/MS study. *Fuel, 139*, 622-628.

Zhao, C., Jiang, E., & Chen, A. (2017a). Volatile production from pyrolysis of cellulose, hemicellulose and lignin. *Journal of the Energy Institute, 90*(6), 902-913.

Zhao, J., Wang, Q., Yu, L., & Wu, L. (2017b). TG–DSC analysis of straw biomass pyrolysis and release characteristics of noncondensable gas in a fixed-bed reactor. *Drying technology, 35*(3), 347-355.

Zhou, N., & Dunford, N. T. (2017). Thermal Degradation and Microwave-Assisted Pyrolysis of Green Algae and Cyanobacteria Isolated from the Great Salt Plains. *Transactions of the ASABE, 60*(2), 561-569.

APPENDICES

Table 1: Experimental design for DSC runs with different weight fraction (wt %) of biomass blends

Combination No.	AB	CW	DS	Catalyst to biomass weight ratio
1	100.00	0.00	0.00	0.0
2	100.00	0.00	0.00	2.0
3	0.00	100.00	0.00	0.0
4	0.00	100.00	0.00	2.0
5	0.00	0.00	100.00	0.0
6	0.00	0.00	100.00	2.0
7	0.00	33.33	66.67	0.0
8	0.00	33.33	66.67	2.0
9	0.00	66.67	33.33	0.0
10	0.00	66.67	33.33	2.0
11	33.33	0.00	66.67	0.0
12	33.33	0.00	66.67	2.0
13	33.33	33.33	33.33	0.0
14	33.33	33.33	33.33	2.0
15	66.67	33.33	0.00	0.0
16	66.67	33.33	0.00	2.0
17	66.67	0.00	33.33	0.0
18	66.67	0.00	33.33	2.0

Table 2: Elemental analysis (wt %) of the three pure biomass [AB = Algal Biomass; CW = Cedar Wood; and DS = Digested Sludge]. Means labeled with the same letters are not significantly different (Tukey's HSD test, $\alpha = 0.05$). [In all the tables under table 1, means comparison is done along the rows]

(a) Ultimate analysis of the three biomass

Biomass	AB	CW	DS
C	43.66 ± 0.64^{c}	39.06 ± 0.64^{b}	33.01 ± 0.07^{a}
H	7.30 ± 0.08^{b}	4.80 ± 0.82^{ab}	5.40 ± 0.48^{a}
N	5.97 ± 0.25^{c}	0.82 ± 0.30^{a}	4.81 ± 0.01^{b}
S	2.09 ± 0.22^{a}	2.24 ± 0.30^{a}	2.57 ± 0.46^{a}
O	41.00 ± 0.09^{a}	53.09 ± 1.46^{b}	54.22 ± 0.08^{b}

(b) Proximate analysis of the three biomass

Biomass	AB	CW	DS
Ash	11.50 ± 0.21^{a}	16.05 ± 1.05^{b}	32.97 ± 0.05^{c}
Moisture	6.13 ± 0.41^{a}	8.29 ± 0.27^{b}	5.96 ± 0.14^{a}
Volatile Matter	75.57 ± 1.30^{c}	66.43 ± 0.28^{b}	58.72 ± 0.67^{a}
Fixed Carbon	6.80 ± 1.92^{ab}	9.23 ± 1.04^{b}	2.35 ± 0.57^{a}

(c) Sulphur analysis of the three biomass

Biomass	AB	CW	DS
Sulphate	0.87 ± 0.04^{b}	0.01 ± 0.00^{a}	1.66 ± 0.01^{c}
Pyritic Sulphur	0.14 ± 0.02^{a}	0.36 ± 0.02^{a}	0.30 ± 0.15^{a}
Organic Sulphur	1.08 ± 0.16^{ab}	1.88 ± 0.27^{b}	0.60 ± 0.32^{a}

(d) Lipid content (wt %) of the three biomass

Biomass	AB	CW	DS
Lipid (dry basis)	7.54 ± 0.19^{c}	1.66 ± 0.03^{a}	6.46 ± 0.38^{b}
Lipid (ash free dry basis, wt %)	8.52 ± 0.21^{b}	1.98 ± 0.04^{a}	9.64 ± 0.57^{b}

Table 3: Particle size (μm) distribution for Cedar wood biomass. Means labeled with the same letters are not significantly different (Tukey's HSD test, $\alpha = 0.05$). Means comparison is done along the columns.

Sieve No.	Particle Size Range	Fraction of particles retained
20	>850	4.31 ± 0.27^{a}
45	355 - 850	40.07 ± 1.77^{d}
60	250 - 355	16.45 ± 0.21^{c}
100	150 - 250	16.93 ± 0.69^{c}
140	106 - 150	6.01 ± 0.35^{a}
200	75 - 106	6.81 ± 0.44^{ab}
Pan	< 75	9.34 ± 0.25^{b}

Table 4: Pre – exponential factor (A) values (min^{-1}) for DSC runs of all the combinations [T =Peak temperature from DSC run in ^{o}C; NA = Not Applicable]

Combo number	Heating Rate (^{o}C/min)	Estimates from DSC runs and FWO Plot for peak number:									
		1		2		3		4		5	
		T	A	T	A	T	A	T	A	T	A
1	10	87	4.4×10^{5}	211.3	9.3×10^{18}	314.9	3.4×10^{10}	NA	NA	NA	NA
	15	92.6		215.3		321.9		NA		NA	
	20	104.1		218.7		330.6		NA		NA	
2	10	94.7	1.1×10^{8}	185.2	2.7×10^{6}	NA	NA	NA	NA	NA	NA
	15	100.5		194.5		362.8		NA		NA	
	20	107.7		205		367		NA		NA	
3	10	79.80	1.7×10^{8}	143.4	5×10^{11}	250.7	4.1×10^{23}	365.8	4.4×10^{12}	NA	NA
	15	87.5		150.6		255.5		374.7		NA	
	20	92		153.1		256.4		380.1		NA	
4	10	79.9	5.3×10^{2}	177.4	2×10^{4}	368.5	3×10^{11}	397.2	8.2×10^{6}	NA	NA
	15	96.1		183.6		376.1		407.7		NA	
	20	112.5		202.8		384.4		423.3		NA	

Table 4 (Continued): Pre – exponential factor (A) values (min^{-1}) for DSC runs of all the combinations [T = Peak temperature from DSC run in ^{o}C; NA = Not Applicable]

Combo number	Heating Rate (^{o}C/min)	Estimates from DSC runs and FWO Plot for peak number:									
		1		2		3		4		5	
		T	A	T	A	T	A	T	A	T	A
5	10	84.7	4.2×10^{5}	244	3.1×10^{21}	324	1.3×10^{14}	NA	NA	NA	NA
	15	97.2		248.4		330.4		NA		NA	
	20	101.3		250.9		336.2		NA		NA	
6	10	90	4.1×10^{4}	183.2	3.8×10^{10}	298	1.4 x 10	362.6	1.8 x 10	NA	NA
	15	106.3		191.8		310.5		369		NA	
	20	108.4		195.1		372.4		434.7		NA	
7	10	80.6	1.8×10^{6}	246	2×10^{20}	327.9	2.5×10^{2}	NA	NA	NA	NA
	15	87.5		249.2		332.9		NA		NA	
	20	96.5		253.3		374.5		NA		NA	
8	10	78	3.9×10^{4}	161.9	1.1×10^{3}	NA	NA	NA	NA	NA	NA
	15	89.5		187.8		328.5		NA		NA	
	20	99		193.7		344.5		NA		NA	

Table 4 (Continued): Pre – exponential factor (A) values (min^{-1}) for DSC runs of all the combinations [T = Peak temperature from DSC run in ^{o}C; NA = Not Applicable]

Combo number	Heating Rate (^{o}C/min)	Estimates from DSC runs and FWO Plot for peak number									
		1		2		3		4		5	
		T	A	T	A	T	A	T	A	T	A
9	10	80.6	2.1×10^{7}	145.4	6.6×10^{8}	239.7	6.3×10^{8}	366.7	NA	NA	NA
	15	86.4		154.5		251.4		NA		NA	
	20	94.3		158.4		255.1		NA		NA	
10	10	81.5	6.8×10^{8}	173.7	6.9×10^{2}	NA	NA	NA	NA	NA	NA
	15	86.4		192		NA		NA		NA	
	20	93		212.6		437.7		NA		NA	
11	10	95.2	5.8×10^{6}	214.1	2.7×10^{2}	320.8	3×10^{9}	NA	NA	NA	NA
	15	101		249.5		325.2		NA		NA	
	20	110.3		251		337.1		NA		NA	
12	10	89.3	2.3×10^{5}	184.6	1.6×10^{3}	250.5	7.5×10^{-1}	373.07	NA	NA	NA
	15	102.3		202.3		354.6		NA		NA	
	20	107		220.7		376.5		NA		NA	

Table 4 (Continued): Pre – exponential factor (A) values (min^{-1}) for DSC runs of all the combinations [T = Peak temperature from DSC run in ^{o}C; NA = Not Applicable]

Combo number	Heating Rate (^{o}C/min)	Estimates from DSC runs and FWO Plot for peak number									
		1		2		3		4		5	
		T	A	T	A	T	A	T	A	T	A
13 (Rep 1)	10	81.9	9.8×10^{3}	156.4	4.6×10^{10}	249.5	3.2×10^{18}	321.4	3×10^{12}	452.3	NA
	15	86.5		160.8		252.2		328.5		NA	
	20	103.4		167.7		257.4		335.1		NA	
13 (Rep 2)	10	76.7	1.8×10^{7}	152	3.6×10^{8}	243.5	2.9×10^{12}	317.8	1.9×10^{8}	447.64	NA
	15	86.2		155.5		251.4		328.2		NA	
	20	89.7		165		255		337.8		NA	
14 (Rep 1)	10	83.7	9.5×10^{7}	163.6	5.8×10^{3}	NA	NA	NA	NA	NA	NA
	15	91.5		181.5		329.1		409.3		NA	
	20	96.4		193.7		422.9		NA		NA	
14 (Rep 2)	10	77.9	1.9×10^{6}	178.9	4.8×10^{3}	NA	NA	NA	NA	NA	NA
	15	86.3		198.8		339		401.5		NA	
	20	93.7		211.7		379.1		NA		NA	

Table 4 (Continued): Pre – exponential factor (A) values (min^{-1}) for DSC runs of all the combinations [T = Peak temperature from DSC run in ^{o}C; NA = Not Applicable]

Combo number	Heating Rate (^{o}C/min)	Estimates from DSC runs and FWO Plot for peak number									
		1		2		3		4		5	
		T	A	T	A	T	A	T	A	T	A
15	10	78.2	4.3×10^{7}	156.3	3.8×10^{8}	207	8.6×10^{7}	314.7	1.7×10^{11}	NA	NA
	15	83		163.5		211.2		323		NA	
	20	91.1		170.7		221.6		328.3		NA	
16	10	77.4	2.7×10^{3}	174.2	5.9×10^{2}	NA	NA	NA	NA	NA	NA
	15	95.5		191.3		NA		NA		NA	
	20	103		213.7		341.8		NA		NA	
17	10	90	6.3×10^{7}	NA	NA	210.7	5×10^{14}	315.4	5×10^{9}	NA	NA
	15	99		161.5		216.4		326.5		NA	
	20	102.8		186.1		220.1		332.2		NA	
18	10	90	5×10^{4}	158.9	1×10^{2}	314.2	9.1×10^{1}	NA	NA	NA	NA
	15	98.6		176.1		356.7		405.2		NA	
	20	111		206.4		373.8		NA		NA	

Table 5: Pyrolysis kinetics parameter estimation (kJ/mol) from DSC runs for the combinations

Combination No.	**Total Activation Energy, E_a**	**Total Change in Enthalpy, ΔH**	**Total Change in Gibb's Free Energy, ΔG**
1	339.74	327.70	363.80
2	118.63	111.64	212.10
3	548.52	532.22	489.77
4	305.80	287.88	555.24
5	418.81	406.37	374.28
6	181.05	163.84	541.86
7	282.89	270.51	380.10
8	65.88	59.03	211.28
9	215.40	204.49	329.99
10	91.83	84.97	210.01
11	192.39	179.96	383.89
12	88.06	75.77	390.39
13	398.55 ± 72.57	382.61 ± 72.53	482.72 ± 0.71
14	87.28 ± 8.80	80.49 ± 8.76	207.62 ± 0.47
15	350.01	334.10	494.75
16	57.03	50.14	213.88
17	308.27	296.12	367.68
18	92.49	80.43	379.54

Table 6: Bio-char yield from various combinations (wt %) at different heating rate (10, 15 and 20 ^{o}C/min)

Combination No	Bio-char at different heating rate (wt %)		
	10 ^{o}C/min	**15 ^{o}C/min**	**20 ^{o}C/min**
1	35.71	34.29	31.43
2	40	31.42	27.14
3	40	37.14	38.57
4	40	31.42	57.14
5	55.71	54.28	48.57
6	61.43	52.86	40
7	50	51.43	45.71
8	48.57	57.14	40
9	35.71	41.42	38.57
10	44.28	61.42	70
11	42.86	47.14	44.29
12	52.86	57.14	61.43
13	37.14	38.57	40
13	44.29	42.85	38.57
14	44.28	57.14	35.71
14	35.71	52.86	31.43
15	35.71	34.28	40
16	40	52.86	48.57
17	40	41.43	44.29
18	57.14	61.42	65.71

Table 7: Analysis of variance (ANOVA) for response surface models (from REG procedure) of different biomass pairs for E_a

Biomass Pairs	Source	Degree of Freedom	Sum of Squares	Mean Square	F – value	Pr > F
AB and CW	Model	5	347665	69533	15.01	<.0001
	Lack of Fit	12	59495	4957.90	1.86	0.40
	Coefficient of Variance	30.60	R^2	0.8298		
CW and DS	Model	5	347665	69533	15.01	<.0001
	Lack of Fit	12	59495	4957.89708	1.86	0.4031
	Coefficient of Variance	29.41	R^2	0.8428		
AB and DS	Model	5	347668	69534	15.01	<.0001
	Lack of Fit	12	59493	4957.72	1.86	0.4032
	Coefficient of Variance	29.41	R^2	0.8428		

$p < 0.15$ signifies statistical significance.

Table 8: Analysis of variance (ANOVA) for response surface models (from REG procedure) of the three different biomass pairs for ΔH

Biomass Pairs	Source	Degree of Freedom	Sum of Squares	Mean Square	F – value	Pr > F
AB and CW	Model	5	328982	65796	13.55	<.0001
	Lack of Fit	12	62627	5218.89	1.96	0.3878
	Coefficient of Variance	31.73	R^2	0.8288		
CW and DS	Model	5	334461	66892	14.99	<.0001
	Lack of Fit	12	57148	4762.34	1.78	0.4147
	Coefficient of Variance	30.43	R^2	0.8426		
AB and DS	Model	5	334463	66893	14.99	<.0001
	Lack of Fit	12	57146	4762.15	1.78	0.4147
	Coefficient of Variance	30.43	R^2	0.8426		

$p < 0.15$ signifies statistical significance.

Table 9: Parameter estimate of the biomass pair of AB and CW for E_a [CatRatio = Catalyst to Biomass Ratio, wt/wt]

Variable	Degree of Freedom	Parameter Estimate	Standard Error	t Value	Pr > |t|
Intercept	1	367.38	43.99	8.35	<.0001
AB	1	-8.95	9.47	-0.94	0.3608
CW	1	-71.93	30.17	-2.38	0.0318
CatRatio	1	-113.89	15.84	-7.19	<.0001
AB * CW	1	11.73	6.60	1.78	0.0972
$(CW)^2$	1	13.43	4.23	3.17	0.0068

$p < 0.15$ signifies statistical significance.

Table 10: Parameter estimate for the biomass pair of AB and CW for ΔH

Variable	Degree of Freedom	Parameter Estimate	Standard Error	t Value	Pr > |t|
Intercept	1	350.72	43.29	8.10	<.0001
AB	1	-8.21	9.32	-0.88	0.3930
CW	1	-68.20	29.69	-2.30	0.0376
CatRatio	1	-112.10	15.58	-7.20	<.0001
AB * CW	1	11.15	6.49	1.72	0.1078
$(CW)^2$	1	12.86	4.16	3.09	0.0080

$p < 0.15$ signifies statistical significance.

Table 11: Parameter estimate of the biomass pair of DS and CW for E_a

Variable	Degree of Freedom	Parameter Estimate	Standard Error	t Value	Pr > |t|
Intercept	1	319.92	42.63	7.51	<.0001
DS	1	-20.82	28.57	-0.73	0.4782
CW	1	28.03	9.30	3.01	0.0093
CatRatio	1	-113.89	15.22	-7.48	<.0001
DS * CW	1	-9.59	5.34	-1.80	0.0938
$(DS)^2$	1	4.49	3.94	1.14	0.2742

$p < 0.15$ signifies statistical significance.

Table 12: Parameter estimate for the biomass pair of DS and CW for ΔH

Variable	Degree of Freedom	Parameter Estimate	Standard Error	t Value	Pr > |t|
Intercept	1	308.63	41.84	7.38	<.0001
DS	1	-21.84	28.04	-0.78	0.4490
CW	1	26.99	9.13	2.96	0.0104
CatRatio	1	-112.10	14.94	-7.50	<.0001
DS * CW	1	-8.98	5.24	-1.71	0.1084
$(DS)^2$	1	4.53	3.87	1.17	0.2615

$p < 0.15$ signifies statistical significance.

Table 13: Parameter estimate of the biomass pair of AB and DS for E_a [CatRatio = Catalyst to Biomass Ratio, wt/wt]

Variable	Degree of Freedom	Parameter Estimate	Standard Error	t Value	Pr > |t|
Intercept	1	516.14	47.63	10.84	<.0001
DS	1	-115.98	30.41	-3.81	0.0019
AB	1	-28.03	9.30	-3.02	0.0093
CatRatio	1	-113.89	15.22	-7.48	<.0001
AB * DS	1	9.59	5.34	1.80	0.0939
$(DS)^2$	1	14.08	4.09	3.44	0.0039

$p < 0.15$ signifies statistical significance.

Table 14: Parameter estimate for the biomass pair of AB and DS for ΔH

Variable	Degree of Freedom	Parameter Estimate	Standard Error	t Value	Pr > |t|
Intercept	**1**	497.56	46.75	10.64	<.0001
DS	**1**	-111.70	29.85	-3.74	0.0022
AB	**1**	-26.99	9.13	-2.96	0.0104
CatRatio	**1**	-112.10	14.94	-7.50	<.0001
DS * AB	**1**	8.98	5.24	1.71	0.1085
$(DS)^2$	**1**	13.51	4.01	3.37	0.0046

$p < 0.15$ signifies statistical significance.

Table 15: Analysis of variance (ANOVA) for response surface models (from REG procedure) of the three different biomass pairs for ΔG

Biomass Pairs	Source	Degree of Freedom	Sum of Squares	Mean Square	F – value	Pr > F
CW and AB	Model	6	168664	28111	3.48	0.0283
	Lack of Fit	11	105069	9551.73	26430.5	<.0001
	Coefficient of Variance	24.70	R^2	0.6162		
DS and CW	Model	5	178450	35690	5.24	0.0064
	Lack of Fit	12	95282	7940.21	21971.30	<.0001
	Coefficient of Variance	22.67	R^2	0.6519		
AB and DS	Model	5	178450	35690	5.24	0.0064
	Lack of Fit	12	95282	7940.21	21971.30	<.0001
	Coefficient of Variance	22.67	R^2	0.6519		

$p < 0.15$ signifies statistical significance.

Table 16: Combinations of the three biomass (with and without catalyst ZSM–5) for furnace runs:

Combination No.	AB	CW	DS	Catalyst to biomass weight ratio
1	100.00	0.00	0.00	0.0
2	100.00	0.00	0.00	2.0
3	0.00	100.00	0.00	0.0
4	0.00	100.00	0.00	2.0
5	0.00	0.00	100.00	0.0
6	0.00	0.00	100.00	2.0
14	33.33	33.33	33.33	2.0
OM	4.29	38.57	57.14	0.0
OM – 0.5	4.29	38.57	57.14	0.5
OM – 1.0	4.29	38.57	57.14	1.0
OM – 2.0	4.29	38.57	57.14	2.0

Table 17: GC – MS analysis of bio-oil obtained all the combinations subjected to pyrolysis in the furnace. Means for different chemical compounds having the same letter are not significantly different (Tukey's HSD test, $p > 0.05$) [- = Not Detected; All comparisons are done along the rows for a given chemical compound within different combinations.]

Chemical Compounds *	Yield (Area %) from combination number:										
	1	**2**	**3**	**4**	**5**	**6**	**14**	**OM**	**OM – 0.5**	**OM – 1.0**	**OC**
AH	-	57.76 ± 1.69^{c}	1.27 ± 0.15^{a}	84.9 ± 1.59^{f}	-	72.3 ± 1.33^{e}	89.38 ± 0.97^{g}	-	22.88 ± 2.09^{b}	62.89 ± 0.68^{d}	83.12 ± 1^{f}
OA	2.46 ± 0.08^{a}	24.67 ± 1.14^{d}	71.71 ± 2.04^{g}	10.48 ± 0.67^{b}	12.98 ± 0.51^{c}	4.09 ± 0.05^{a}	2.4 ± 0.11^{a}	44.32 ± 4.42^{f}	37.51 ± 1.3^{e}	10.78 ± 0.24^{bc}	-
Acids	52.47 ± 1.07^{d}	-	2.09 ± 0.16^{a}	-	3.87 ± 0.05^{a}	-	-	22.14 ± 1.42^{c}	9.23 ± 1.62^{b}	3.55 ± 0.62^{a}	-
Aldehydes	16.18 ± 0.64^{c}	-	-	-	3.03 ± 0.2^{b}	-	0.7 ± 0.01^{a}	-	-	-	-
Ketones	-	-	1.65 ± 0.31	-	-	-	-	-	-	-	-
Alcohols	4.75 ± 0.49^{c}	7.45 ± 0.09^{e}	9.93 ± 0.64^{f}	-	6.19 ± 0.19^{d}	1.48 ± 0.04^{a}	1.08 ± 0.01^{a}	9.21 ± 0.02^{f}	1.57 ± 0.02^{a}	3.36 ± 0.12^{b}	0.69 ± 0.03^{a}
Amines	0.47 ± 0.06	-	-	-	-	-	-	-	-	-	-
Amides	6.9 ± 1.93	-	-	-	-	-	-	-	-	-	-
Paraffins	3.43 ± 0.34^{a}	2.65 ± 0.02^{a}	-	-	4.93 ± 0.93^{a}	-	-	-	-	-	-
Olefins	3.27 ± 0.23^{b}	1.74 ± 0.02^{a}	7.83 ± 0.36^{d}	4.62 ± 0.49^{a}	9.39 ± 0.21^{e}	-	2.02 ± 0.2^{a}	4.15 ± 0.22^{bc}	10.61 ± 0.62^{f}	7.42 ± 0.03^{d}	5.25 ± 0.09^{c}
Alkynes	3.22 ± 0.27^{a}	3.15 ± 0.01^{a}	-	-	-	-	-	-	-	-	-
Esters	1.8 ± 0.56^{a}	2.58 ± 0.11^{a}	-	-	2.32 ± 0.05^{a}	-	-	-	-	-	-
Nitriles	5.05 ± 0.5^{b}	-	-	-	3.33 ± 0^{a}	-	-	-	-	-	-
Furans	-	-	5.51 ± 0.72	-	-	-	-	-	-	-	-
CDC	-	-	-	-	53.97 ± 0.75^{e}	22.13 ± 1.6^{d}	4.42 ± 0.22^{a}	20.18 ± 1.08^{d}	18.2 ± 4.22^{cd}	12.01 ± 0.01^{bc}	10.94 ± 0.99^{ab}

*AH = Aromatic hydrocarbons; OA = Other Aromatics; CDC = Cholesterol Derived Compounds

Table 18: ASPEN PLUS simulation findings for the heat duty (kJ/hr) of the PYROLYSI and CONDENSE block for the various biomass combinations

Blend #	PYROLYSI	CONDENSE
1	8.68	-2.05
3	8.80	-1.69
5	6.93	-1.23
7	7.56	-1.39
9	8.18	-1.54
11	7.51	-1.50
13	8.14	-1.66
15	8.72	-1.93
17	8.09	-1.77

Fig 1: Pyrolysis unit setup – (a) Muffle furnace unit used for pyrolysis; (b) Condenser unit of the pyrolysis system and; (c) quartz reactor containing sample to be pyrolysed in a quartz crucible

(a)

(b)

(c)

Fig 2: DSC thermogram for AB, CW, DS, and Combo 13 run at 10 ºC/min heated from 25 to 500 ºC. [Color pattern for different curves of biomass are as follows: AB = Red; CW = Purple; DS = Blue; and Combo 13 = Orange]

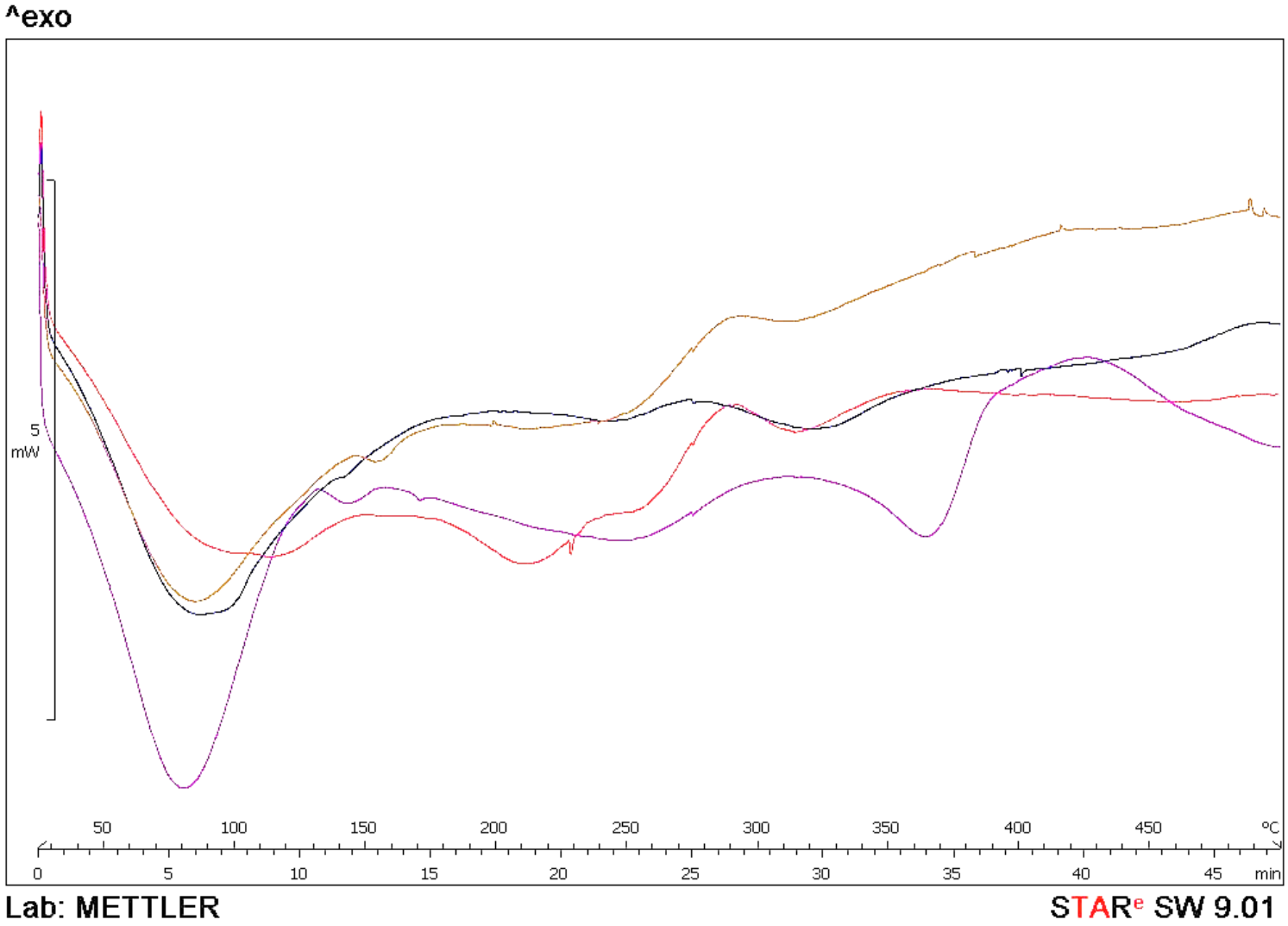

Fig 3: DSC thermogram for AB, CW, DS, and Combo 13 run at 15 ºC/min heated from 25 to 500 ºC. [Color pattern for different curves of biomass are as follows: AB = Orange; CW = Red; DS = Blue; and Combo 13 = Green]

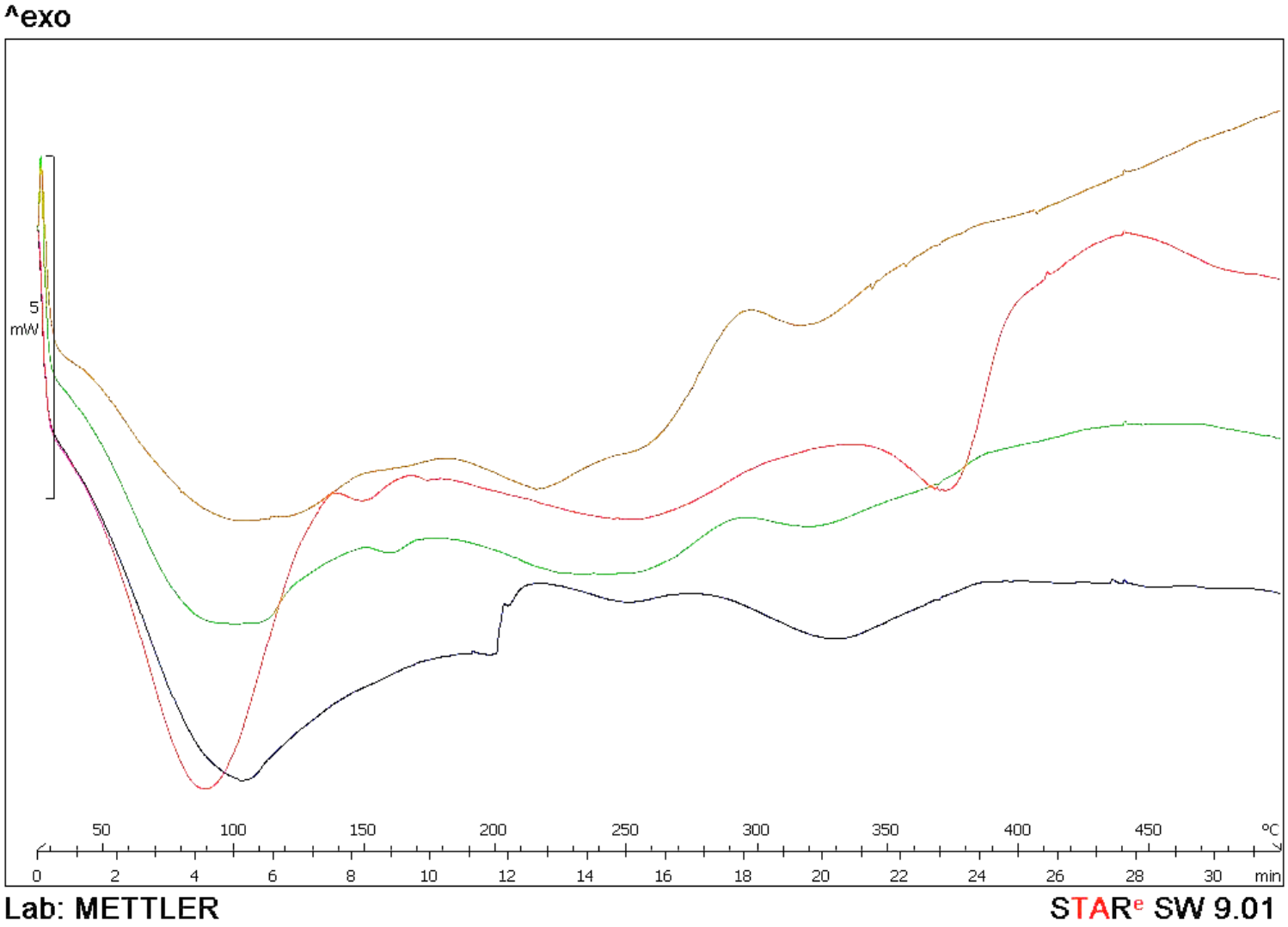

Fig 4: DSC thermogram for AB, CW, DS, and Combo 13 run at 20 ºC/min heated from 25 to 500 ºC. [Color pattern for different curves of biomass are as follows: AB = Green; CW = Orange; DS = Red; and Combo 13 = Purple]

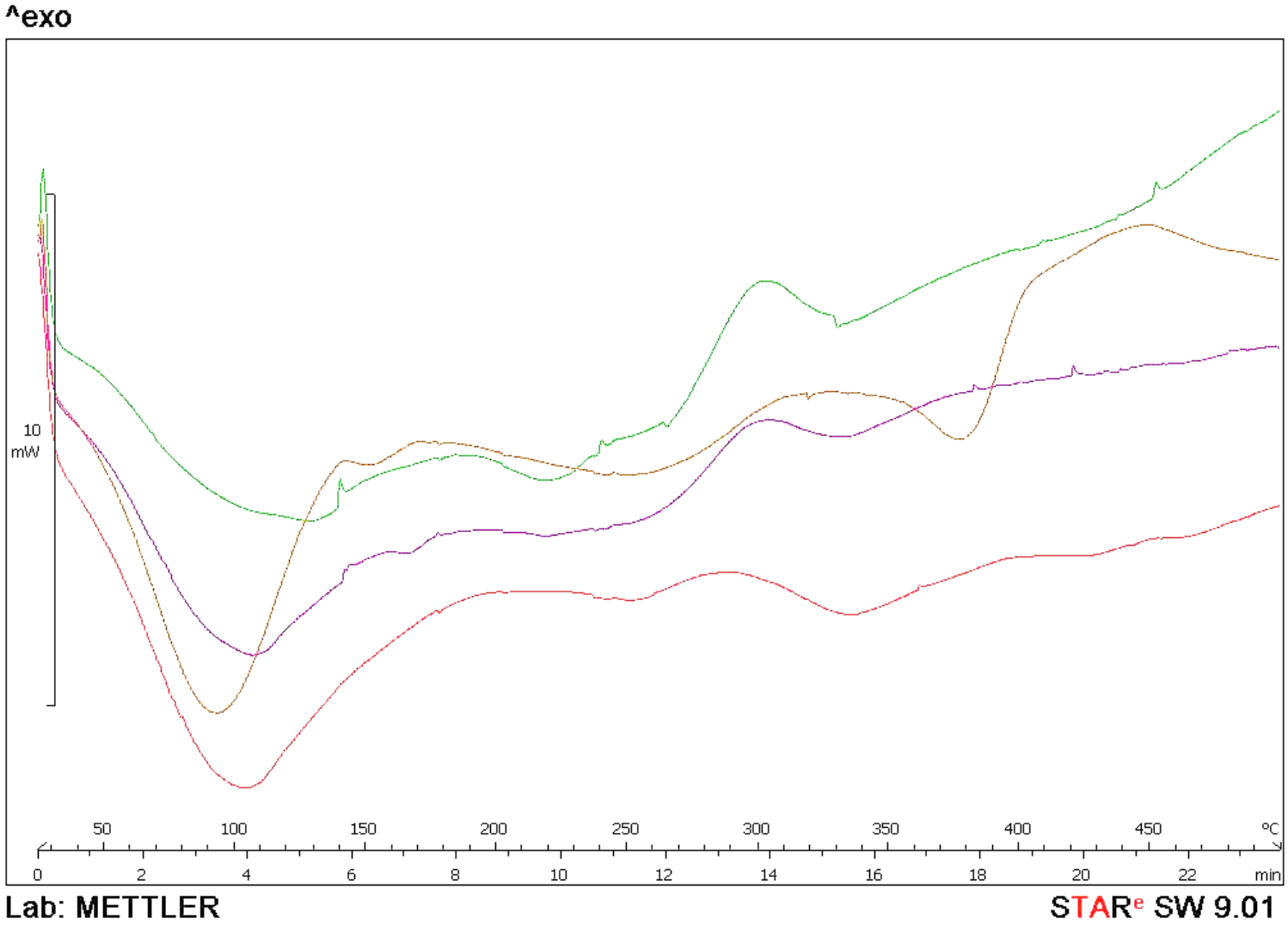

Fig 5: (a) DSC thermogram for combination 16 at 20 ºC/min heated from 25 to 500 ºC.

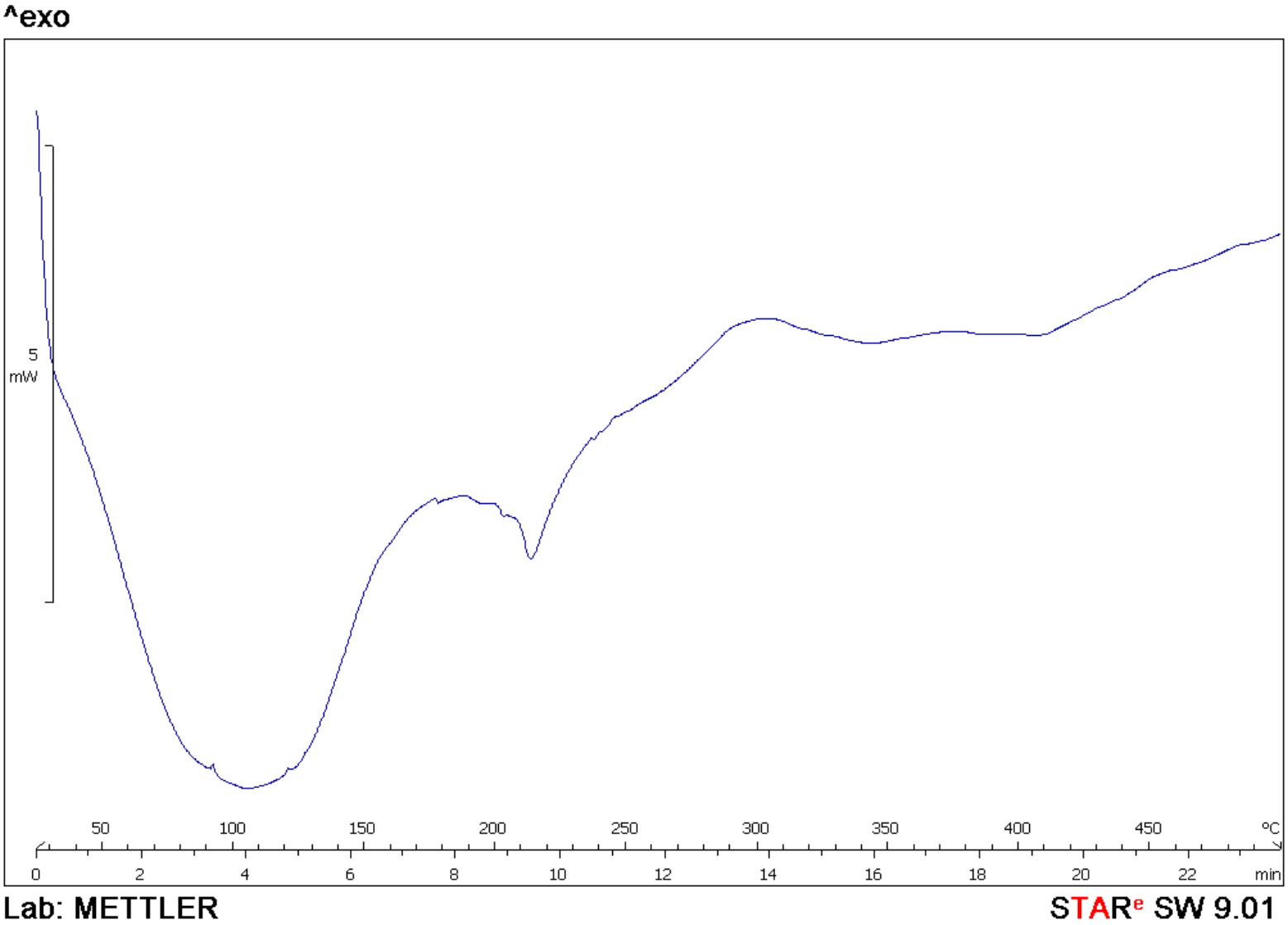

Fig 5: (b) DSC thermogram for combination 16 at 10 ºC/min heated from 25 to 500 ºC.

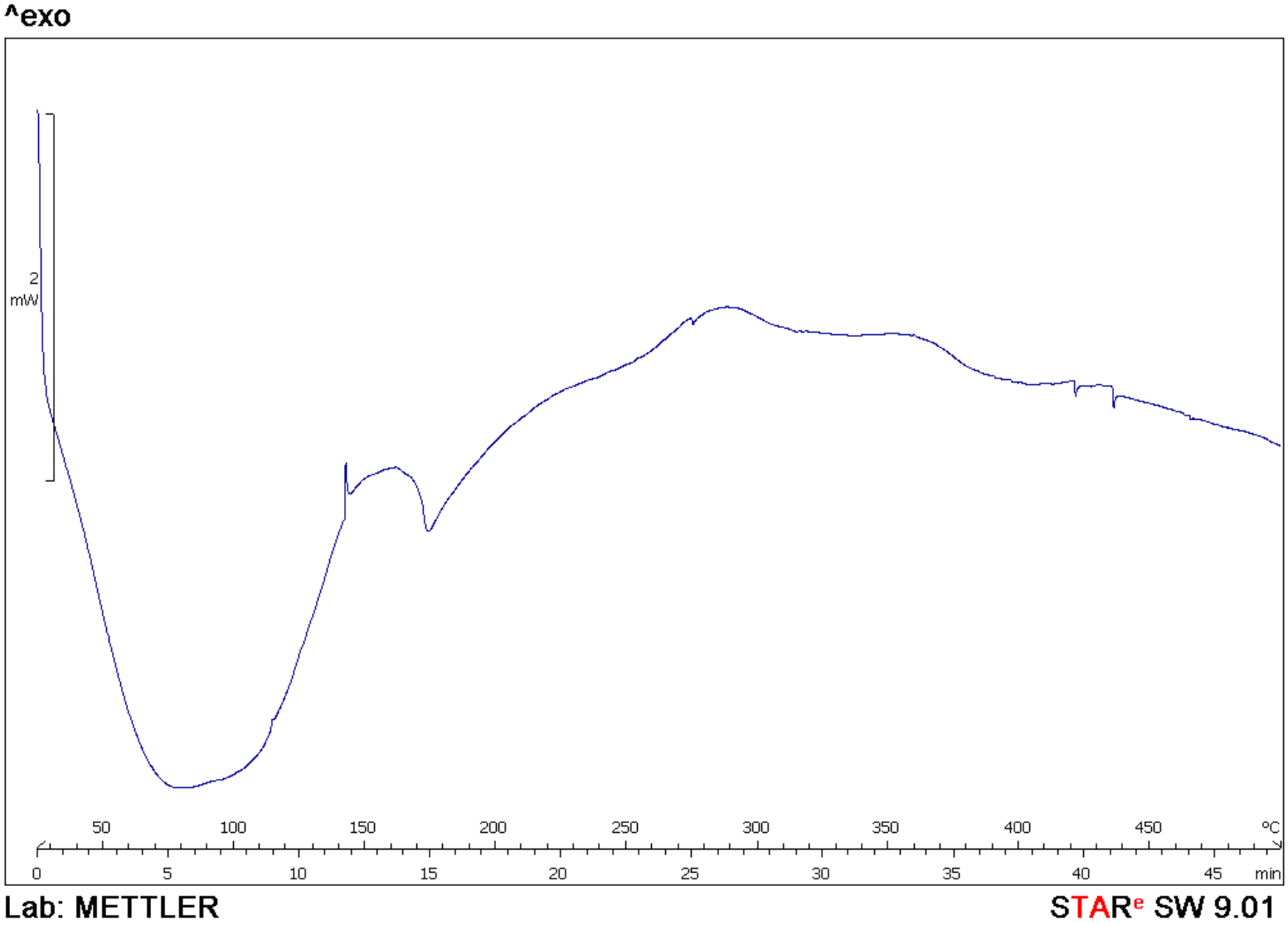

Fig 5: (c) DSC thermogram for combination 16 at 15 ºC/min heated from 25 to 500 ºC.

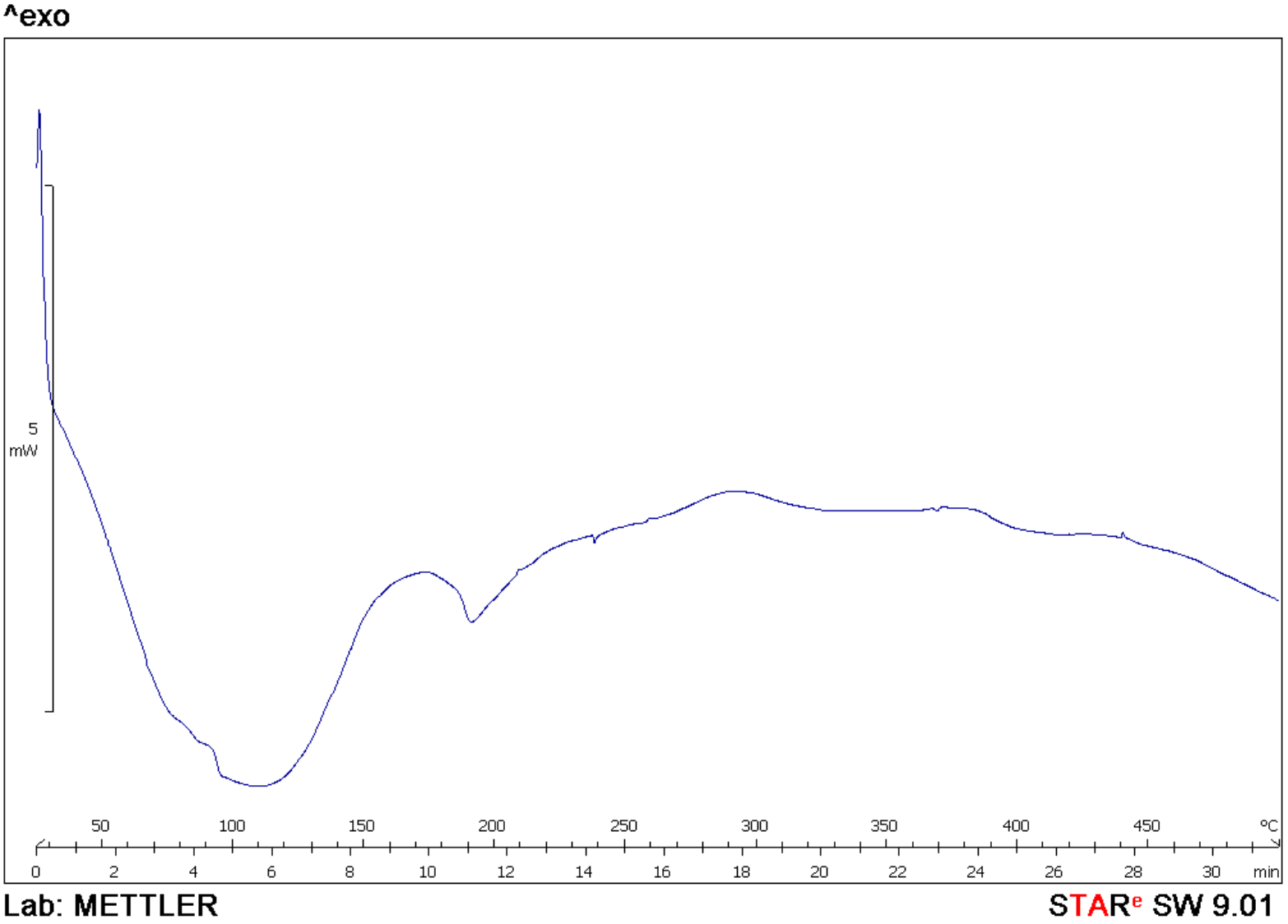

Fig 6: 3D surface plot for the response surface model based on the biomass pair of CW and AB for E_a without ZSM–5,

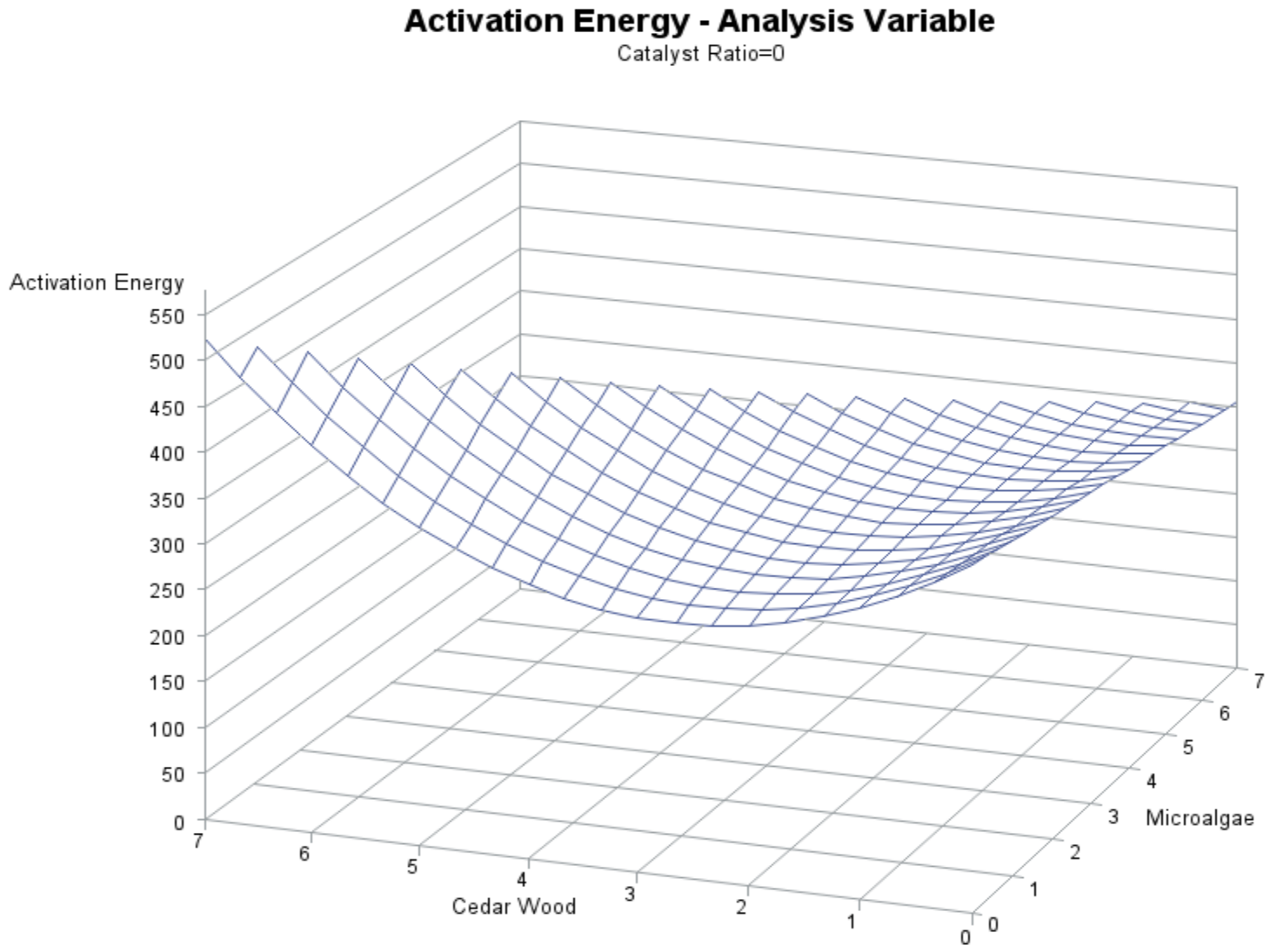

Fig 7: Contour plot for the response surface model based on the biomass pair of AB and CW for E_a without ZSM–5,

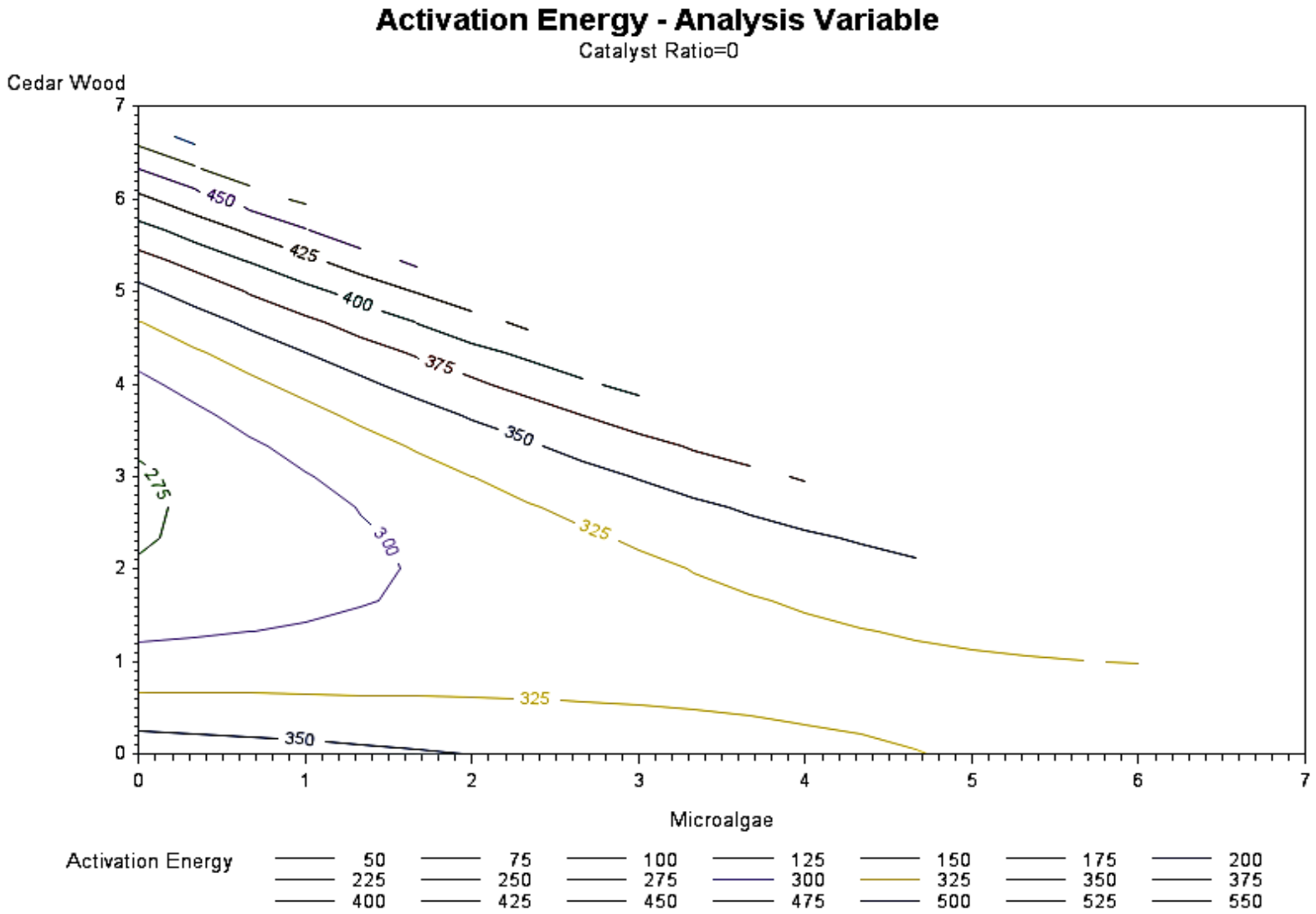

Fig 8: 3D surface plot for the response surface model based on the biomass pair of CW and AB for E_a with ZSM–5,

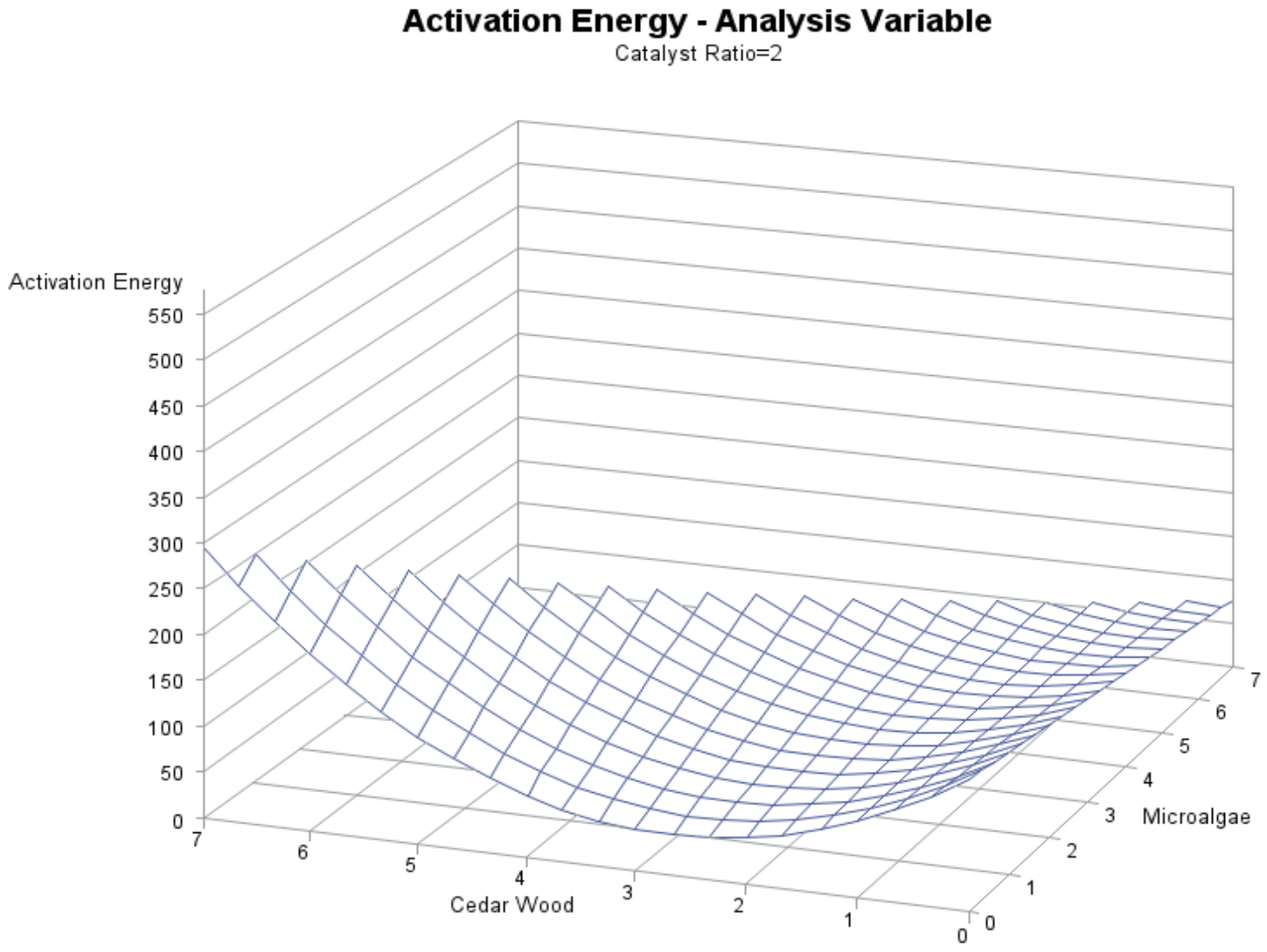

Fig 9: Contour plot for the response surface model based on the biomass pair of CW and AB for E_a with ZSM–5,

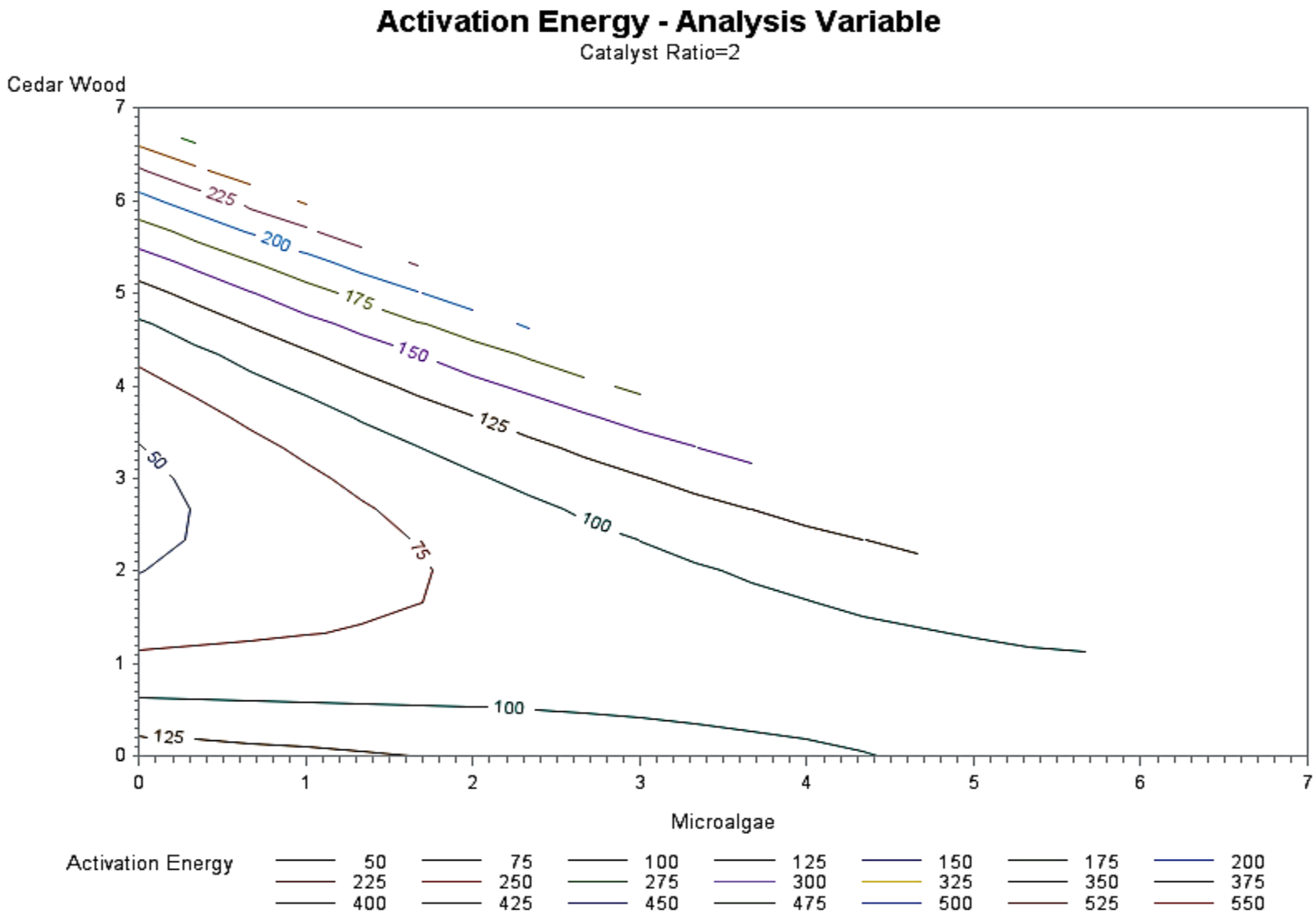

Fig 10: 3D surface plot for the response surface model based on the biomass pair of CW and AB for ΔH without ZSM–5,

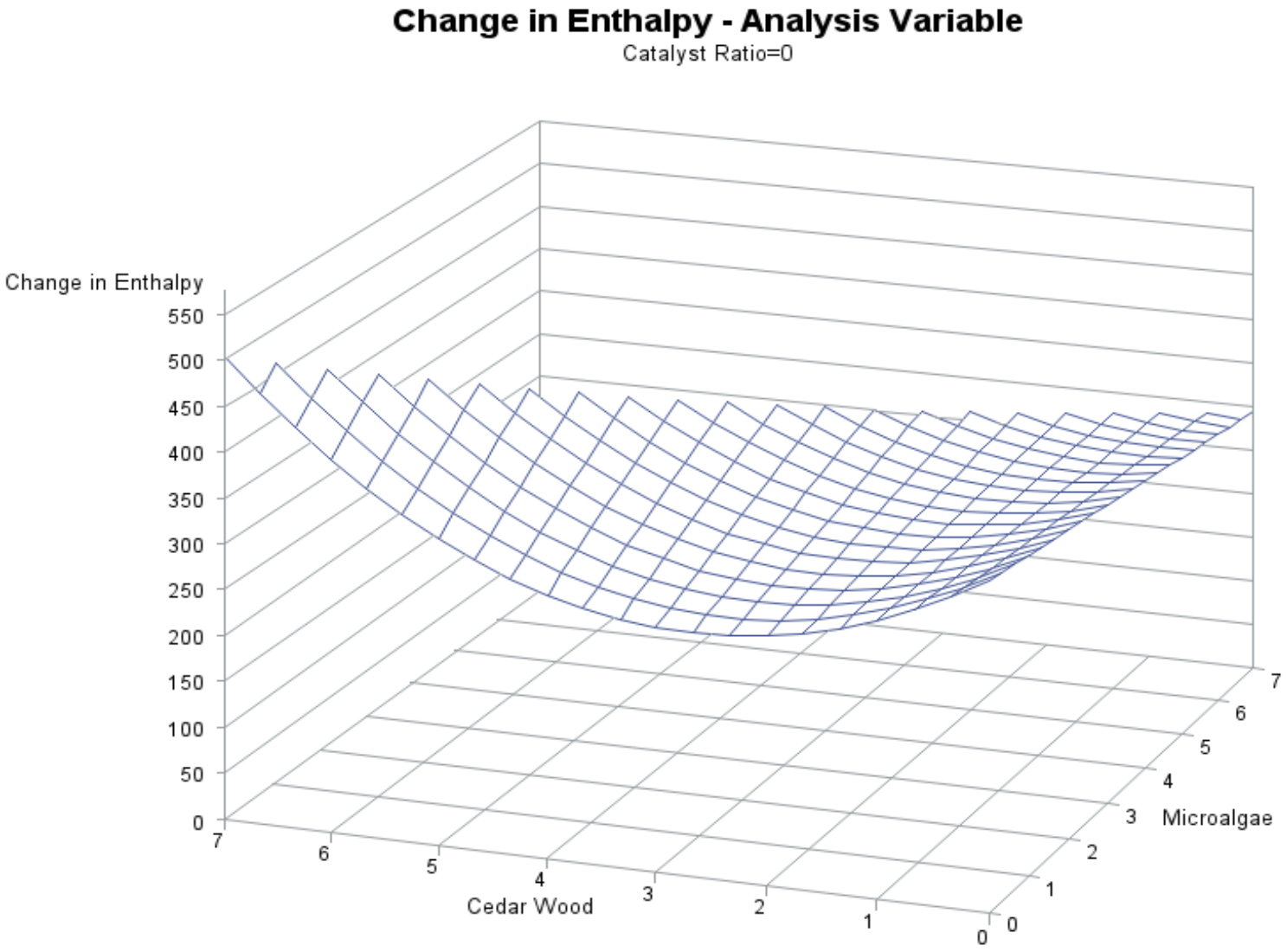

Fig 11: Contour plot for the response surface model based on the biomass pair of CW and AB for ΔH without ZSM–5,

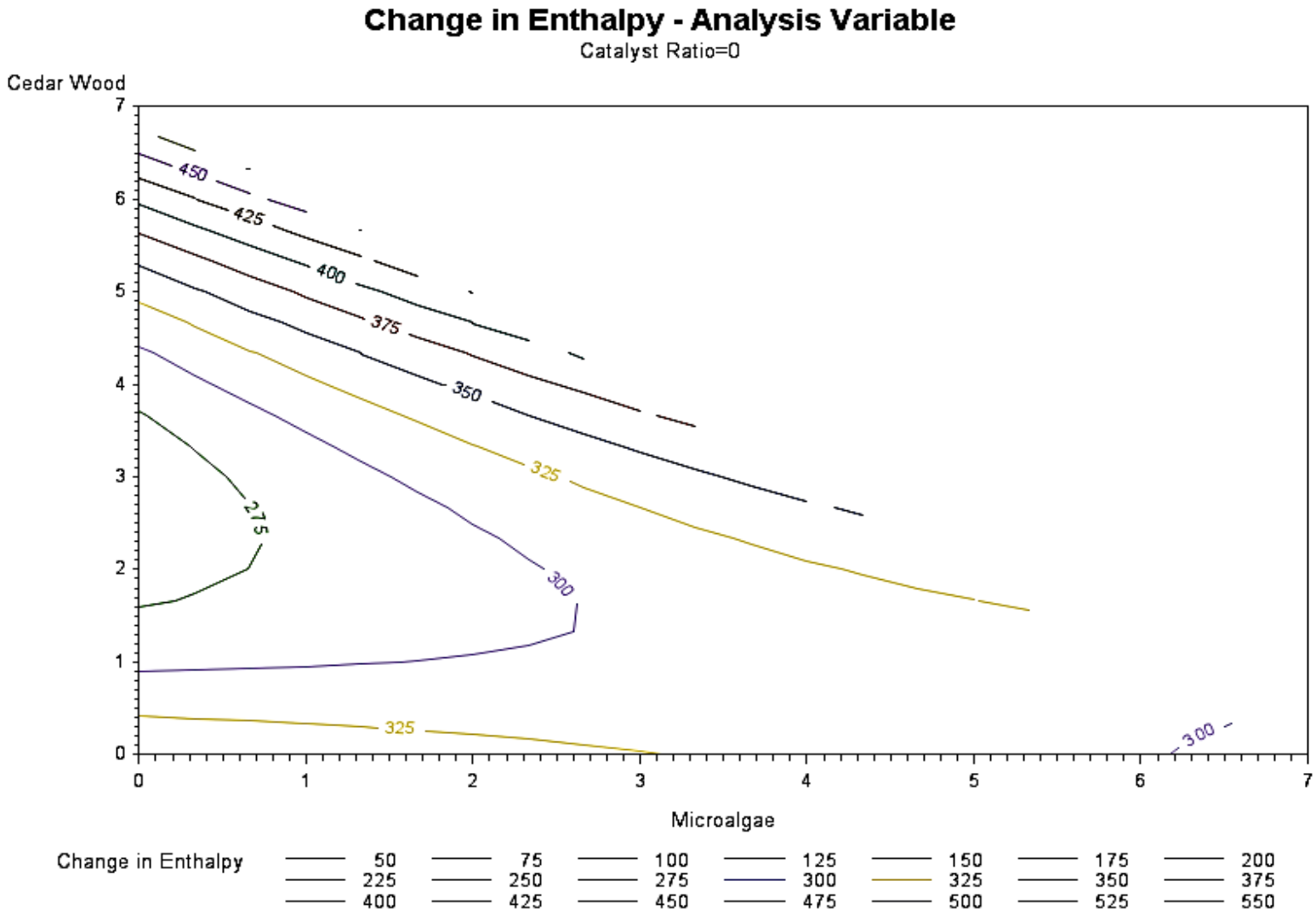

Fig 12: 3D surface plot for the response surface model based on the biomass pair of CW and AB for ΔH with ZSM–5,

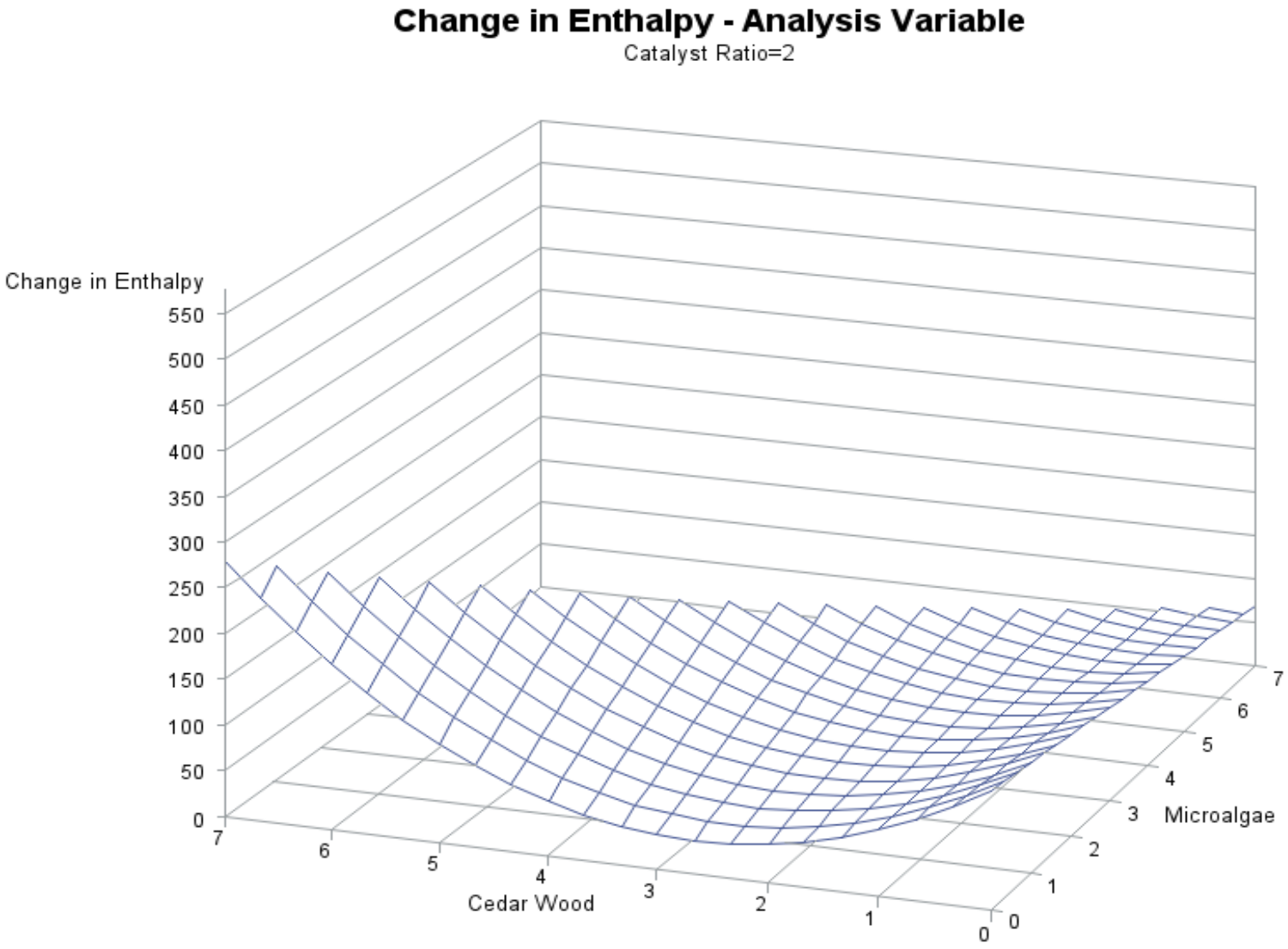

Fig 13: Contour plot for the response surface model based on the biomass pair of CW and AB for ΔH with ZSM–5,

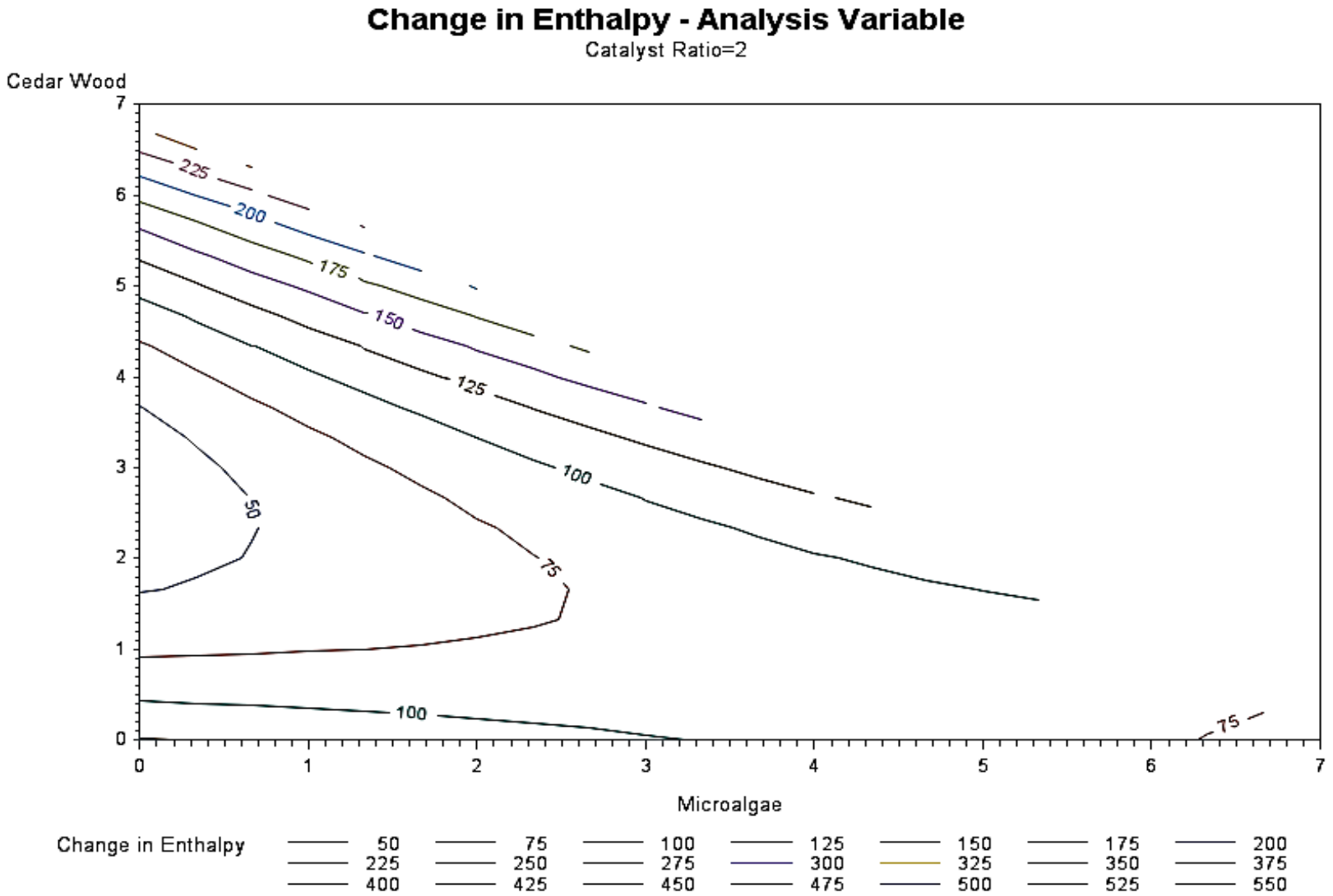

Fig 14: 3D surface plot for the response surface model based on the biomass pair of DS and CW for E_a without ZSM–5,

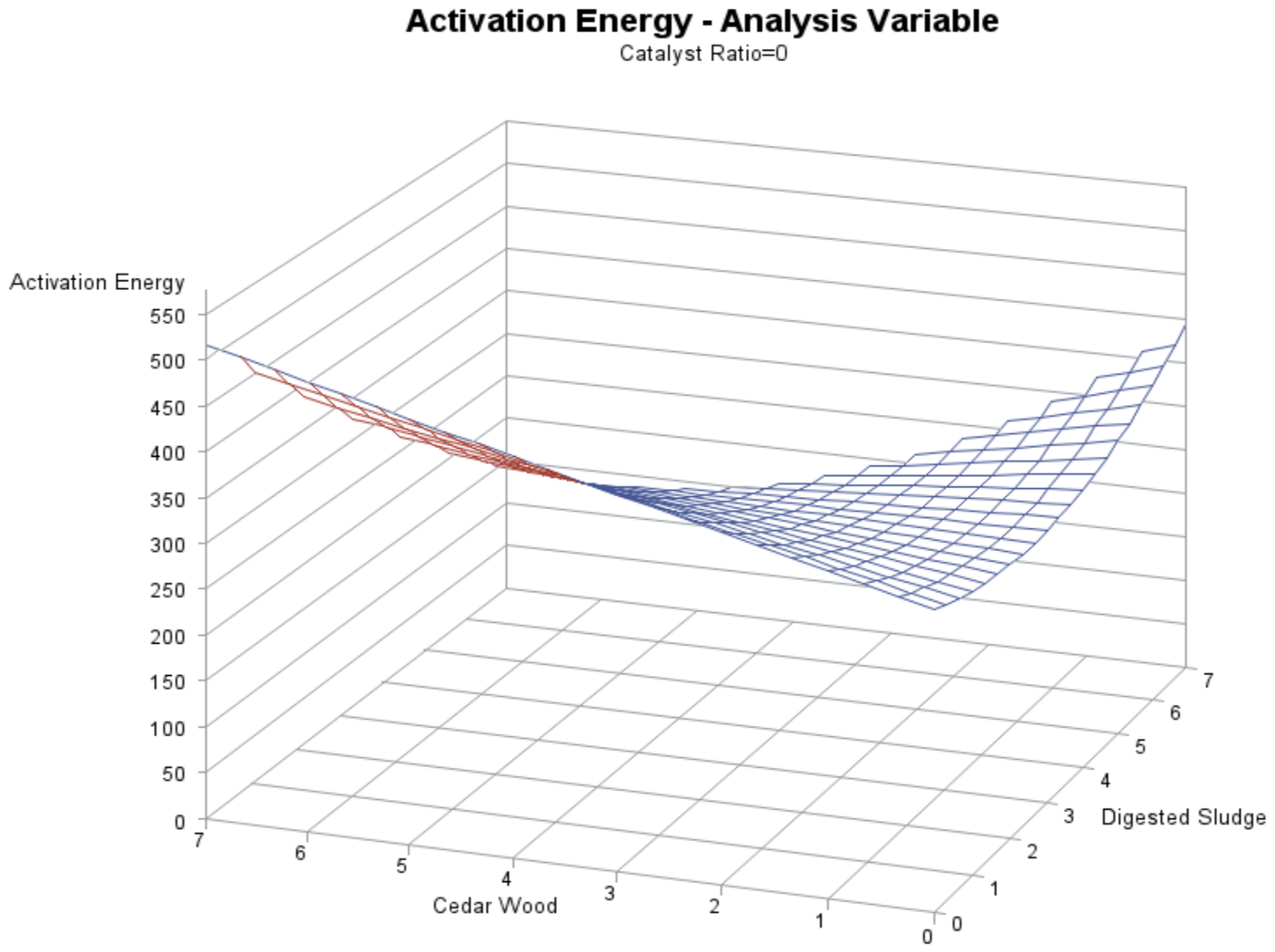

Fig 15: Contour plot for the response surface model based on the biomass pair of DS and CW for E_a without ZSM–5,

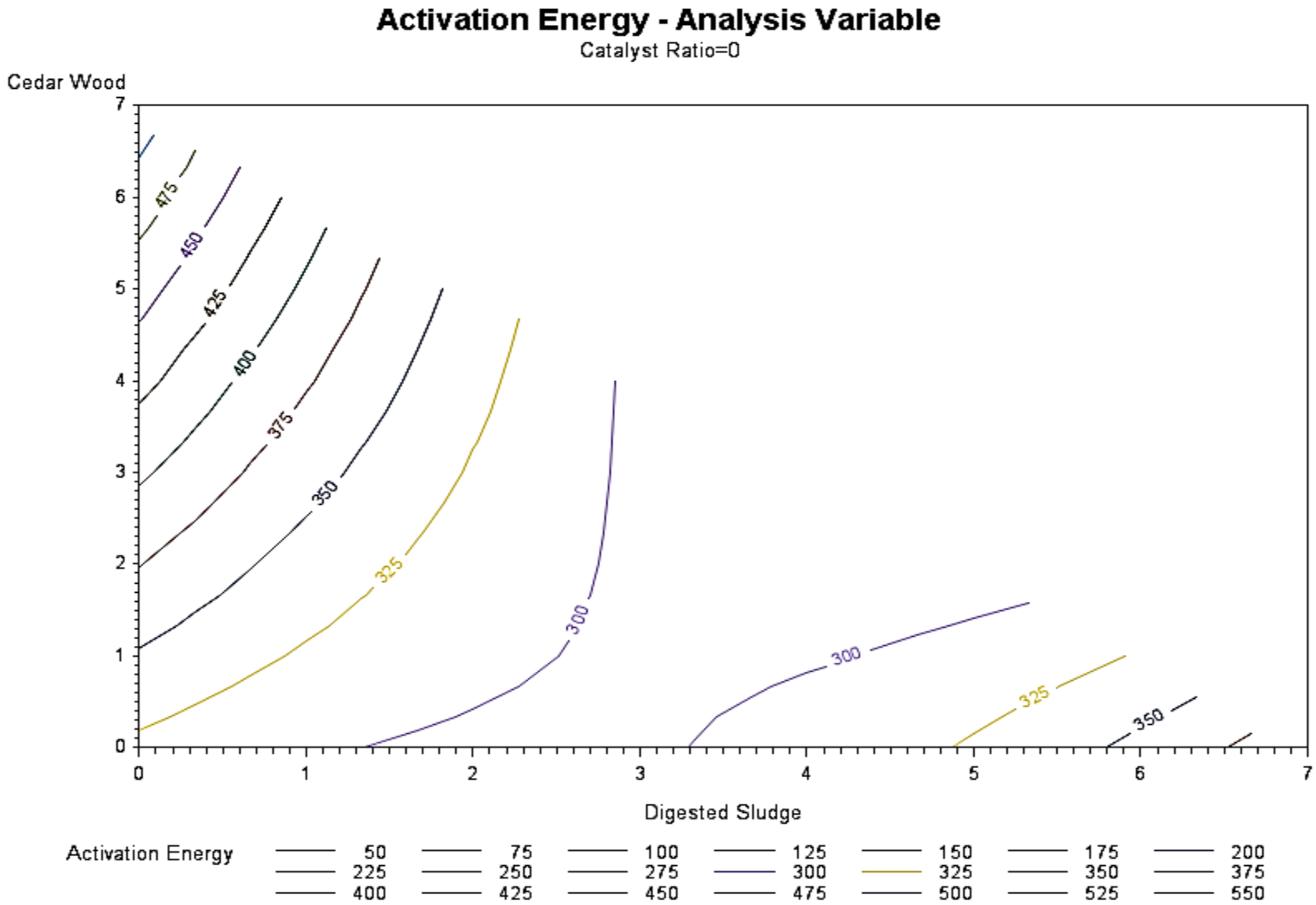

Fig 16: 3D surface plot for the response surface model based on the biomass pair of DS and CW for E_a with ZSM–5,

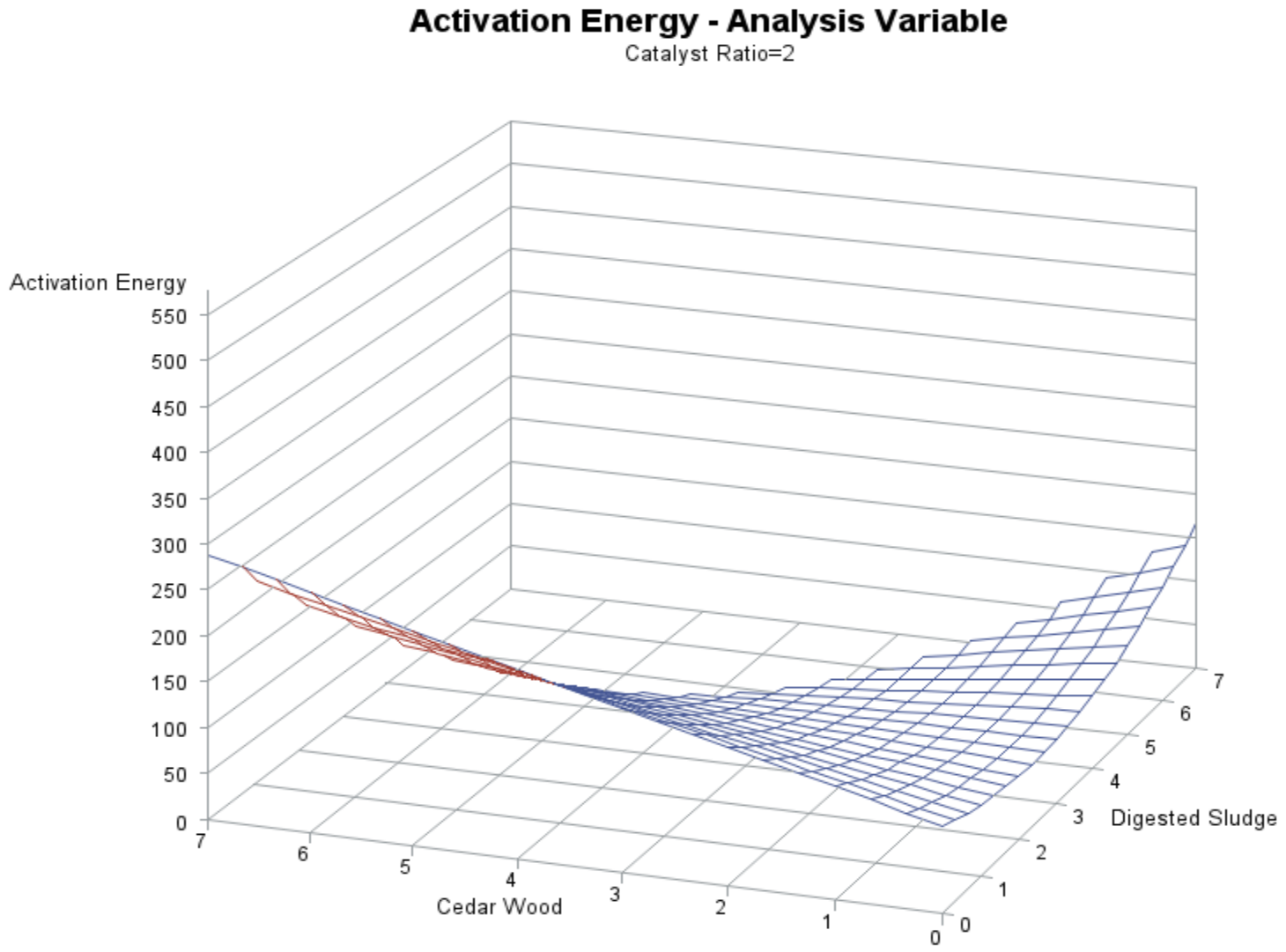

Fig 17: Contour plot for the response surface model based on the biomass pair of DS and CW for E_a with ZSM–5,

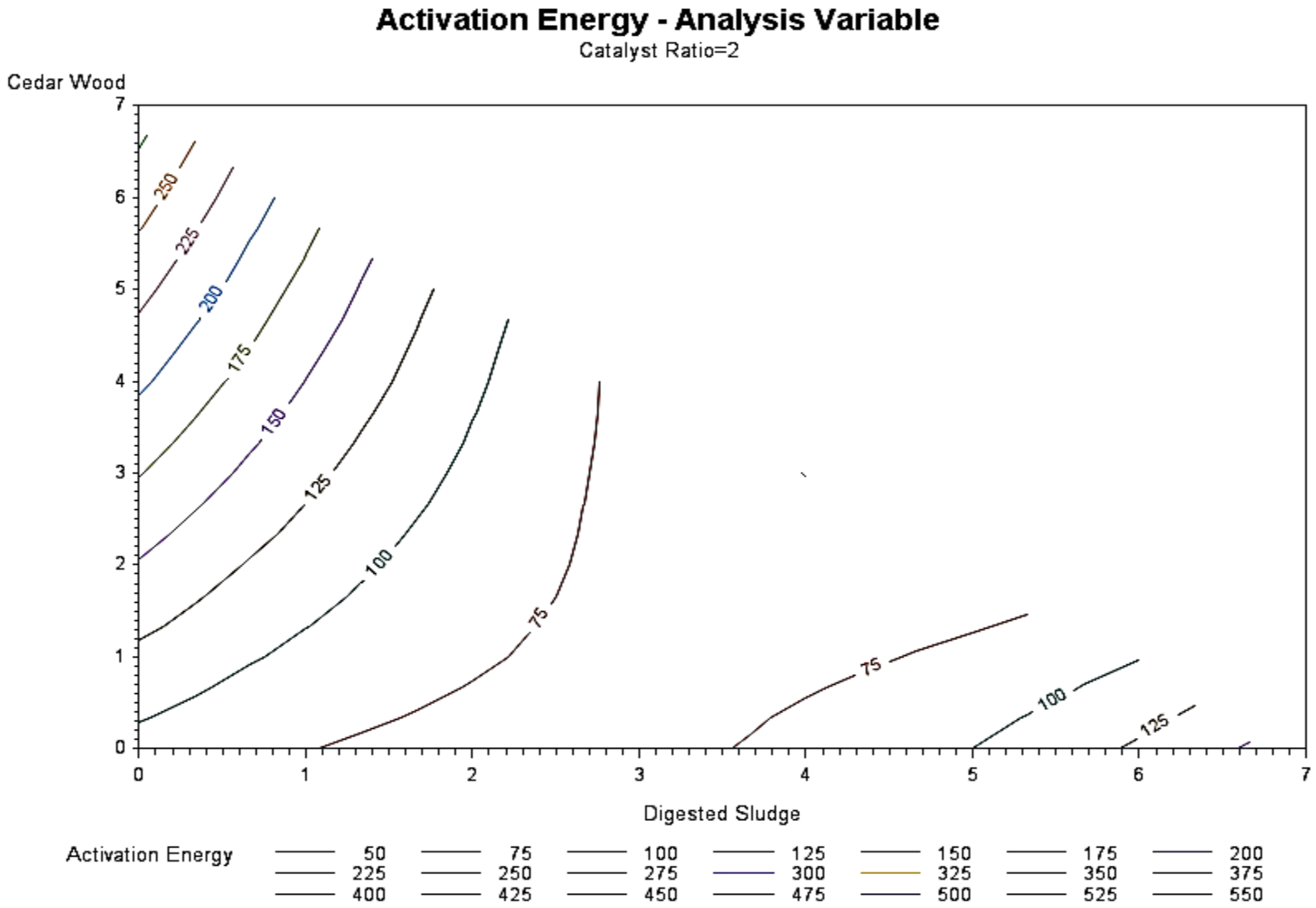

Fig 18: 3D surface plot for the response surface model based on the biomass pair of DS and CW for ΔH without ZSM–5,

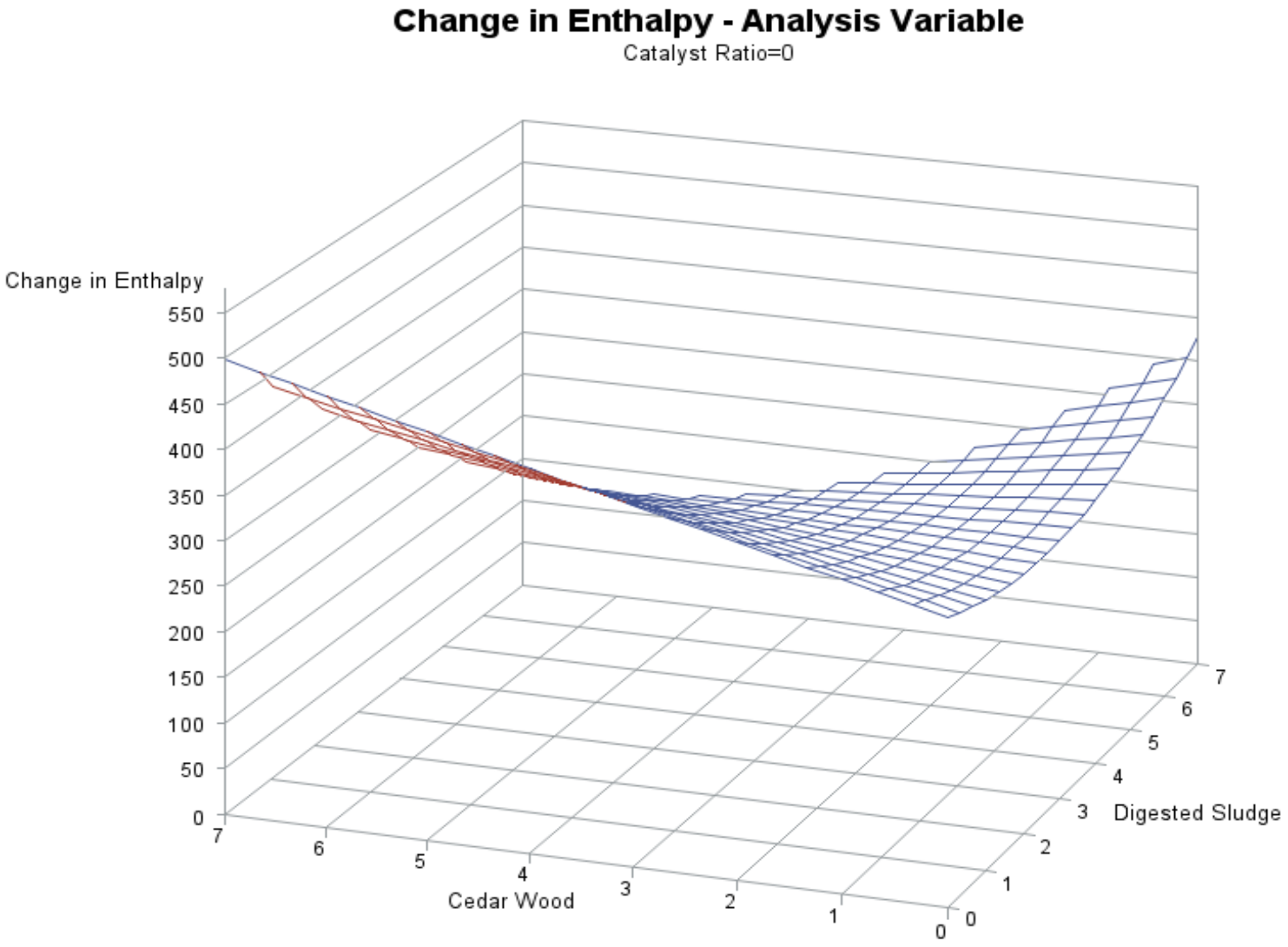

Fig 19: Contour plot for the response surface model based on the biomass pair of DS and CW for ΔH without ZSM–5,

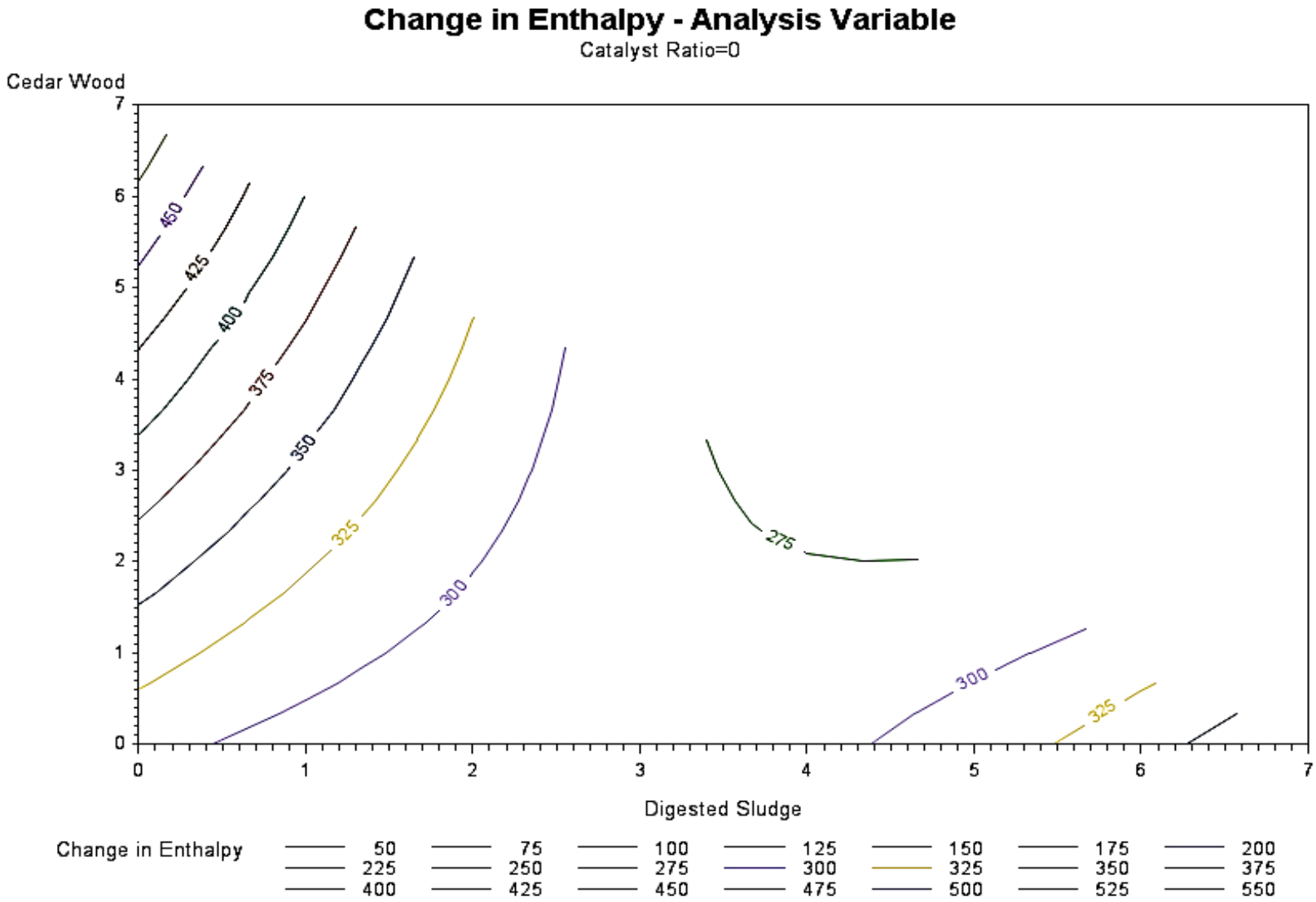

Fig 20: 3D surface plot for the response surface model based on the biomass pair of DS and CW for ΔH with ZSM–5,

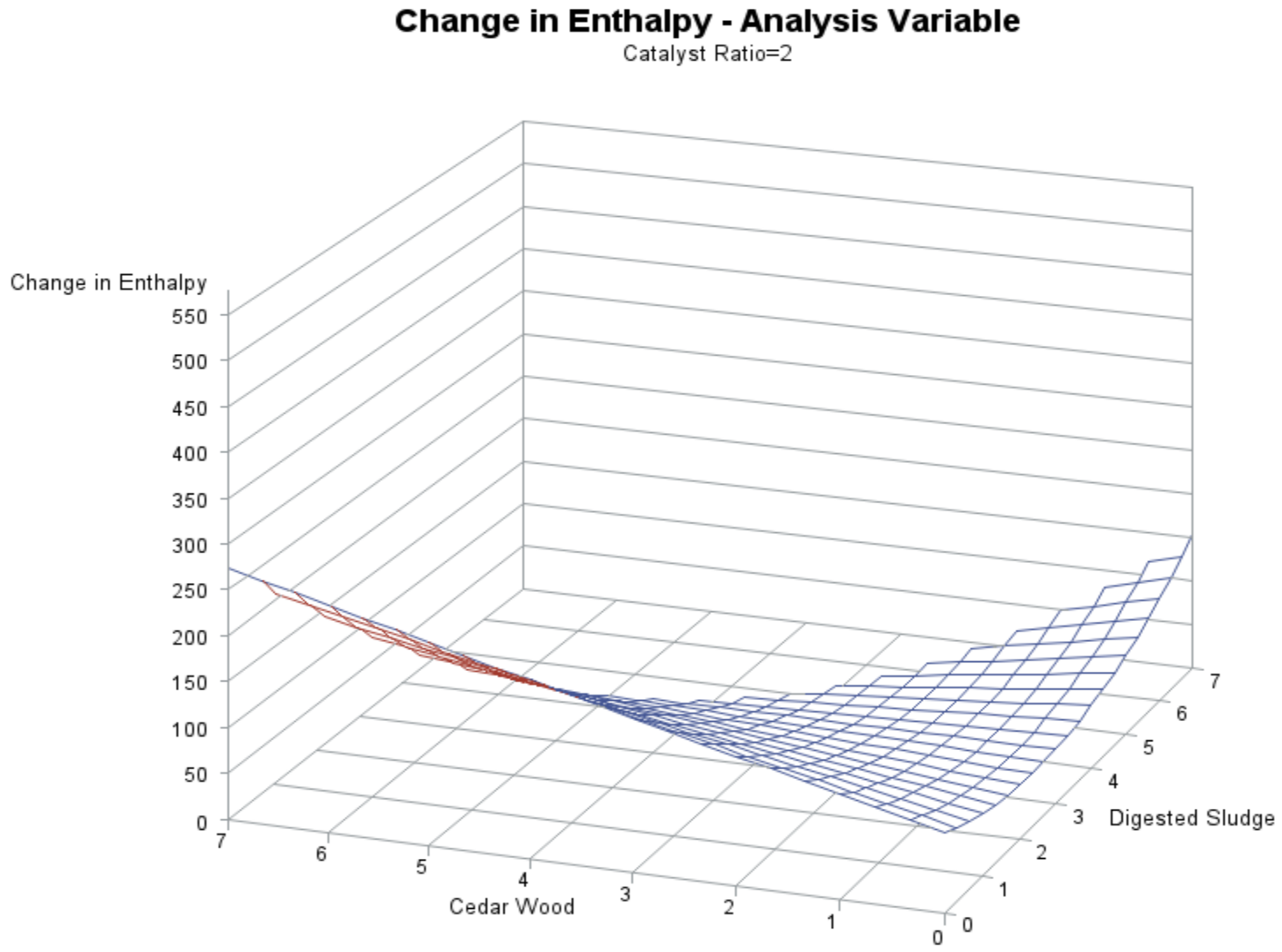

Fig 21: Contour plot for the response surface model based on the biomass pair of DS and CW for ΔH with ZSM–5,

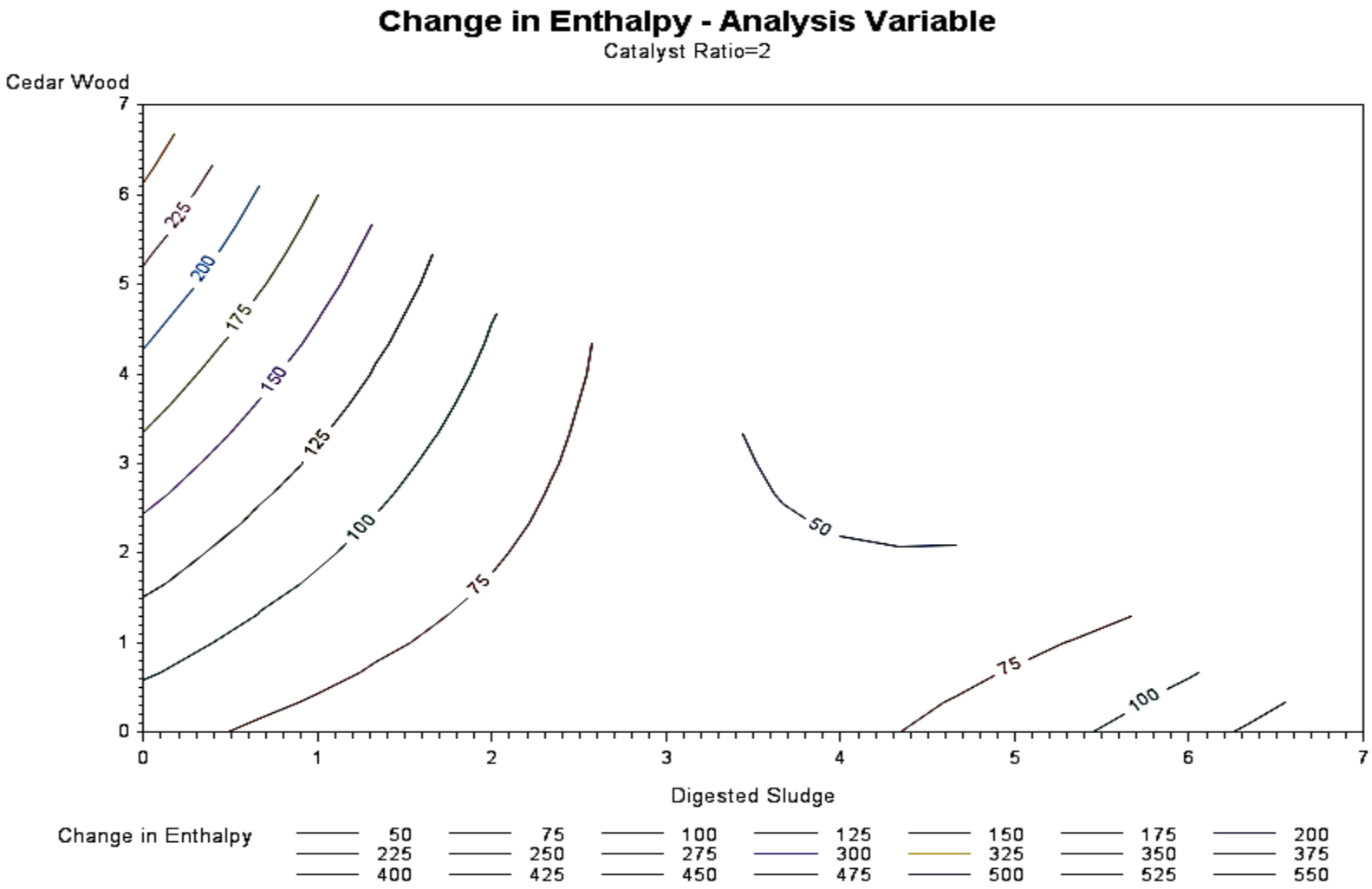

Fig 22: 3D surface plot for the response surface model based on the biomass pair of DS and AB for E_a without ZSM–5,

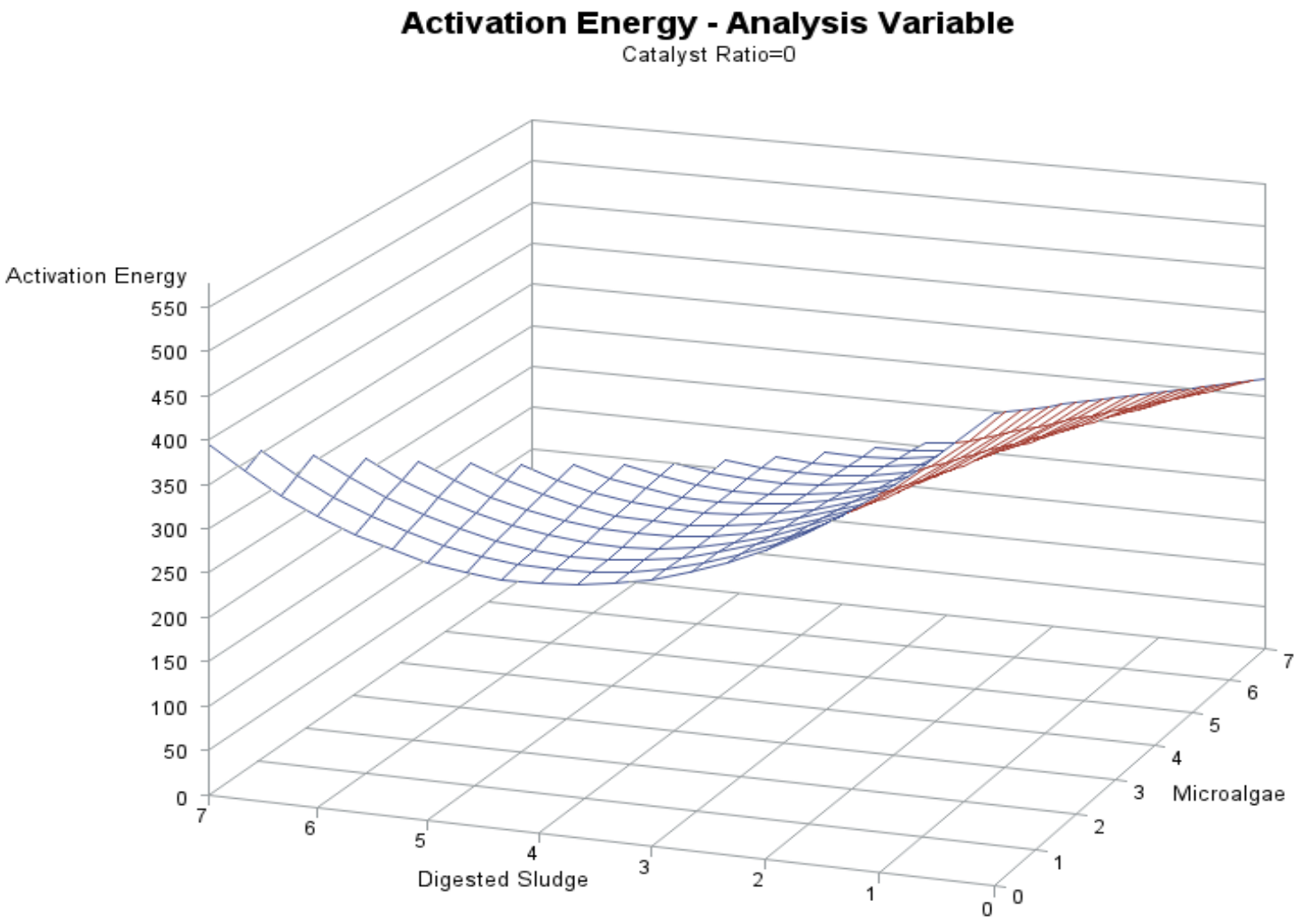

Fig 23: Contour plot for the response surface model based on the biomass pair of DS and AB for E_a without ZSM–5,

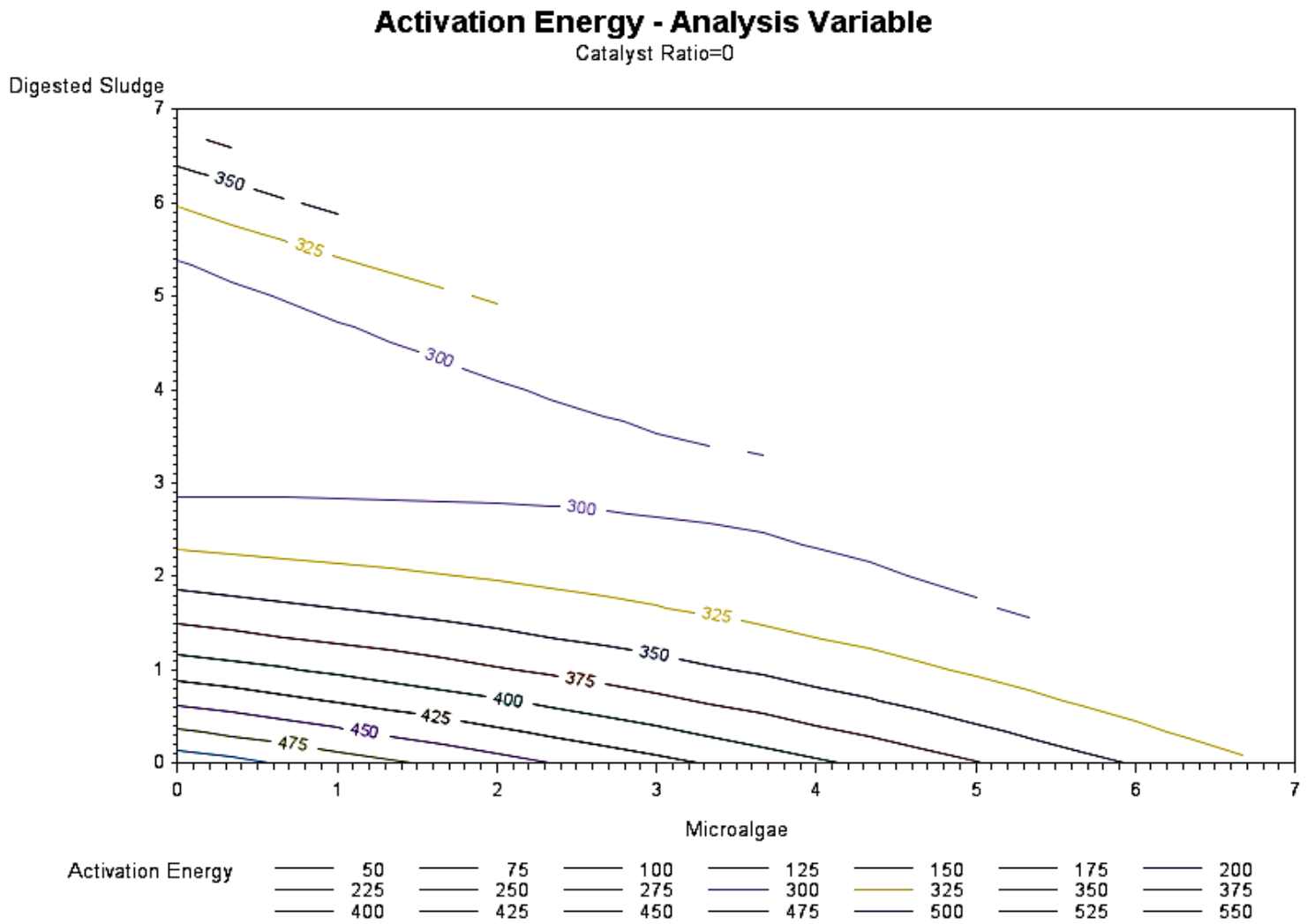

Fig 24: 3D surface plot for the response surface model based on the biomass pair of DS and AB for E_a with ZSM–5,

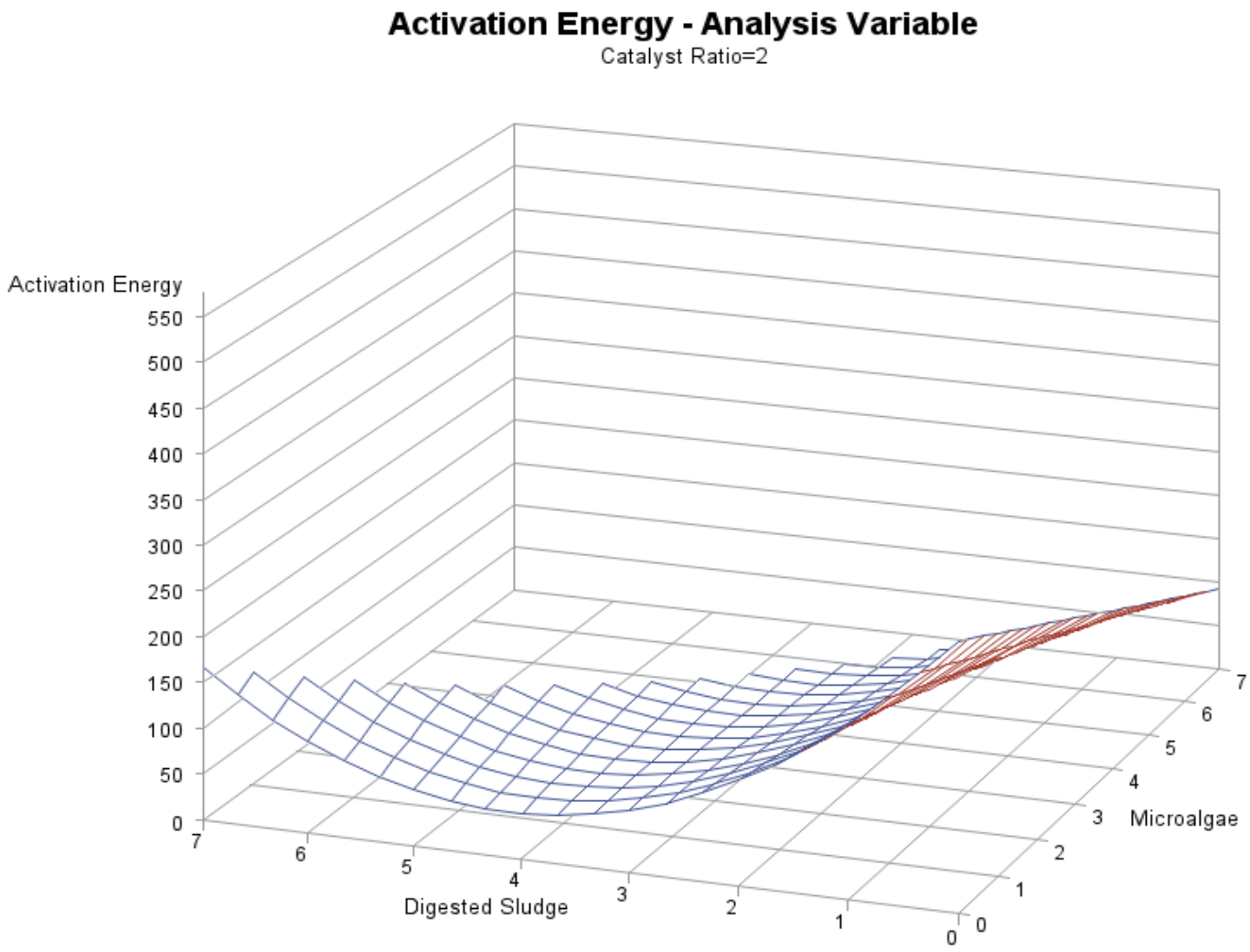

Fig 25: Contour plot for the response surface model based on the biomass pair of DS and AB for E_a with ZSM–5,

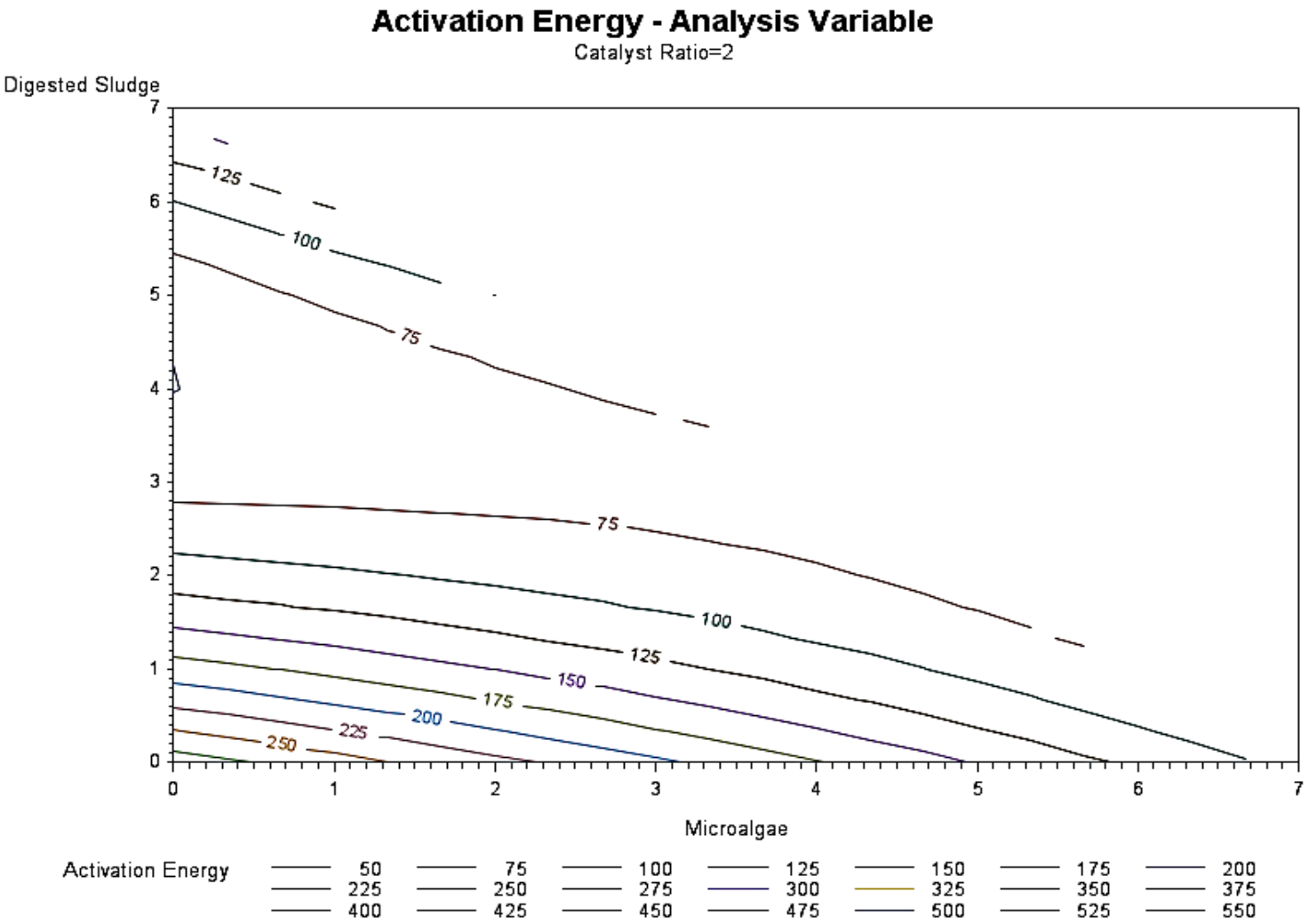

Fig 26: 3D surface plot for the response surface model based on the biomass pair of DS and AB for ΔH without ZSM–5,

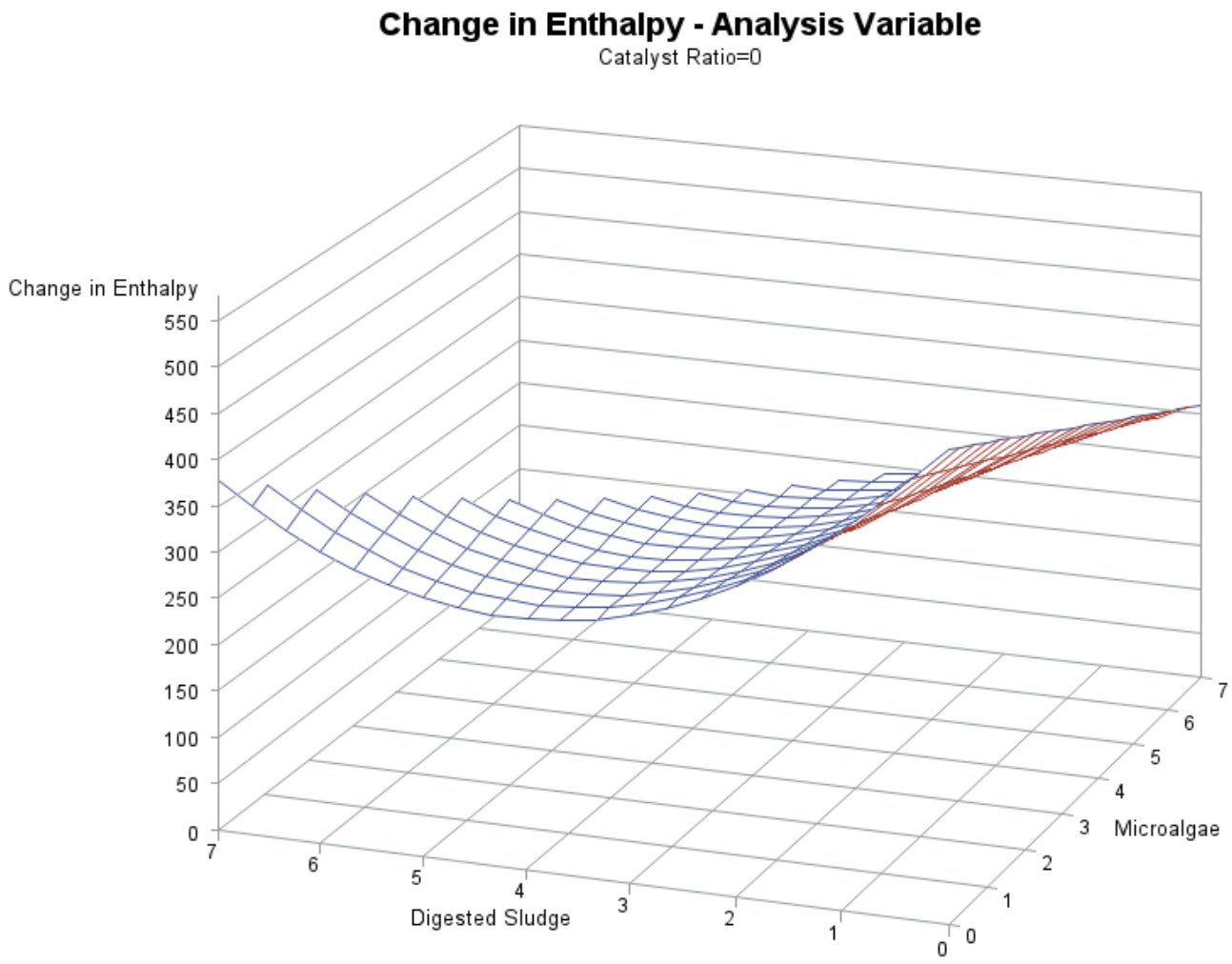

Fig 27: Contour plot for the response surface model based on the biomass pair of DS and AB for ΔH without ZSM–5,

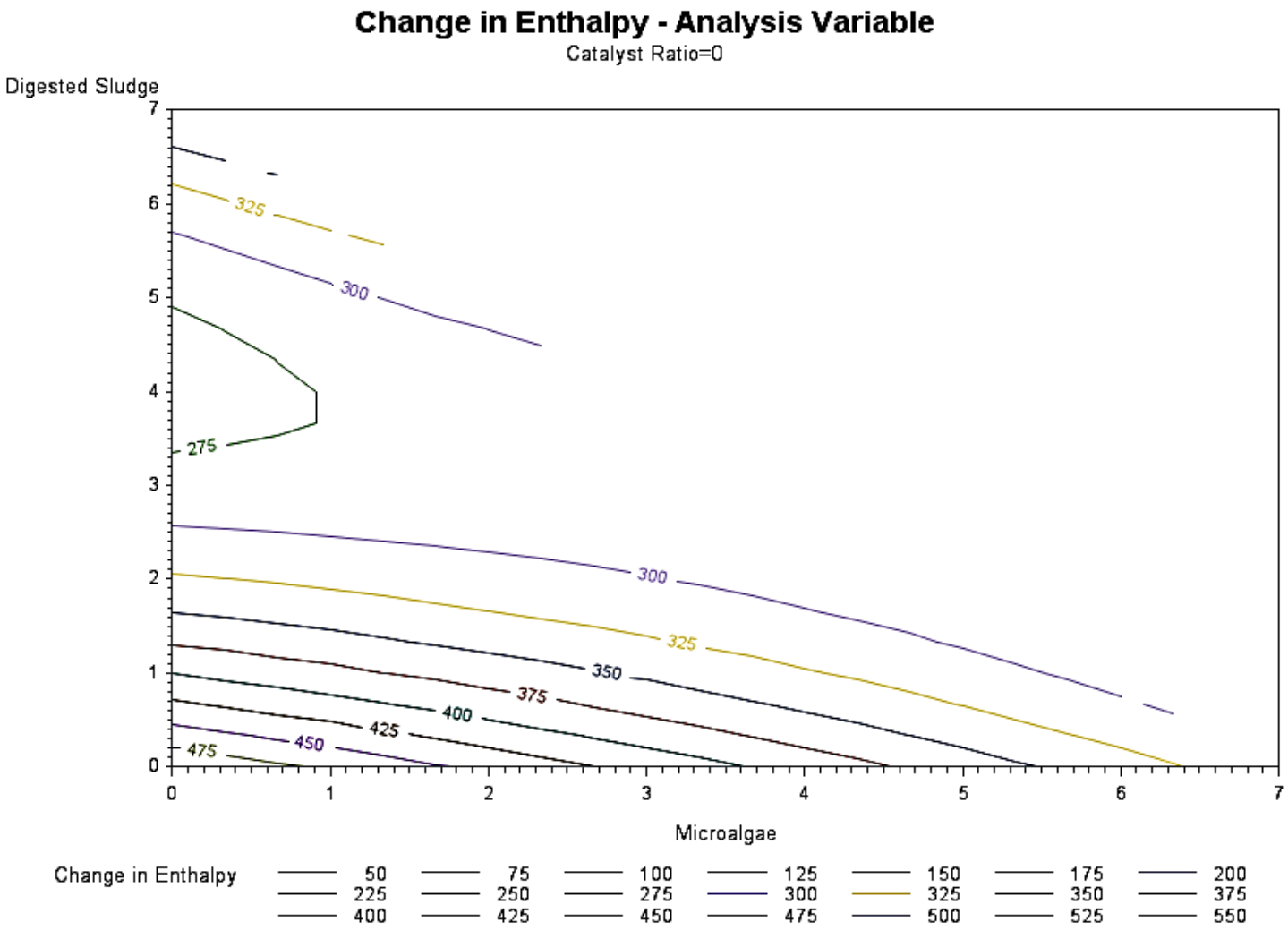

Fig 28: 3D surface plot for the response surface model based on the biomass pair of DS and AB for ΔH with ZSM–5,

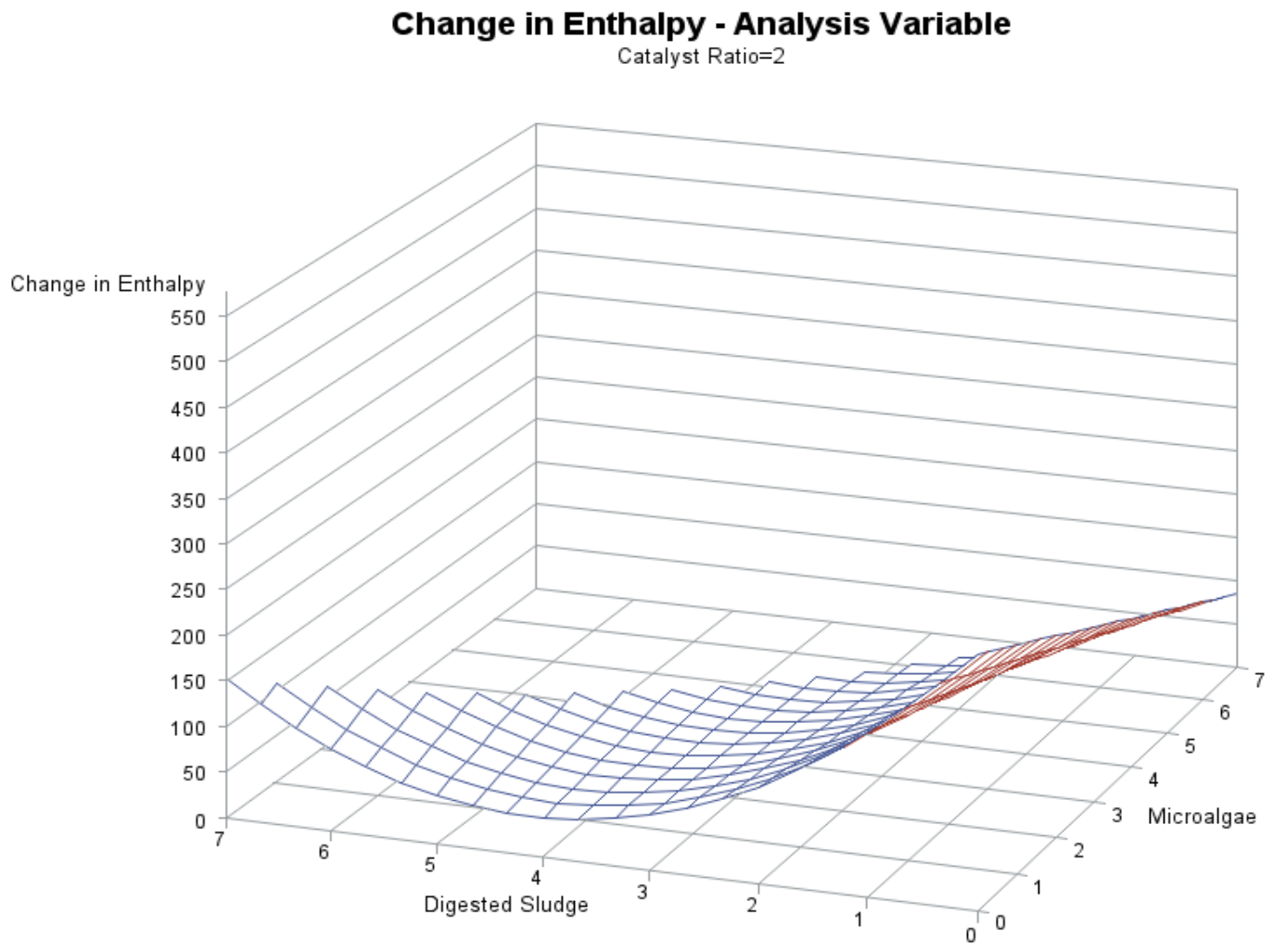

Fig 29: Contour plot for the response surface model based on the biomass pair of DS and AB for ΔH with ZSM–5,

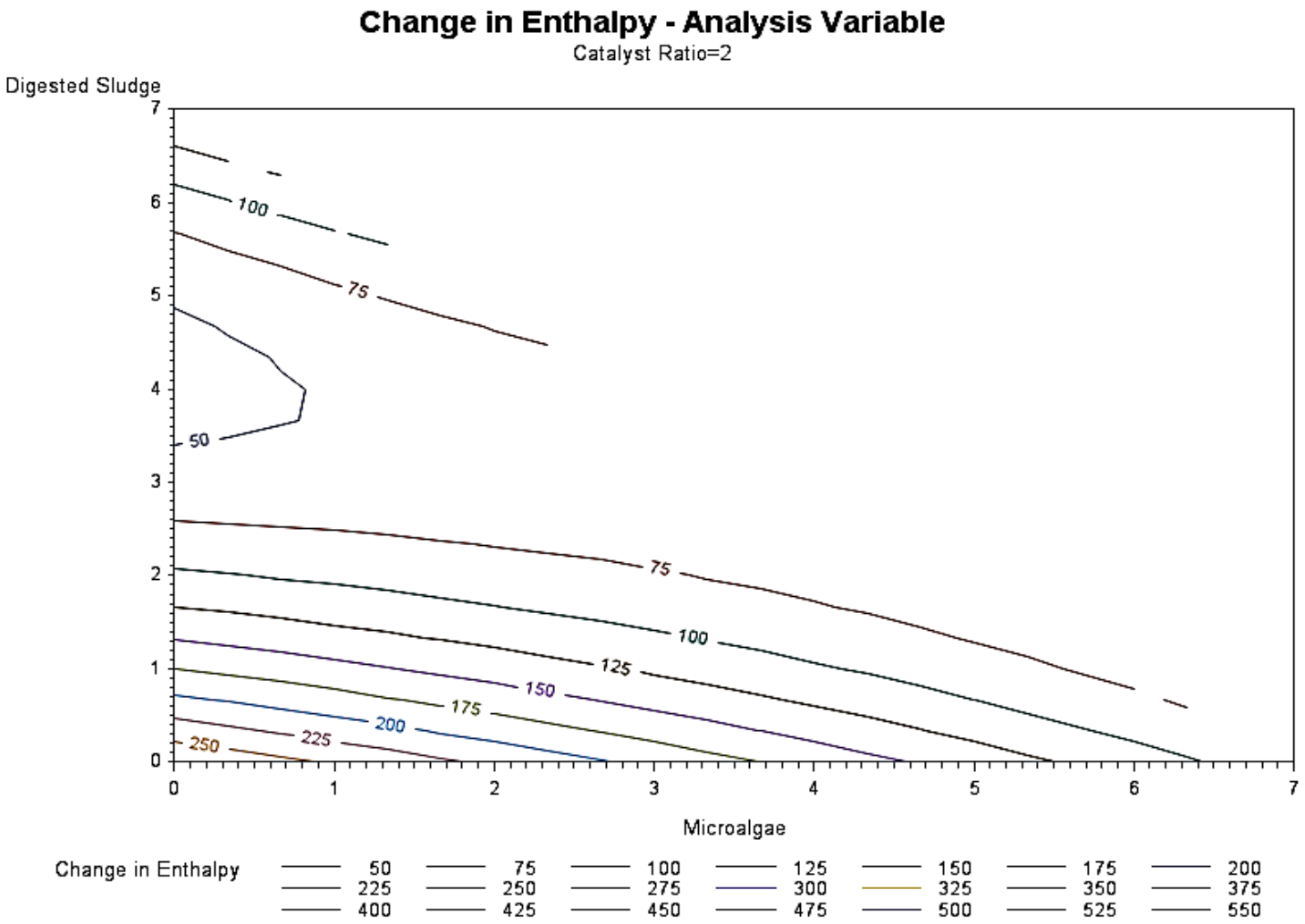

Fig 30: Graph depicting the pyrolysis product yields for the 11 different combinations ran in the furnace.

[OM – Optimum Mixture with biomass composition (wt %) of 57.14 DS; 4.29 AB and 38.57 CW;

OM – 0.5 = ZSM–5: OM wt/wt ratio = 0.5:1 wt/wt;

OM – 1.0 = ZSM–5: OM wt/wt ratio = 1:1 wt/wt;

OM – 2.0 = ZSM–5: OM wt/wt ratio = 2:1 wt/wt.]

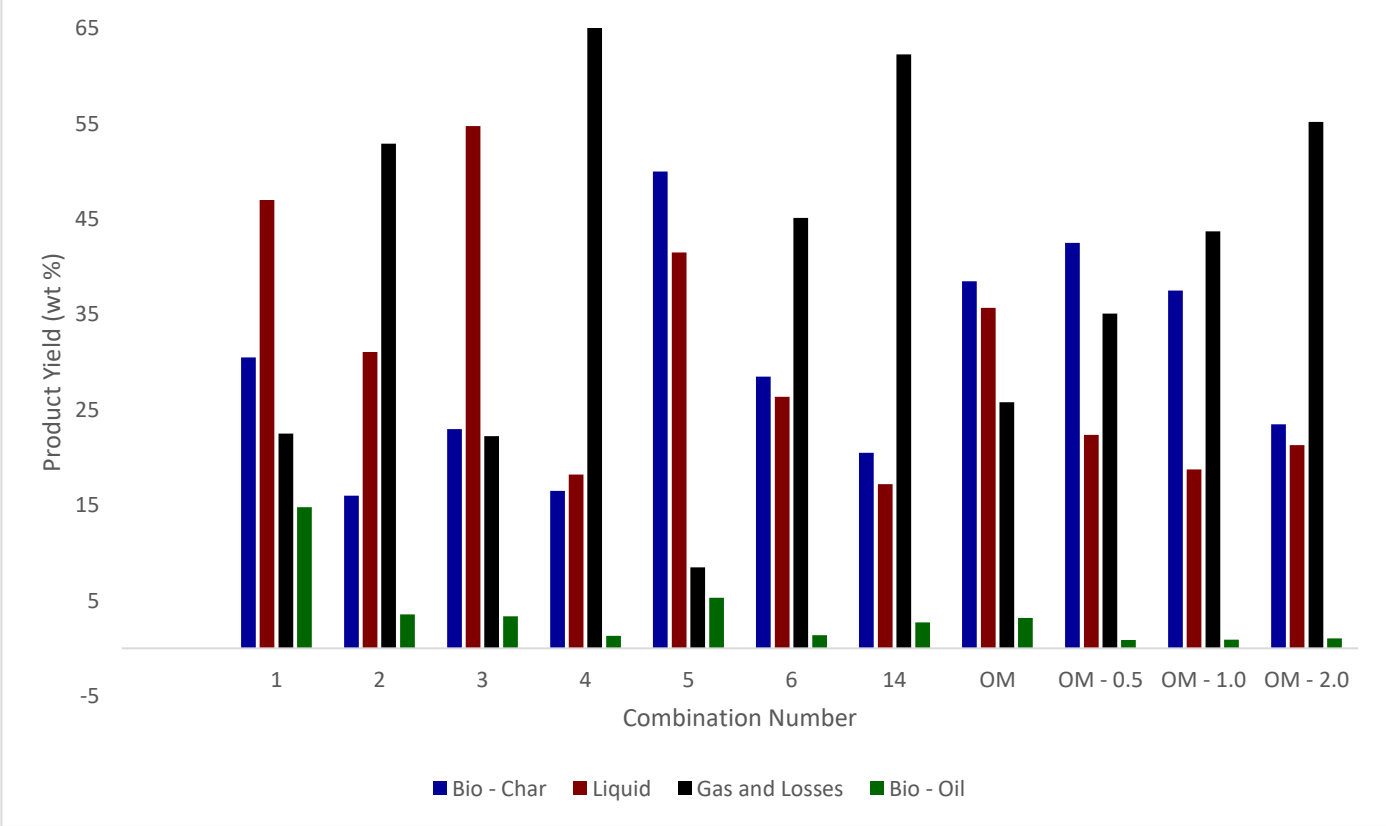

Fig 31: ASPEN PLUS simulation flowsheet

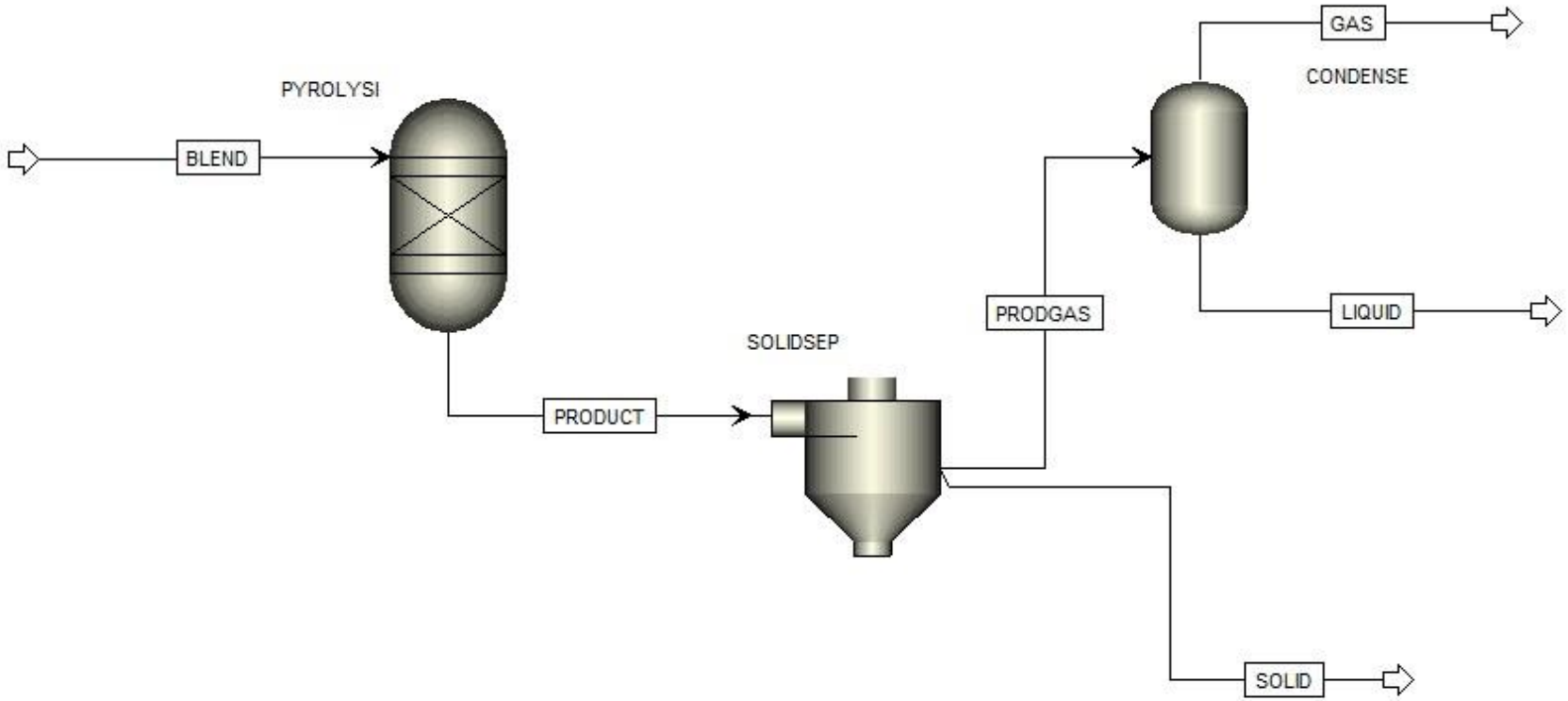

Fig 32: ASPEN PLUS simulation results for mass balance of different biomass mixtures from DSC runs

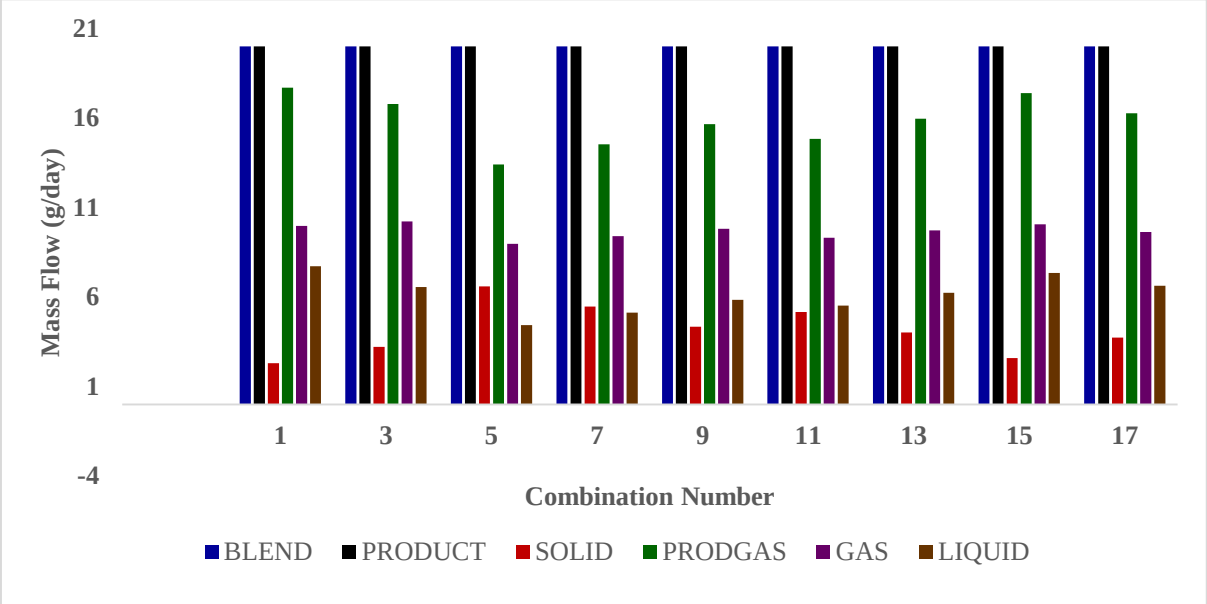

Fig 33: ASPEN PLUS simulation results for energy balance of different biomass mixtures from DSC runs

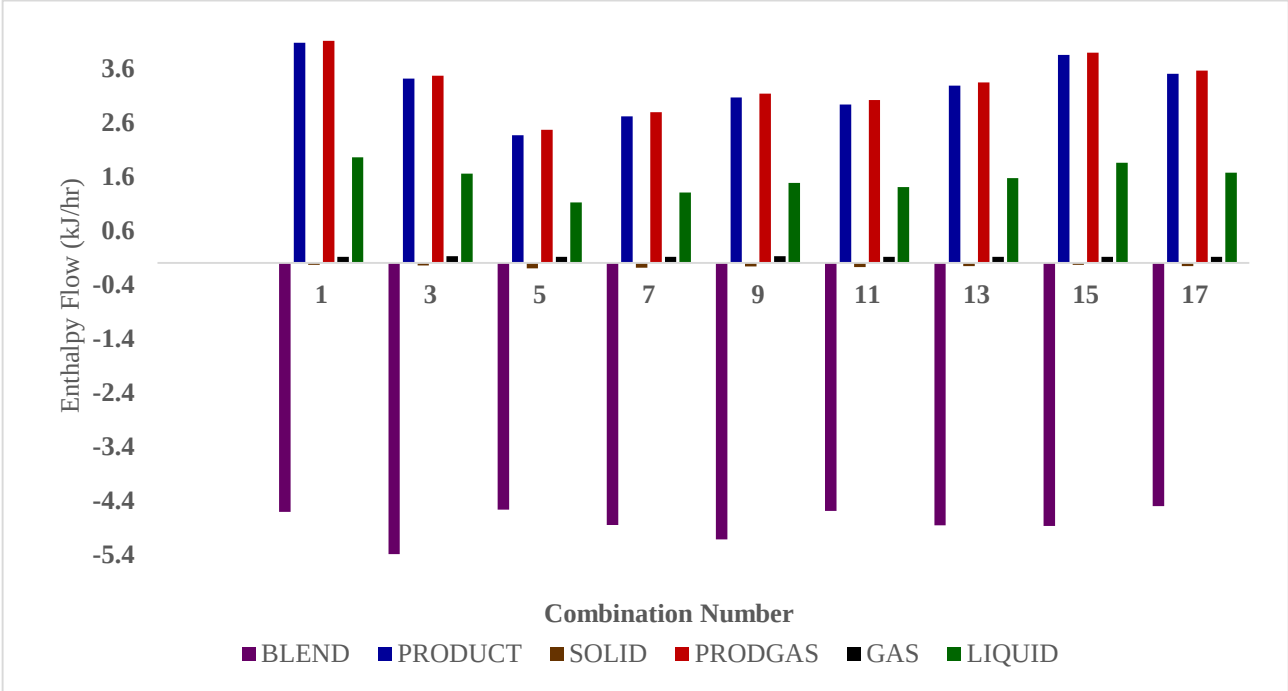

VITA

Sourabh Chakraborty

Candidate for the Degree of

Doctor of Philosophy

Dissertation: CO-PYROYLSIS OF MICROALGAE, SLUDGE, AND LIGNOCELLULOSIC BIOMASS FOR AROMATIC HYDROCARBON PRODUCTION

Major Field: Biosystems and Agricultural Engineering

Biographical:

Education:

Completed the requirements for the Doctor of Philosophy in Biosystems and Agricultural Engineering at Oklahoma State University, Stillwater, Oklahoma in December, 2019.

Completed the requirements for the Master of Technology in Biotechnology and Biochemical Engineering at Indian Institute of Technology – Kharagpur, Kharagpur, West Bengal/India in 2015.

Completed the requirements for the Bachelor of Technology in Biotechnology at Heritage Institute of Technology, Kolkata, West Bengal/India in 2013.

Experience: Graduate Research Assistant at Oklahoma State University
Stillwater, OK, August 2016 to December 2019.

Professional Memberships: ASABE